Mechanisms of Microbiologically Influenced Corrosion Caused by Corrosive Biofilms and its Mitigation Using Enhanced Biocide Treatment

A dissertation presented to

the faculty of

the Russ College of Engineering and Technology of Ohio University

In partial fulfillment

of the requirements for the degree

Doctor of Philosophy

Ru Jia

December 2018

This dissertation titled

Mechanisms of Microbiologically Influenced Corrosion Caused by Corrosive Biofilms and its Mitigation Using Enhanced Biocide Treatment

by

RU JIA

has been approved for

the Department of Chemical and Biomolecular Engineering

and the Russ College of Engineering and Technology by

Tingyue Gu

Professor of Chemical and Biomolecular Engineering

Dennis Irwin

Dean, Russ College of Engineering and Technology

Abstract

JIA RU, Ph.D., December 2018, Chemical Engineering

Mechanisms of Microbiologically Influenced Corrosion Caused by Corrosive Biofilms and its Mitigation Using Enhanced Biocide Treatment

Director of Dissertation: Tingyue Gu

Corrosion influenced or driven by the presence or activities of microorganisms is known as biocorrosion or microbiologically influenced corrosion (MIC). MIC has been recognized as a significant problem in many industrial systems such as power plant cooling systems, oil and gas transportation, and water utilities. In nature, different types of microorganisms live in a community that attaches to materials such as metals to form a biofilm. Microbes in the biofilm are responsible for MIC. Thus, it is critical to understand the corrosion mechanisms that are caused by different microbes and find better ways to treat biofilms.

The main importance of this work is listed below:

(1) H_2S is not the primary contributing factor in carbon steel MIC by sulfate reducing bacteria (SRB).

(2) Sulfate reducing archaeon (SRA) is corrosive against C1018 carbon steel at 80^{o}C because SRA can utilize extracellular electrons for sulfate respiration just like SRB.

(3) A nature-inspired anti-biofilm peptide at ppb (w/w) levels are found in lab tests to enhance a popular commercial biocide in treating a corrosive oilfield biofilm consortium on C1018 carbon steel.

Many people mistakenly believe that biogenic H_2S is the major contributing factor in sulfate reducing microbes (SRM) MIC on carbon steel. In this project, a nitrate reducing *Pseudomonas aeruginosa* biofilm that does not have H_2S corrosion complication was evaluated for its corrosivity against carbon steel. It was found that *P. aeruginosa* grown as an NRB (nitrate reducing bacterium) was very corrosive against C1018 carbon steel because starved sessile cells switched from organic carbon to elemental iron as electron donor, thus causing more corrosion. A causal-relationship experiment was designed to prove a hypothesis that the Fe^{2+} acceleration of SRB MIC of carbon steel is primarily attributed to reduced H_2S toxicity that leads to a higher sessile cell count, rather than an elevated $[H_2S]$ during incubation. A higher Fe^{2+} concentration in the culture medium can counter the toxic effects of H_2S to promote SRB planktonic and sessile cell growth with increased dissolved $[H_2S]$. A previous work demonstrated that lower $[H_2S]$ due to H_2S escape to a larger headspace led to accelerated corrosion because of better sessile cell growth. In the two cases, $[H_2S]$ had opposite trends, suggesting that H_2S was not the primary causal factor in the corrosion. In both cases, the increase of weight loss was due to increased electron uptake as evidenced by the increased sessile cell count in both cases. The combination of the headspace work with the Fe^{2+} work provides conclusive evidence that H_2S is not the primary contributing factor in carbon steel MIC by SRB, thus solving a long-time mystery in SRB MIC of carbon steel.

There are lots of data on MIC at mild temperatures such as 37°C. However, in a deep reservoir, much higher temperatures (e.g., 80°C) are encountered. *Archaeoglobus fulgidus*, a thermophilic SRA, was found to be corrosive against C1018 carbon steel at

80ºC. It was also found that under different levels of carbon source starvation, the thermophilic SRA became more corrosive against carbon steel. This work proved that SRA also can utilize extracellular electrons for sulfate respiration just like SRB. This will inspire new research into the extracellular electron transfer (EET) mechanisms in archaea.

In enhanced oil recovery (EOR), polymers are usually injected to increase the viscosity of injection water that is needed the push out viscous crude oil. EOR polymers, which are organic molecules, may be utilized by microbes as an organic carbon source. In this project, a commercial EOR polymer was degraded by an oilfield biofilm consortium (labeled as Consortium II) in an artificial seawater medium during a 30-day incubation period resulting in reduced viscosity by 34.5%. An efficient biocide treatment in the presence of EOR chemicals and other oilfield chemicals is desired. An equimolar D-amino acid mixture (D-mix) containing four different D-amino acids (D-tyrosine, D-methionine, D-leucine, and D-tryptophan) was tested to enhance tetrakis hydroxymethyl phosphonium sulfate (THPS) against Consortium II in the presence of EOR chemicals and other oilfield chemicals in this work. The combination of 100 ppm (w/w) THPS + 100 ppm (w/w) D-mix achieved further logarithmic reductions of sessile cell counts compared with the 100 ppm THPS alone treatment, thus further reduced carbon steel coupon weight loss and pitting corrosion. The test results suggest that D-amino acids are compatible with the other oilfield chemicals.

Facing escalating biocide dosages, it is desirable to find biocide enhancers that make biocides more effective in biofilm treatment. Peptide A, a 14-mer cyclic peptide, was inspired by the anti-biofilm Equinatoxin II protein found in a sea anemone that

exhibits biofilm-free exteriors. Peptide A at ppb levels was found to enhance 100 ppm THPS in treating biofilm Consortium II on C1018 carbon steel in an enriched artificial seawater medium. The enhanced biocide treatment reduced sessile cells on the carbon steel thus decreasing the coupon weight loss and pitting corrosion.

Properly conducted electrochemical measurements such as linear polarization resistance (LPR), electrochemical impedance spectroscopy (EIS) and potentiodynamic sweep (PDS) can be used to support weight loss and pitting data and provide transient corrosion trends in MIC mechanistic studies and in biocide efficacy assessment.

Dedication

To

All the people who helped me during my PhD degree pursuit

And especially my wife: Dongqing Yang

Acknowledgments

I would like to give my sincere appreciation to Prof. Tingyue Gu for his support, patience and advice during my Ph.D. study. His rigorous training helped me to improve my technical writing and logical thinking skills. His enthusiasm and motivation encouraged me to be an independent researcher. He committed time and efforts to all of my projects and paper writings. I could not have completed my study without his continuous help. I really appreciate his supervision.

I am highly grateful to Prof. Srdjan Nešić, Prof. Tadeusz Malinski, Prof. Monica Burdick and Prof. Rebecca Barlag for serving on my dissertation committee. I sincerely thank for their time and contribution. I thank the support from Prof. Srdjan Nešić who has provided a professional working environment in the Institute for Corrosion and Multiphase Technology (ICMT). I also appreciate Prof. Valerie Young for her help in my professional growth. My many thanks go to our MIC group members both past and present: Dr. Dake Xu, Dr. Yingchao Li, Dongqing Yang, Dr. Jin Xu, Di Wang, Dr. Tuba Unsal, Dr. Jie Long Tan, Dr. Wenwen Dou, Jialin Liu, Zhong Li, Jike Yang, Fazlollah Madani Sani, Saeed Seyfi Kakhki, Amy Lindenberger and Weizhen Cai for their help in my academic study and experimental work. A special thanks goes to Dr. Peng Jin, Dr. Bruce Brown, Alexis Barxias, Dr. Marc Singer, Dr. David Young, Dr. Yoon-Seok Choi, Rebecca Gill and other staff and students at ICMT for their support and help in my research. I would like to express my appreciations to Dr. Amir Zlotkin at Hutchison Biofilm Solutions, Limited, and Earl Harlow at SABIC Innovative Plastics for valuable suggestions to my research. I would like to thank Joey Boyle and James Caesar for their

technical support on setting up experiments. I also want to thank Thomas Riggs and Carrie Linscott for their administrative support.

I would like to express my sincere appreciation to TOTAL, SABIC, the Pipeline and Hazardous Materials Safety Administration (PHMSA) of the U.S. Department of Transportation (DOT), Hutchinson Biofilm Solutions, Limited, Petronas, PTTEP, Chinese Society for Corrosion and Protection for their financial support in the projects that I participated.

Last but not least, my heartfelt thanks go to my wife, Dongqing Yang for her unwavering love and support. I also want to express my deep appreciation to our parents and other family members for their unconditional love, care and support during my Ph.D. study.

Table of Contents

Page

List of Tables

Page

List of Figures

Page

Nomenclature

ρ	Density, kg/m^3
$C_{SO_4^{2-}}$	Sulfate concentration in liquid, mol/m^3
$i_{a(Fe)}$	Anodic iron dissolution reaction current density, A/m^2
$i_{c(H^+)}$	H^+ reduction current density, A/m^2
$i_{c(SO_4^{2-})}$	Sulfate reduction current density, A/m^2
α_c	Cathodic charge transfer coefficient
CPE_b	Capacitance of the corrosion product film or the biofilm, F
CPE_{dl}	Capacitance of the electrical double layer, F
CR	Corrosion rate, mm/y
D	Diffusion coefficient, m^2/s
E	Redox potential/reduction potential, V
E_{corr}	Corrosion potential, V
E_e	Equilibrium potential, V
F	Faraday constant, A·s/mol
i	Current density, A/m^2
i_0	Exchange current density, A/m^2
i_{corr}	Corrosion current density, A/m^2
i_{ct}	Charge transfer current density, A/m^2
i_{lim}	Mass transfer limiting current density, A/m^2
M	Molecular weight
n	Constant phase element parameter
R	Universal gas constant, J/mol/K

R_b	Corrosion product film or biofilm resistance, $\Omega \cdot m^2$
R_c	Consumption rate of sulfate in biofilm, $mol/m^3/s$
R_{ct}	Charge transfer resistance, $\Omega \cdot m^2$
R_p	Polarization resistance, $\Omega \cdot m^2$
R_s	Solution resistance, $\Omega \cdot m^2$
T	Temperature in Kelvin, K
Y_0	Constant phase element parameter, $s^n/\Omega/cm^2$
z	Number of electrons transferred in an electrode reaction
β	Tafel slope, V/decade
ΔE	Cell potential of a redox reaction, V
ΔG	Gibbs free energy change, kJ/mol
ω	Angular frequency, rad/s

Chapter 1: Introduction

1.1 Background

Corrosion is the deterioration of materials as a result of chemical, physical and biological processes [1]. Corrosion influenced or driven by the presence or activities of microorganisms is known as biocorrosion or microbiologically influenced corrosion (MIC) [2]. It is widely accepted that MIC accounts for 20% of all corrosion damages. In the United State, billions of dollars are lost due to MIC every year [3]. Microbes were known to be associated with corrosion as early as 1910 [4]. MIC has been recognized as a significant problem in the oil and gas industry since the 1980s [5]. MIC is a serious risk in many industrial systems such as power plant cooling systems, oil and gas transportation pipelines, and water utilities [6–8]. MIC was blamed as a culprit for the 2006 Alaska oil pipeline leak [9]. An MIC failure of an offshore 16-inch ID (inner diameter) pipeline used to transport a mixture of oil, gas, and water occurred in only 2.5 years [10]. Bhat et al. reported that an 8-inch ID pipeline used to transport oil and produce water failed in only 8 months due to MIC [11]. MIC has been studied for decades. However, much confusion still remains in MIC because this study involves multidisciplinary knowledge such as corrosion engineering, microbiology, chemical engineering, and electrochemistry.

In nature, different types of microorganisms live in a community that attaches to materials such as metals to form a biofilm [12]. Microbes embedded in the biofilm are called sessile microbes while those in the bulk fluid are planktonic microbes [13]. It is widely known that biofilms are responsible for MIC [14]. Other corrosion processes such as under-deposit corrosion [15], crevice corrosion [16] and stress corrosion cracking [17]

can cooperate with MIC. Many materials are degraded by MIC, for example, carbon steel, which is commonly used in piping [18]. Stainless steel is prone to MIC pitting attack even though it is resistant against corrosion by atmospheric oxygen [19,20]. Other materials such as magnesium [21], aluminum alloy [22], and zinc [23] can also be corroded by biofilms. Various microbes such as bacteria, archaea and fungi are frequently found to cause MIC [24]. To detect and perform case analysis, it is critical to understand various MIC mechanisms.

Since biofilms are responsible for MIC, MIC mitigation is about biofilm mitigation. Biofilms can protect sessile cells from hazardous chemicals [25]. Therefore, it is more difficult to treat sessile cells in a biofilm than to treat planktonic cells. In the oil and gas industry, pigging and biocide dosing are the most widely used techniques to mitigate field biofilms [26]. Pigging can remove deposits and biofilms in the pipeline. Pigs are used to apply biocides as well. Biocides such as tetrakis hydroxymethyl phosphonium sulfate (THPS) and glutaraldehyde are widely used because they are biodegradable and offer broad-spectrum efficacy [26]. Certain parts of the pipeline such as dead ends are not piggable. In oilfield applications, a particular biocide is usually licensed. The biocide kills vulnerable microbes allowing resistant microbes to step in. The increased resistance of microbes against the biocide leads to higher dosages. This could result in environmental concerns and increased costs. Thus, it is desirable to enhance biocide treatment using various biocide enhancers.

In this work, MIC mechanisms and its mitigation were investigated in order to further understand MIC and efficiently treat corrosive biofilms. Different tools were used to study MIC mechanisms and to assess biofilm treatment.

Chapter 2: Literature Review

This chapter provides a sufficient background to elucidate the rationale behind this work. It includes a wide range of contents, such as biofilms, corrosive microorganisms, anaerobic MIC mechanisms, and MIC mitigation.

2.1 Biofilms

Biofilm is a multicellular community composed of sessile cells embedded in a matrix [27]. It is widely accepted that in the lab and field, the planktonic cells do not cause MIC pitting [28]. Biofilms are associated with corrosion and fouling, which lead to economic losses in many industries [27]. The removal of biofilms is desired and necessary to maintain pro oil and gas pipelines, cooling water systems, and water utility systems [29].

Figure 1 shows the process of biofilm formation. In the beginning, planktonic cells first need to attach to the surface and form an early structure. After that, mixed and integrated colonies form for optimum metabolic cooperations. Some sessile cells in biofilms detach under shear stress. Microorganisms in biofilms are held together by extracellular polymeric substances (EPS), which are composed of polysaccharides, proteins, and nucleic acids [30]. Many microorganisms secrete EPS to form biofilms (Figure 2). EPS function as a way of protection, adhesion, and aggregation for the sessile cells [31].

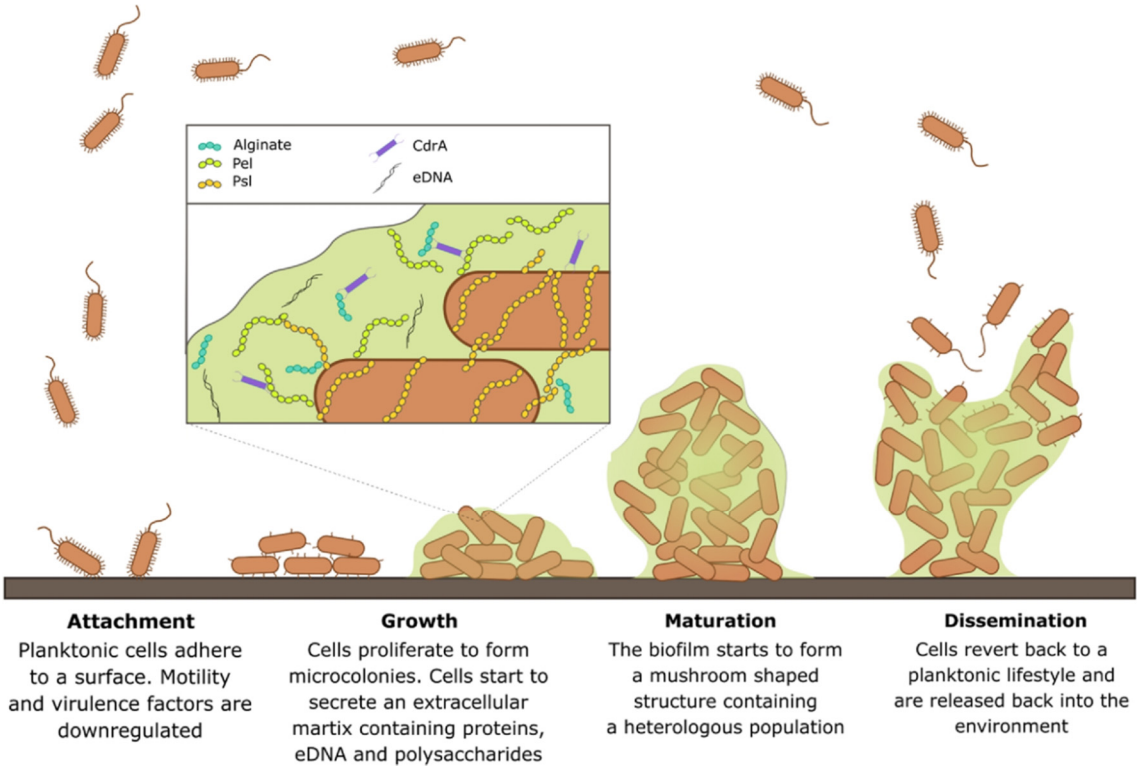

Figure 1. Biofilm formation [32]. (Open access under the terms of the Creative Commons Attribution License.)

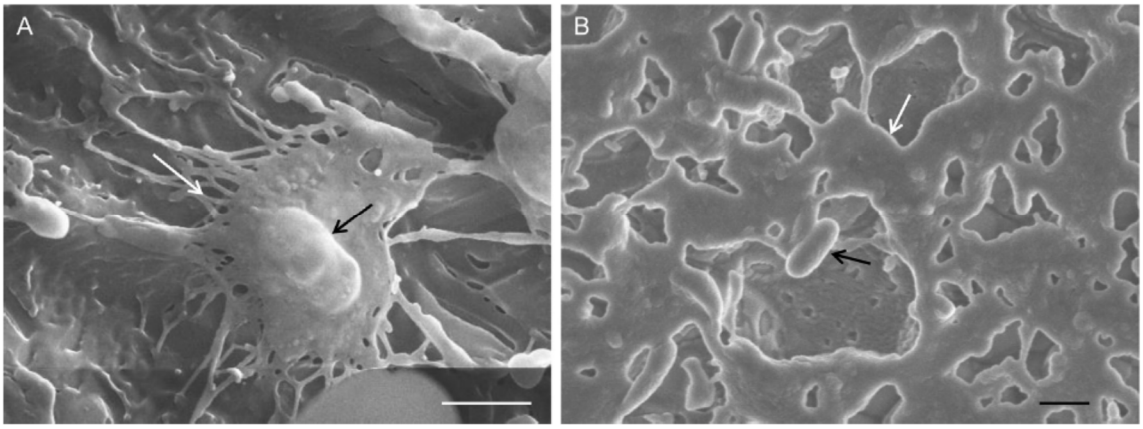

Figure 2. Scanning electron microscope (SEM) of microorganisms (black arrow) and EPS (white arrow) on a mild steel surface after 3 days (scale bar = 1 μm) [18]. (Reproduced with permission from Elsevier.)

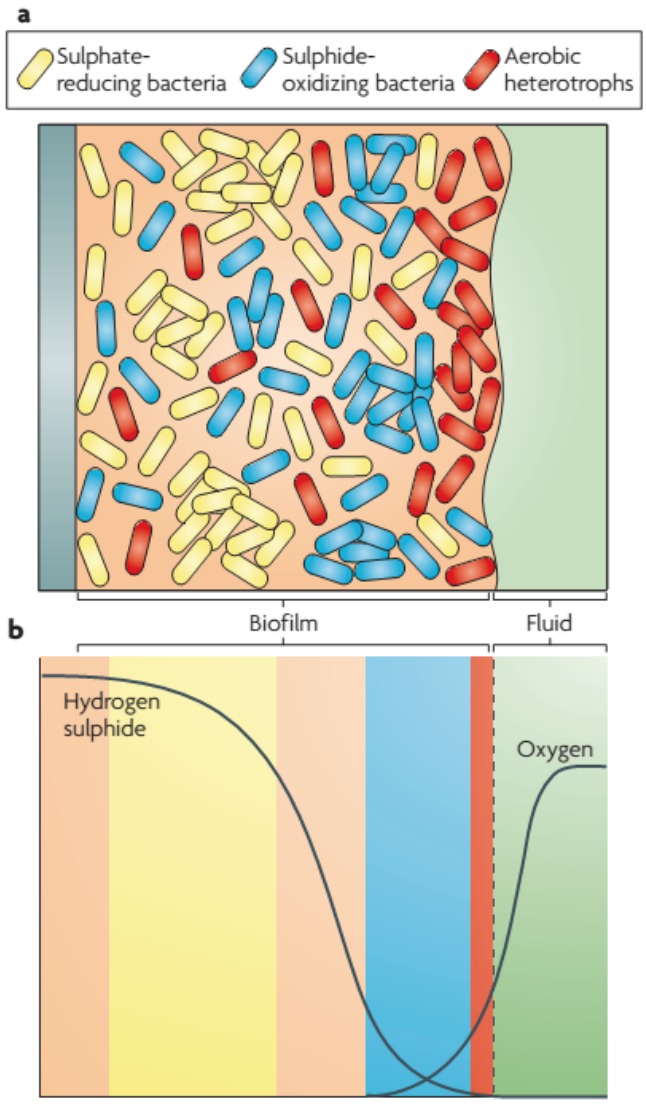

Figure 3. The physiological heterogeneity of a mixed species biofilm [33]. Red cells are facultative heterotrophs. (Reproduced with permission from Nature.)

In mechanistic MIC research, a pure strain is usually used in laboratories to reduce the number of variables. However, the electrochemical processes in natural communities are different from that in a single species. As shown in Figure 3, anaerobic bacteria grow underneath facultative bacteria. The concentrations of oxygen, metabolites and nutrients vary within biofilms [33]. Microorganisms can alter their metabolisms and

release different compounds in response to others in biofilms [18]. Different species in biofilms can utilize the cooperative benefits, sequestrate a nutrient-rich area for colonization, and protect them from harmful conditions [34]. Biofilms protect sessile cells from hazardous chemicals.

Several possible defensive mechanisms are employed by biofilms. The EPS matrix of biofilms could limit the penetration of antimicrobial agents. As a result, the matrix protects sessile cells from hazardous chemicals [25]. Microbes can slow down their metabolic rate to reduce the intake of hazardous chemicals. There is a nutrient concentration gradient in biofilms. Deeper area bacteria in biofilms experience a starvation, their growth is suppressed. As a result, the low growth or no growth condition helps increase the resistance to hazardous environments [35]. The heterogeneity feature of biofilms is also considered to promote resistance to harmful environments [36]. Persister cells are tougher than others. They survive even though neighbors in the same biofilm community are dead. They can even benefit from the nutrients released by dead cells. The regrowth occurs when the antimicrobial stress is removed [27]. It is known that bacteria pass antimicrobial genes in plasmids to each other for enzyme inactivation of antimicrobial agents to counter their harmful effects [37]. Therefore, the long-term use of a particular antibiotic may lead to resistant bugs. Biocides are broad-spectrum antimicrobials. It is difficult for a certain microbe to develop resistance. However, when vulnerable microbes are killed, resistant microbes in the environment will step in to fill the niche. Another way for microbes to defend against hazardous chemicals is to perform active transport against diffusion to pump out unwanted toxic substances [37]. These defense mechanisms contribute to the recalcitrance of biofilms toward biocide treatment.

2.2 Corrosive Microbes

2.2.1 Sulfate reducing bacteria (SRB)

More than a hundred years ago, SRB were found to be involved in anaerobic corrosion [4]. SRB are commonly found in many industries. In the oil and gas industry, the harmful activities of SRB causing corrosion and reservoir souring are well accepted [38]. In the petroleum industry, SRB are also a major concern due to their hydrogen sulfide metabolite, which leads to reservoir souring, pitting, and stressed corrosion cracking [39]. SRB are widely spread in oil reservoirs. Crude oil contains hydrocarbon and volatile fatty acids such as propionic and acetic acids that are organic carbon molecules for SRB growth [40]. Sulfate comes from seawater injection, which is widely used in enhanced oil recovery (EOR) by maintaining reservoir pressure [41]. In oil pipelines, SRB can come from oil reservoirs. Moreover, SRB can be introduced by hydrotesting using contaminated seawater [42]. Hydrotesting is used to check the mechanical strength and integrity of pipelines before they are commissioned. Lake water, seawater, and produced water are usually utilized in hydrotesting. These water sources could bring microorganisms as well as nutrients. Hydrotest itself may last for only a few hours or a day, but the pipeline is usually shut-in to wait for other installations to be ready. During the extended shut-in time, which can last for months, SRB can grow in the pipeline.

The normal respiration of SRB is usually a reduction of sulfate (electron acceptor) combined with an oxidation of a carbon source (electron donor) [43]. Sulfate is reduced to form bisulfide. Some SRB can also reduce nitrite, nitrate, and elemental sulfur [43].

Lactate is a common carbon source for SRB growth. The oxidization of lactate is shown in Reaction (1), and the reduction of sulfate in Reaction (2) [43].

$$CH_3CHOHCOO^- + H_2O \rightarrow CH_3COO^- + CO_2 + 4H^+ + 4e^- \qquad E^{o'} = -430 \text{ mV} \qquad (1)$$

$$SO_4^{2-} + 9H^+ + 8e^- \rightarrow HS^- + 4H_2O \qquad E^{o'} = -217 \text{ mV} \qquad (2)$$

The redox potential (also known as reduction potential) ($E^{o'}$) is often calculated at modified standard conditions. The standard conditions are 1 M of each substance (1 bar gas) and 25°C, which are denoted by superscript o. Apostrophe in E denotes pH 7 because 1 M $[H^+]$ (pH 0) is too extreme for biological systems. The cell potential ($\Delta E^{o'}$) of the redox reaction coupling Reactions (1) and (2) is 213 mV (–217 mV – (–430 mV)) at the modified standard conditions. The corresponding Gibbs free energy change ($\Delta G^{o'}$) can be calculated in equation below,

$$\Delta G^{o'} = -zF\Delta E^{o'} \qquad (3)$$

where z is the number of electrons in the redox reaction (z = 8 here), F the Faraday's constant (96.4 kJ mol^{-1} $volt^{-1}$), and $\Delta E^{o'}$ the change in redox potential. It yields $\Delta G^{o'}$ = −164 kJ/mol sulfate, which is thermodynamically favorable. Pyruvate, formate, and methanol can be potentially used as carbon sources by SRB in their respiration [44]. SRB in a mixed-culture community are often found to be the main cause of MIC because SRB dwell at the bottom of a biofilm right on a metal surface.

2.2.2 Nitrate reducing bacteria (NRB)

Nitrate is sometimes injected into oil reservoirs to increase NRB growth that can compete with SRB growth to suppress biogenic H_2S production, which causes pipeline corrosion and reservoir souring [45,46]. Iron oxidation coupled with nitrate reduction is thermodynamically favorable [47]. *Pseudomonas aeruginosa* and *Bacillus licheniformis*

can grow as NRB using nitrate as electron acceptor under anaerobic condition for their respiration. Nitrate reduction requires biocatalysis. A wide-type *P. aeruginosa* biofilm anaerobically grown on 304 stainless steel caused pitting corrosion during a 14-day incubation period [48]. It was found that a *B. licheniformis* biofilm grown on carbon steel during a 7-day lab test caused more corrosion than a pure-strain SRB biofilm [47]. Thus, nitrate injection in souring mitigation should be operated carefully so that unspent nitrate will not enter pipelines. In soil MIC studies, NRB MIC is significant because agricultural runoff brings nitrate to soil [49].

2.2.3 Acid producing bacteria (APB)

An acidic environment can be present underneath APB biofilms due to secreted organic acids that can cause MIC [50]. Iron oxidation coupled with proton reduction is thermodynamically favorable. Unlike sulfate or nitrate reduction, proton reduction does not need biocatalysis [51]. Organic acids produced by planktonic cells suspended in the bulk fluid can help maintain a low pH environment. The pH underneath an APB biofilm can be much lower than that in the bulk fluid. This is because the volumetric density of sessile cells in the APB biofilm is much higher than the density of planktonic cells in the bulk fluid [51]. Organic acid attack is far more corrosive than strong acids at the same pH. This is because organic acids are weak acids. Undissociated organic acids serve as a reservoir to release more protons [52]. A low pH environment can also prevent or damage the formation of passivation films such as a siderite film in CO_2 corrosion [53].

2.2.4 Archaea

Archaea have been found to be abundant in nature in recent decades [54]. Similar to bacteria, there is no membrane-bound nucleus or organelles in archaea [55]. One

difference between archaea and bacteria is that archaea do not have peptidoglycans in cell walls [56]. Some archaea can be sulfate or nitrate reducers [57,58]. Some archaea are methanogens [59]. Some archaea can live in extreme conditions with very high temperatures and pressures [60]. Thermophilic sulfate reducing archaea (SRA) were found abundant in marine hydrothermal systems in many places including Alaskan oil reservoirs and North Sea [61,62]. SRA utilize sulfate as electron acceptor during their respiration. Therefore, SRA can be corrosive just like SRB.

2.3 MIC Mechanisms

2.3.1 Bioenergetics of MIC

Microbes require electron acceptor and electron donor to generate energy for their metabolism [24]. In 2009, a theory called biocatalytic cathodic sulfate reduction (BCSR) for MIC due to SRB was proposed by Gu et al. [63]. This theory applied bioenergetics to elucidate SRB MIC against carbon steel. In this theory, it is assumed that electrons released by iron oxidation in Reaction (4) are used by sulfate reduction in Reaction (2) to produce energy in SRB. In reality, the concentration of S^{2-} is much smaller than HS^- under physiological pH. Thus S^{2-} should be replaced with HS^- in Reaction (2). The actual cathodic reactions are more complex than Reaction (2). This theory only considers the terminal electron acceptor utilization step. There is no physical cathode in this theory like in CO_2 corrosion which treats the iron surface as both anode and cathode. SRB biofilms serve as biocathodes because the sulfate reduction occurs inside SRB cells. Cross-cell wall electron transport is required because the electrons are released extracellularly by iron oxidation but they are used in sulfate reduction in the SRB

cytoplasm. Reaction (2) occurs at a negligible rate if there is no biocatalysis from biofilms.

$$Fe \rightarrow Fe^{2+} + 2e^{-} \qquad E^{o'} = -447 \text{ mV} \qquad (4)$$

SRB cells can live as planktonic cells in the bulk fluid while sessile cells are embedded in the biofilm. The reduction of sulfate and the oxidation of a carbon source such as the lactate as electron donor provide energy for SRB respiration (Reaction (1) coupled with Reaction (2)). The cell potential of the reaction ($\Delta E^{o'}$) is 213 mV. The corresponding Gibbs free energy change $\Delta G^{o'}$ is −164 kJ/mol sulfate, which is thermodynamically favorable. For iron oxidation coupled with sulfate reduction (Reaction (4) coupled with Reaction (2)), the cell potential of the reaction ($\Delta E^{o'}$) is 230 mV (–217 mV – (–447 mV)), which yields a Gibbs free energy change ($\Delta G^{o'}$) of −178 kJ/mol sulfate. This means that just like lactate, iron can serve as an electron donor for SRB to produce energy via sulfate reduction.

SRB cells can attach to a metal surface to form biofilms. These sessile cells on the metal surface can catalyze sulfate reduction by accepting electrons released from extracellular metal oxidation. This process leads to direct corrosion by SRB. It should be notified that not all sessile cells in a biofilm can directly uptake the electrons from the metal for sulfate reduction. Only those sessile cells on or close to the metal surface cause corrosion [63]. Sessile cells have limited access to the organic carbon because of mass transfer resistance presented by biofilms. SRB sessile cells need to find another electron donor when there is a local shortage of organic carbon in biofilms. In this situation, iron can serve as an energy source as illustrated in Figure 4. Lactate oxidation coupled with sulfate reaction and iron oxidation coupled with sulfate reduction both can produce

energy for SRB. The difference between them is that lactate oxidation occurs in the cytoplasm (normal respiration), while iron oxidation occurs outside the SRB cells. It was found that SRB attacked iron more aggressively under the organic carbon shortage condition [64]. Xu et al. [64] observed that *Desulfovibrio vulgaris* (ATCC 7757) biofilms were firstly grown on C1018 carbon steel in ATCC 1249 medium for 3 days to obtain mature biofilms on the coupons. After switching to fresh media with decreased levels of organic carbon, there were more weight losses and deeper pits despite decreases in sessile cell counts compared with the case with full-strength culture medium after the 3-day pre-growth.

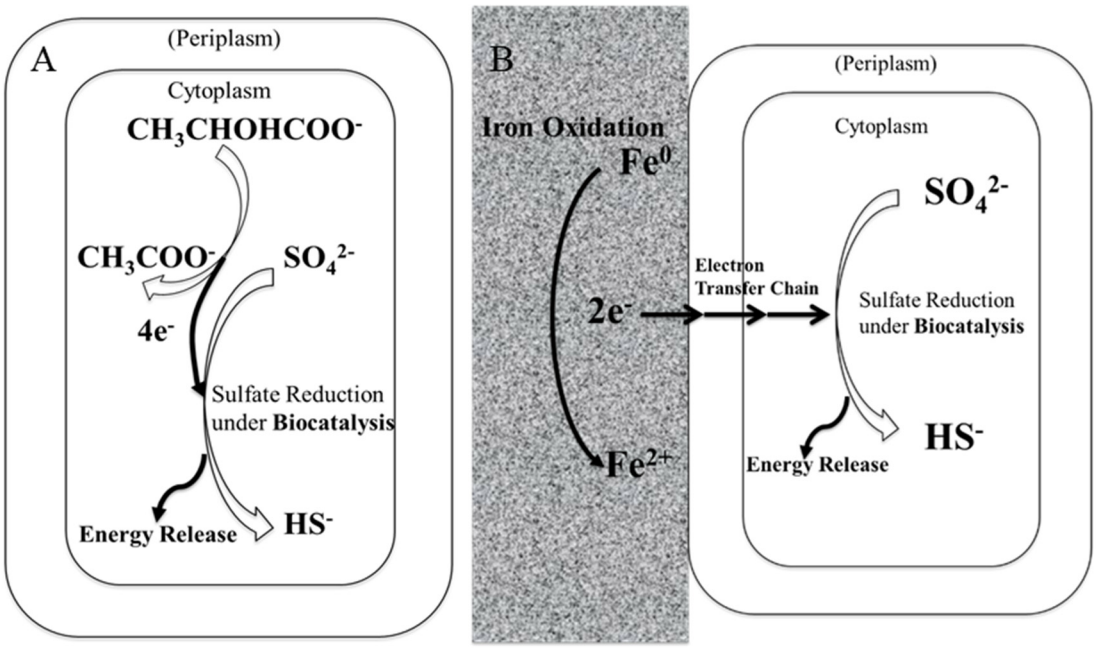

Figure 4. Schematic drawing of SRB respiration using (A) lactate and (B) elemental iron as electron donor [24]. (Reproduced with permission from Elsevier.)

Moreover, BCSR can be expanded to explain MIC caused by other strains, such as NRB. *B. licheniformis* was reported to grow as an NRB at 37°C on C1018 carbon steel coupons for 7 days. The results showed that the coupon weight loss was about 0.89 mg/cm^2 and the largest pit depth found in the C1018 carbon steel was 14.5 μm [47]. Therefore, the BCSR theory could be modified to become biocatalytic cathodic nitrate reduction (BCNR). The anodic reaction in this theory is the same as that in the BCSR theory. The cathodic reactions of nitrate reduction are listed in Reactions (5) and (6) below:

$$2NO_3^- + 10e^- + 12H^+ \rightarrow N_2 + 6H_2O \qquad E^{o'} = +749 \text{ mV} \tag{5}$$

$$NO_3^- + 8e^- + 10H^+ \rightarrow NH_4^+ + 3H_2O \qquad E^{o'} = +358 \text{ mV} \tag{6}$$

The redox potential ($E^{o'}$) in Reactions (5) and (6) are calculated at modified standard conditions. The standard conditions are 1 M of each substance (1 bar gas) and 25°C, which are denoted by superscript o. Apostrophe in E denotes pH 7 because 1 M $[H^+]$ (pH 0) is too extreme for biological systems. The calculated $\Delta E^{o'}$ for Reaction (4) with Reactions (5) and (6) are 1196 mV (749 mV – (–447 mV)) and 805 mV (358 mV – (–447 mV)), respectively. The Gibbs free energy changes ($\Delta G^{o'}$) are −577 kJ/mol nitrate and −621 kJ/mol nitrate, respectively at the modified standard conditions. The negative values show that the coupled reactions are thermodynamically favorable. Thus, MIC by NRB is thermodynamically favorable.

Theories such as BCSR and BCNR are capable of explaining MIC caused by corrosive bacteria (SRB and NRB). The corrosive microbes are collectively called "XRB", in which "X" stands for the non-oxygen oxidant such as sulfate, nitrate/nitrite, or CO_2 and "B" represents bugs such as archaea, bacteria, and eukaryotes [65].

Another important point is why sessile cells on the metal surface, rather than planktonic cells in the bulk fluid are responsible for MIC. This is because electrons released by iron oxidation could not freely "swim" to the cytoplasm of a planktonic cell. A biofilm is required to perform cross-cell wall electron transfer, also known as extracellular electron transfer (EET) [66–68]. Microbes capable of EET are known as electrogens [69]. EET is bidirectional. Extracellular electrons (e.g., from iron oxidation) can move from outside of a cell to the cell's cytoplasm. Electrons from organic carbon oxidation can move from cytoplasm via EET to outside. In microbial fuel cells (MFCs) research, electrogenic microbes are used to generate bioelectricity.

The EET mechanisms for electron transfer between an external solid surface and a cell wall are classified into two categories: direct electron transfer (DET) and mediated electron transfer (MET) as shown in Figure 5. DET requires protein-based cellular structures such as pili or *c*-type cytochromes to contact the iron surface. MET requires redox mediators that are externally added or secreted by bacteria to facilitate the electron transfer [70,71].

Figure 6 shows the carbon steel surface morphology with SRB attachment when there is a shortage of organic carbon in the culture medium. The SRB cells grew pili, which are conductive nanowires to link the cells with the carbon steel surface to harvest electrons [72]. Here, pili are used to transfer electrons from extracellular iron oxidation to SRB cells, which belongs to the DET mechanism. It was found that for this system, when the SRB cells were grown with organic carbon, pili were not formed [72]. This was because organic carbon oxidation in the SRB cytoplasm provided electrons for sulfate reduction. Thus, there was no need for extracellular electrons. This means that EET was

not needed as shown in Fig. 4. Pili can form an electron transfer network to link cells in more than a monolayer [69].

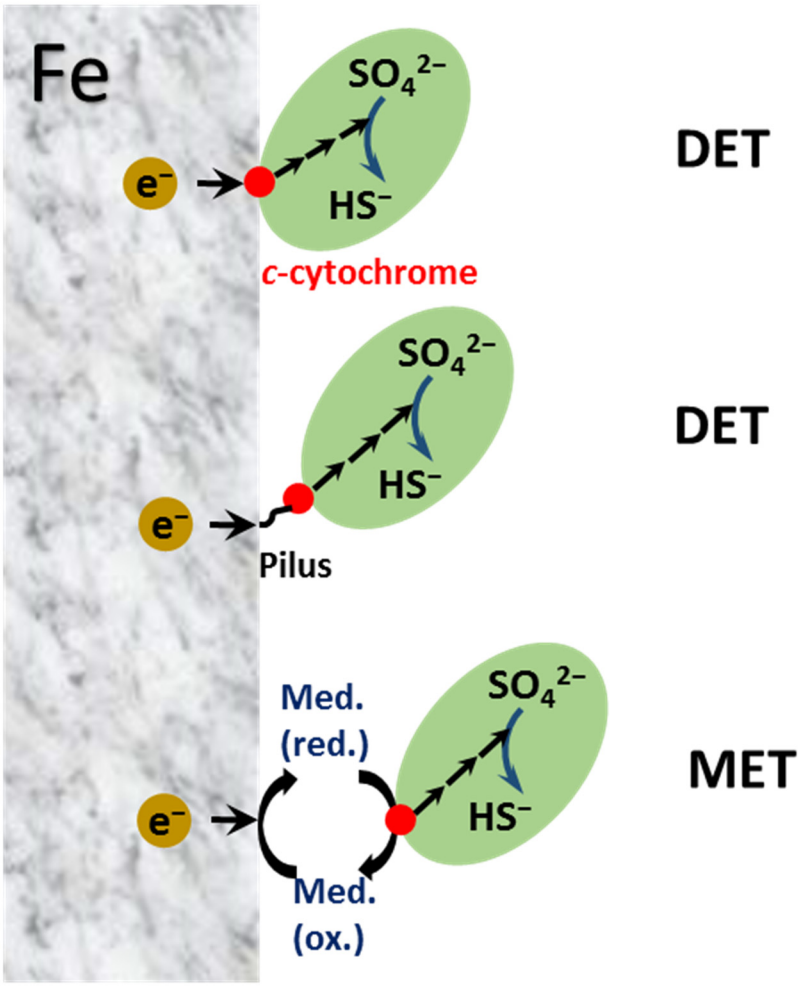

Figure 5. Schematic drawing of DET and MET mechanisms for EET between an iron surface and an SRB cell wall.

MET is another electron transfer method for microbes [65]. *D. vulgaris* (ATCC 7757) biofilms were grown in ATCC 1249 medium supplemented with one of the two common electron mediators (riboflavin and flavin adenine dinucleotide (FAD)) on 304

stainless steel for 7 days. The results showed that both 10 ppm (w/w) led to pitting corrosion and more weight loss because of enhanced electron transfer [73]. In a biofilm consortium, electron mediators can be supplied by some non-corrosive microbes to corrosive microbes to increase energy production for the entire biofilm community [69].

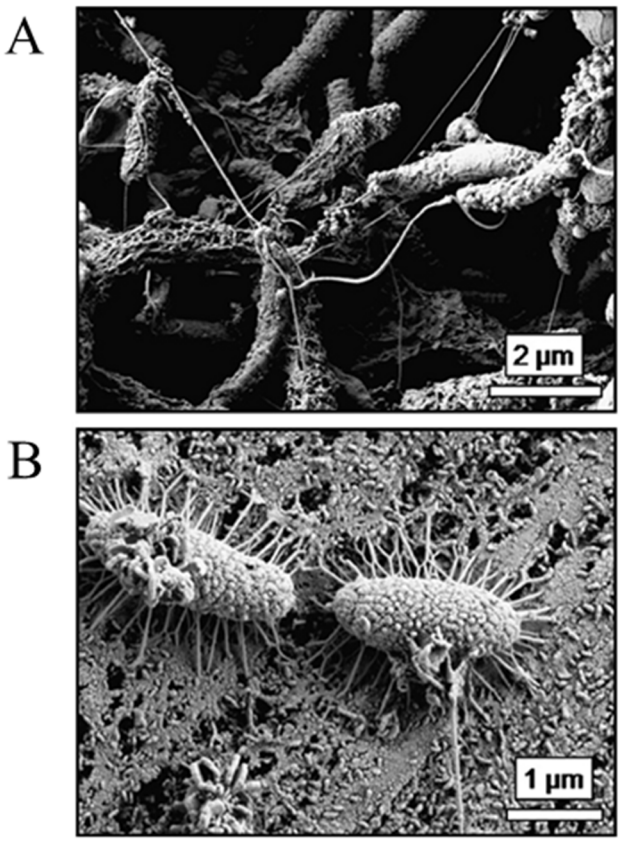

Figure 6. SEM images of SRB cells in a culture medium lacking carbon source: (A) in a colony, and (B) individual cells [72]. (Reproduced with permission from Elsevier.)

2.3.2 Classifications of MIC caused by microbes

It is known that SRB and NRB are corrosive because their respiration can use extracellular electrons from iron oxidation. Some other microbes are also known to be

corrosive, for example, APB. The metabolic products of APB contain organic acids that are corrosive. Their accumulation underneath biofilms can form a locally acidic environment. Biogenic hydrogen sulfide can also cause corrosion because it is a corrosive metabolite.

Different MIC mechanisms can occur for the same microbe if it attacks two different materials. For example, MIC caused by *D. vulgaris* against copper is not due to extracellular electron utilization by SRB respiration [74], but rather due to H_2S. The Gibbs free energy change for the coupled redox reaction of sulfate reduction and copper oxidation is not negative which means it is not thermodynamically favorable [74]. Thus, electron harvest for energy production by *D. vulgaris* cannot happen. Corrosion must be due to another mechanism. It was found that the Reaction (7) is thermodynamically favorable [75]. Therefore, there are more than two different types of anaerobic MIC mechanisms caused by microbes.

$$2Cu_{(crystal)} + HS^- + H^+ \rightarrow Cu_2S_{(crystal)} + H_{2(g)} \qquad \Delta G^{o\prime} = -98.2 \text{ kJ/mol} \qquad (7)$$

MIC caused by anaerobes can be classified into three types. In the first type (Type I), corrosion is due to the respiration by bacteria, which utilize the extracellular electrons from metals for respiration. Bacteria in this type should be capable of EET. They include SRB or NRB [6]. Oxidation of the metal coupled with sulfate or nitrate reduction must be thermodynamically favorable. This means the metal must be "energetic" enough. Note that sulfate and nitrate reductions both require biocatalysis. Sessile cells are needed to perform EET and sulfate or nitrate reduction. Otherwise, sulfate or nitrate reduction reaction rate is negligible. In this type of MIC, cross-cell wall EET is necessary to

transport electrons from outside and the inside of a cell. Thus, Type I MIC is also called EET-MIC [76].

The second type (Type II) of MIC is often caused by fermentative microbes that secrete organic acids in their metabolites. A typical example is APB MIC. H_2S secreted by SRB can also cause Type II MIC. Copper MIC by SRB belongs to this category. Therefore, this type of MIC is called metabolite MIC (M-MIC) [76].

Although in M-MIC, corrosive metabolites are biogenic, their reactions with metal surfaces do not need biocatalysis. APB can secrete organic acids such as volatile fatty acids. They dissociate to release protons. The undissociated weak acids serve as proton reservoirs in a buffering system. Proton reduction does not need biocatalysis. The sulfide corrosion reaction in Reaction (7) does not need biocatalysis either. The pH underneath an APB biofilm can be much lower than that in the bulk fluid because a biofilm has a higher cell density than that in the bulk fluid. It is said that the pH difference could be greater than 2 [77]. It should be noted that M-MIC is also electrochemical corrosion just like EET-MIC. This is because the oxidant reduction and iron oxidation are separable half reactions.

The third type (Type III) of MIC mechanism is known as biodegradation MIC (BD-MIC). Microbes attack organic substances such as polymers or plasticizer molecules in polymers. This biodegradation progress can be considered a corrosion progress when the scope of corrosion is expanded beyond metals. In BD-MIC, enzymes are secreted by microbes to degrade large organic molecules in order to harvest small organic carbon molecules as nutrient molecules [78]. Both aerobic and anaerobic microbes can cause this corrosion.

2.3.3 Mechanistic modeling

The BCSR theory describes the thermodynamics behind EET-MIC by SRB on carbon steel (Reactions (2) and (4)). Therefore, various SRB biofilms can be modeled. The $E^{o\prime}$ value for SO_4^{2-}/HS^- redox couple is −217 mV/SHE and for Fe^{2+}/Fe^0 is −447 mV/SHE at the modified standard conditions (1 M for solutes and 1 bar partial pressure for gases at pH 7.0 and 25°C). The equilibrium potentials can be calculated using the Nernst equation since $E^{o\prime}$ is defined [47] as shown in Equations (8) and (9). The pH term in Equation (9) impacts the equilibrium potential considerably. The reduction reaction occurs in the cytoplasm of SRB cells that are close to the metal surface [64]. An optimal pH was maintained by cells for metabolic activities in the cytoplasm. This pH can be different from the one in the bulk fluid. Slightly acidic pH in some SRB cytoplasm has been reported before [79]. In this work, pH 7 was used.

Fe^{2+}/Fe^0: $$E_e\ (\text{vs. SHE}) = -0.447\ \text{V} + \frac{RT}{2F}\cdot\ln [Fe^{2+}] \quad (8)$$

SO_4^{2-}/HS^-: $$E_e\ (\text{vs. SHE}) = 0.249\ \text{V} - \frac{2.591RT}{F}\text{pH} + \frac{RT}{8F}\cdot\ln\frac{[SO_4^{2-}]}{[HS^-]} \quad (9)$$

Abiotic acetic acid corrosion has been modeled for the oil and gas industry [80]. The net corrosion effect can be considered proton attached with the following proton reduction reaction coupled with iron oxidation,

Proton reduction: $$2H^+ + 2e^- \rightarrow H_2 \quad (10)$$

This proton reduction reaction occurs on a metal surface. The Nernst equation below shows the pH term is essential [50],

$2H^+/H_2$: $$E_e\ (\text{vs. SHE}) = -\frac{2.303RT}{F}\text{pH} + \frac{RT}{2F}\cdot\ln\frac{p_{H_2}}{p^o} \quad (11)$$

In Equation (11), the p^o is set to 1 bar. The hydrogen partial pressure is often set to 1 bar due to a lack of experimental data. Hence, the value of the ln term is zero. Any error is hoped to be calibrated by experimental data [81]. Based on Equation (11), pH 7 and 25°C leads to an equilibrium potential of −414 mV vs. SHE for $2H^+/H_2$, which is close to the $E^{o\prime}$ value for Fe^{2+}/Fe^0. This means the pH needs to be much lower than 7 for the acid attack to be significant.

The equilibrium potentials above showed the thermodynamic driving force of corrosion. Thermodynamics only tells whether the corrosion can occur or not. It does not indicate how fast the corrosion rate will be.

The corrosion rate is determined by mass transfer and kinetics. Both mass transfer resistance and charge transfer resistance should be considered. The charge transfer resistance $1/i_{ct}$ is modeled using the Butler-Volmer equation as shown below [50],

$$\frac{i}{i_0} = \exp\left[\frac{(1-\alpha_c)zF}{RT}(E-E_e)\right] - \exp\left[-\frac{\alpha_c zF}{RT}(E-E_e)\right] \quad (12)$$

in which E is corrosion potential E_{corr}. Gu et al. defined the aggressiveness of an SRB biofilm as the exchange current density ($i_{0(SO_4^{2-})}$) for sulfate reduction [63]. It describes an SRB biofilm's ability to use extracellular electrons for sulfate reduction. The aggressiveness can vary because sessile cell density or enzyme activities vary even for the same biofilm during incubation [50]. SRB pitting data can be applied to calibrate the value used for modeling.

Exchange current densities (i_0) for iron oxidation and proton reduction have been explained in the CO_2 corrosion [81]. The corrosion rate (CR) in mm/year in this 1-D

model can be calculated from the anodic current density of iron oxidation ($i_{a(Fe)}$) in A/m^2 by plugging in the molecular weight (M_{Fe}) and density (ρ_{Fe}) of iron as shown below [50],

$$CR = \frac{M_{Fe} i_{a(Fe)}}{2F\rho_{Fe}} = 1.16 i_{a(Fe)} \tag{13}$$

The anodic current density is equal to the overall cathodic current density contributed by different cathodic reactions such as sulfate reduction and proton reduction as shown below [50],

$$i_{a(Fe)} = i_{c(SO_4^{2-})} + i_{c(H^+)} \tag{14}$$

$i_{a(Fe)}$ is evaluated using Equation (12) without mass transfer resistance. The cathodic current density for sulfate reduction is calculated following the classical electro-kinetics approach similar to that used in mechanistic abiotic CO_2 corrosion modeling [81],

$$\frac{1}{i_{c(SO_4^{2-})}} = \frac{1}{i_{ct(SO_4^{2-})}} + \frac{1}{i_{lim(SO_4^{2-})}} \tag{15}$$

In Equation (15), the two terms on the right hand side are charge transfer resistance and mass transfer resistance. i_{ct} is calculated using Equation (12) for the SO_4^{2-}/HS^- couple.

The i_{lim} is calculated from the Fick's law as shown in Equation (16). $D_{SO_4^{2-}}$ is the diffusivity (m^2 s^{-1}) of sulfate in the biofilm and $C_{SO_4^{2-}}$ is the sulfate concentration (mol m^{-3}) inside the biofilm [51],

$$i_{lim(SO_4^{2-})} = -zFD_{SO_4^{2-}} \cdot \frac{\partial C_{SO_4^{2-}}}{\partial x} \tag{16}$$

Mass transfer becomes considerably significant when an MIC pit becomes deeper. This is because sulfate has a longer distance to travel to the pit bottom. Figure 7 shows an MIC pit covered with an SRB/APB biofilm and an optional film on top. The top film can be an aerobic biofilm or a mineral film. To be simplistic, the top film could be replaced by liquid water for mass transfer purposes.

The SRB biofilm can be treated with a fixed thickness (usually 50 μm as noted in experiments) that moves with the pit increases. Equation (17) describes the transient transport in which R_c is the consumption rate of sulfate by sessile cells in the SRB biofilm [50].

$$\frac{\partial C_{SO_4^{2-}}}{\partial t} = D_{SO_4^{2-}} \cdot \frac{\partial^2 C_{SO_4^{2-}}}{\partial x^2} + R_c \tag{17}$$

Some sulfate is consumed by SRB sessile cells in the biofilm during the diffusion from the bulk-liquid phase to the pit bottom. This shows a negative R_c value. The R_c value can be treated as zero during the modeling. Experimental calibration is hoped to compensate for any error caused by the R_c value.

The cathodic current density for proton reduction is calculated from the following equation [50],

$$\frac{1}{i_{c(H^+)}} = \frac{1}{i_{ct(H^+)}} + \frac{1}{i_{lim(H^+)}} \tag{18}$$

The pit bottom pH is assumed to be fixed or change with time with a given profile. Thus, the mass transfer resistance for proton reduction is not considered. The i_{ct} value is calculated using Equation (12) for the $2H^+/H_2$ couple. The MICORP software covers MIC due to BCSR and proton reduction due to the presence of an APB biofilm [50].

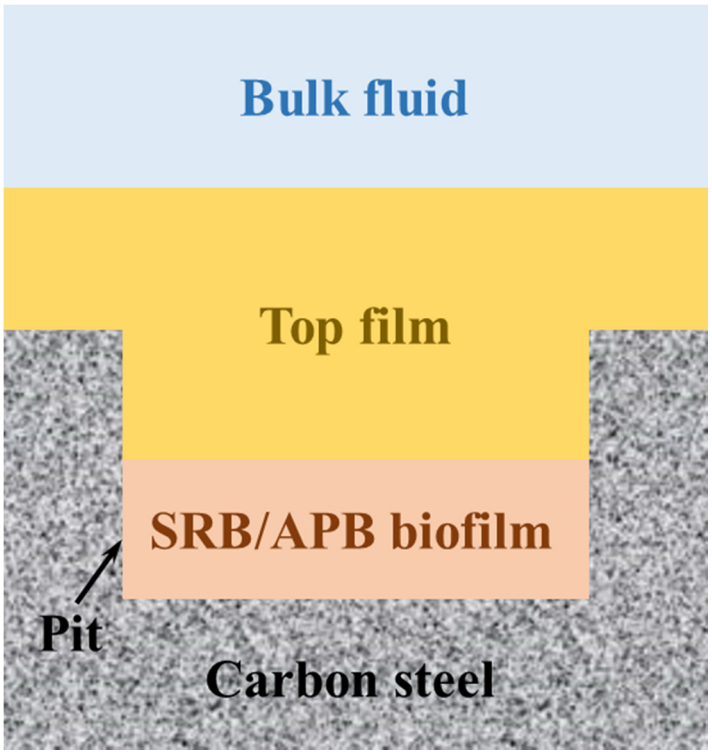

Figure 7. An MIC pit covered with an SRB/APB biofilm and an optional top film. (Redrawn after Xu et al. [50].)

Equation (14) can be solved after plugging in i_a and i_c expressions. Using trial and error, E_{corr} is obtained. Thus $i_{a(Fe)}$ is known, which is the same as i_{corr}. Equation (14) can then be used to calculate CR in this 1-D model.

2.4 Mitigation of Biofilms

2.4.1 Traditional mitigation methods of biofilms

It is obvious that biofilms are responsible for MIC from the discussion above about the relationship between biofilms and MIC mechanisms. Thus, MIC mitigation requires biofilm mitigation. In the industrial field, mechanical cleaning and biocides are traditional ways to mitigate biofilms [26]. Mechanical cleaning can be effective in removing biofilms and corrosion products from metal surfaces. There are various

mechanical cleaning methods such as rubber spheres for heat-exchangers. Pigging is widely used in the oil and gas industry. It is driven by pressurized flow or the built-in electric motor in pipes. A common combination application is to put a biocide solution between two pigs to move the biocide “plug” downstream. A slower pigging speed allows a longer biocide exposure time, but it takes a longer time to complete the operation. Unfortunately, not all pipelines are piggable [82]. For example, some small diameter pipelines are too restrictive to pig because pigs are designed for large diameter pipelines. In addition to small diameters, bends and connections cause pigs to get stuck inside pipelines.

Biocides are usually added to treat biofilms in the industrial field. THPS and glutaraldehyde are commonly used biocides for large-scale applications because they are biodegradable and highly effective against microbes. The disulfide bond in proteins in microbes can be disrupted by THPS. THPS is degraded into trishydroxymethyl phosphine oxide, which is no longer biocidal [83]. Glutaraldehyde is known to be a cross-linking agent, which can cross-link amino acids in cell walls [84]. A high biocide concentration is needed to treat sessile cells in the field due to the protection offered by biofilms to sessile cells. It was reported that sessile cells in biofilms can be 10−1,000 times more resistant to antimicrobial agents than planktonic cells [36]. The use of a particular biocide in the field can promote resistant cells by suppressing weak cells, which leads to increased biocide dosages. High biocide dosages can result discharge problems that cause environmental issues in addition to increased costs.

2.4.2 Biocide enhancers

Since sessile cells in biofilms are more difficult to treat, especially for a biofilm community in the field, a high biocide concentration is required [14]. In the field, a complete eradication is often not practical because flow will introduce microbes and nutrients again. This means a cyclic treatment is needed since biofilms will likely bounce back. The repeated use of a biocide may promote resistant cells. This may lead to higher biocide concentrations over time [85], causing both environmental and economic issues. For large-scale field applications, only a few biocides such as THPS and glutaraldehyde are widely used due to various operational concerns. Thus, it is desirable to enhance current biocides instead of waiting for new blockbuster biocides coming to the market.

Biocide enhancers are applied to enhance biocides by reducing the dosage of biocides. The enhancers do not have to be biocidal. However, they enhance biocides through various mechanisms so that they can reduce the dosage of biocides or make the biocides more effective at the same concentrations. Ethylenediaminetetraacetic acid (EDTA) chelator was reported to be a biocide enhancer to mitigate biofilms [86]. Its sodium salt was used to avoid acidity of the acid form. EDTA is found to accumulate in water systems because it is slowly biodegradable. Ethylenediaminedisuccinate (EDDS) is used to replace EDTA because EDDS is readily biodegradable. It was reported that 2000 ppm EDDS can enhance 30 ppm THPS and 30 ppm glutaraldehyde against planktonic cells of *D. vulgaris* and *Desulfovibrio alaskensis*, respectively [87]. EDDS was also found to enhance glutaraldehyde in SRB biofilm prevention and removal tests [88]. In oil and gas operations, methanol is used as a winterizing agent. The cocktail of 1,000 ppm EDDS, 10% (v/v) methanol and 30 ppm glutaraldehyde achieved excellent efficacies in

inhibiting SRB growth, SRB biofilm establishment, and souring in a 9-day incubation test in 125 mL anaerobic vials [89]. So far, EDDS has not been used in large-scale applications because it is easily consumed by various ions in a liquid and thus high dosage is required.

D-amino acids are natural chemicals in plants, animals and even humans [90]. D-amino acids have been found to be able to disperse biofilms. Kolodkin-Gal et al. found that several D-amino acids, including D-tyrosine (D-tyr), D-methionine (D-met), D-leucine (D-leu), and D-tryptophan (D-trp) can trigger disassembly of *Bacillus subtilis, Staphylococcus aureus*, and *P. aeruginosa* biofilms [91]. It was reported that 6 ppm D-tyr can reduce up to 60% biomass in membrane fouling [92]. Kao et al. found that D-met, D-leu, D-trp did not completely prevent the *P. aeruginosa* biofilm formation [93]. It was possible that a biocidal effect is required for a recalcitrant biofilm to be dispersed by D-amino acids.

D-tyr and D-met were found to enhance 50 ppm THPS and 10 ppm alkyldimethylbenzylammonium chloride (ADBAC) in the *D. vulgaris* biofilm prevention and removal tests [94–96]. D-amino acids also enhanced antibiotics against medical pathogenic biofilms [97,98]. Two ppm D-tyr enhanced 30 ppm ciprofloxacin against the *P. aeruginosa* biofilm by achieving an extra 2-log sessile cell count reduction compared with the 30 ppm ciprofloxacin alone treatment [99]. For industrial biofilm consortia, a mixture of D-amino acids may be required since different microbes may have different responses to D-amino acids. A mixture of D-amino acids (including D-met, D-trp, D-leu and D-tyr) was found to enhance 50 ppm THPS against two recalcitrant oilfield biofilm consortia [100]. The same D-amino acid mixture also enhanced ADBAC and tributyl

tetradecyl phosphonium chloride (TTPC) against a tough field consortium [101,102]. Glutaraldehyde is not compatible with D-amino acids because it is a cross-linking agent that will react with D-amino acids.

The mechanisms of why D-amino acids disperse biofilms are still not fully understood. Several D-amino acid dispersal mechanisms were proposed. For instance, it was proposed that D-amino acids contributed to the remodeling of the cell wall structure [103]. Lam et al. stated that the synthesis of peptidoglycan can be down-regulated by D-amino acids [104]. Peptidoglycan is a strong polymer that serves as a stress-bearing component in bacteria cell walls. Similarly, Kolodkin-Gal et al. thought that D-alanine in the peptidoglycan molecules in bacterial cell walls was replaced by other D-amino acids, while L-amino acids had no effect [91]. There are two types of peptidoglycan molecules shown in Figure 8 in which D-alanine terminus is found [105]. It was confirmed that the addition of 1,000 ppm D-alanine inhibited the efficacy of 100 ppm D-met to enhance 50 ppm THPS against the SRB biofilm [94]. It was speculated that D-alanine in the treatment liquid makes the D-met replacement of the D-alanine terminus in peptidoglycan less likely. In addition to the mechanism of replacement of D-alanine terminals, Leiman et al. proposed that D-amino acids hindered protein synthesis [106]. Thus, well selected D-amino acids will contribute to enhancing biocides against biofilms. In addition to D-amino acids, other green chemicals with low dosages and inexpensive price should also be developed as biocide enhancers.

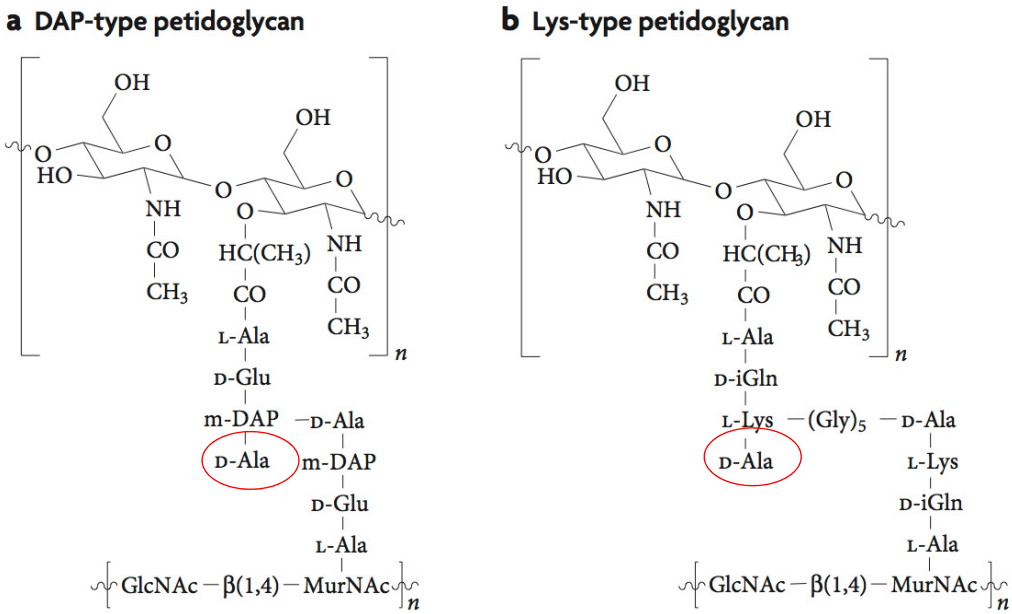

Figure 8. D-alanine terminus is found in two types of peptidoglycan in bacterial cell walls [105]. (Reproduced with permission from Nature.)

2.5 Electrochemical Techniques Applied to MIC

It is desirable to develop effective methods to evaluate electrochemical properties of biofilms on metal surfaces in MIC testing and biocide efficacy assessment [107]. Different non-destructive electrochemical techniques are used to study MIC, including open circuit potential (OCP), polarization resistance (R_p), and electrochemical impedance spectroscopy (EIS) [108]. Potentiodynamic sweep (PDS) are also commonly applied to study MIC with a wide potential range [109], but it can damage surface films. Thus, PDS is typically used only once for biotic working electrode at the end of a test. These techniques are more sensitive than weight loss to measure low corrosion rates in laboratory corrosion tests [107]. They can also be used to corroborate weight loss and

pitting data trends. Unlike one-shot weight loss data in MIC, electrochemical tests (except PDS) can provide transient data.

2.5.1 OCP

OCP has been used by different researchers in biocorrosion systems for many years. Measuring OCP as a function of time is useful to detect the growth of microbes and the initiation of corrosion [107]. It provides a thermodynamic tendency of a sample to lose electrons. A more negative OCP suggests that the working electrode has a higher thermodynamic tendency for corrosion (losing electrons). Thus, it is often seen that when an SRB biofilm covers a working electrode, its OCP shifts in the negative direction [75]. When a working electrode is passivated (e.g., with a coating), its OCP shifts in the positive direction [110]. Note that a more negative OCP does not necessarily result in a higher corrosion rate. The actual corrosion rate also depends on kinetics, which depends on the exchange current density in addition to the potential driving force in the Butler-Volmer equation. Other kinetic electrochemical techniques such as polarization resistance or EIS should be used in addition to OCP to explain corrosion results since corrosion mechanisms are complex in different situations. Sometimes, a more negative OCP is accompanied with lower corrosion rate because the corrosion kinetics is slow which offsets the high thermodynamic tendency for corrosion [111].

2.5.2 Linear polarization resistance (LPR)

LPR is a convenient technique that can continuously measure corrosion rates in near real-time in the field because it is a non-destructive technique. LPR is a simplification of the polarization resistance technique in which it is assumed that in a narrow range the relationship between potential and current is linear. The applied

potential range is usually ±10 mV or ±5 mV to the OCP. It is also a method for fast corrosion analysis to study MIC [112,113]. Polarization resistance (R_p) is defined as the slope of a potential (E) versus current density (i) at OCP. It can be used to measure the instantaneous corrosion rate continuously [108].

The relationship between the corrosion current density (i_{corr}) and R_p is shown below,

$$i_{corr} = \frac{1}{2.3R_p} \cdot \frac{\beta_a \beta_c}{\beta_a + \beta_c} \quad (19)$$

The calculation of corrosion current density requires measurements of R_p and anodic and cathodic Tafel slopes (β_a and β_c) (absolute value of β_c). Equation (19) shows that R_p is inversely proportional to corrosion rate. Polarization resistance techniques have been reported in many MIC studies, especially in recent years [114,115]. It should be noticed that the solution resistance is also included in R_p. Significant errors of corrosion rates can occur in a low conductivity electrolyte without a correction for the solution resistance [108]. Unlike in abiotic CO_2 corrosion in which Tafel slopes are relatively constant, in MIC, Tafel slopes vary greatly even for the same biotic system at different times. Thus, R_p is often not converted into i_{corr} for corrosion rate calculations. Rather, R_p or $1/R_p$ is used qualitative to study corrosion trends.

2.5.3 EIS

EIS is a popular non-destructive technique in corrosion investigations because it provides detailed information on the structures of films on a metal surface. It can be applied to all types of corrosion [116]. It is sensitive and can be used in situ. It can also monitor corrosion processes in electrolytes with low conductivity [117]. An alternating current (AC) potential (5−10 mV in amplitude) is usually applied over a frequency range

between 100 kHz and 10 mHz. Applications of EIS in MIC include corrosion processes monitoring of carbon steel exposed to SRB [118], biocide treatment to sessile cells on carbon steel coupons [119], and the formation of biofilms on stainless steel exposed to natural seawater [120]. Small amplitude signals applied in EIS is one of the advantages in MIC studies [116]. It was reported that repeated uses of EIS analysis did not alter the biofilms and caused no change in the OCP [121], unlike PDS that often shifts OCP [76]. It was also confirmed by Franklin et al. that EIS used to study MIC mechanisms had little or no damage to the activity of sessile cells in biofilms [122]. Nyquist and Bode plots are plotted from EIS spectra. A smaller semi-circle diameter in a Nyquist plot means a lower corrosion resistance, which in turn corresponds to a higher corrosion rate. Equivalent electrical circuits are often used to fit EIS data. A well-fitted model is required to explain the EIS data. The circuit components such as resistance and capacitor (or constant phase element) are matched with physical structures in the film(s) on a metal surface. Because different circuits may fit the same EIS data with good accuracy sometimes, fitted results should be supported by other analyses.

2.5.4 PDS

PDS is a polarization technique, which requires a wide potential range usually from −200 mV to 200 mV, or −300 mV to 300 mV, or negative several hundred millivolts to several volts (relative to stable OCP), depending on the objective of the sweeps. Corrosion current density (i_{corr}), corrosion potential (E_{corr}) and Tafel slopes (β_a and β_c) can be determined in polarization curves by Tafel extrapolation. Numerous researchers have used polarization curves to determine corrosion processes resulted from microbes attached to a metal surface. Li et al. reported that the polarization curve of the *P.*

aeruginosa biofilm in the 2216E medium showed a positive shift in the E_{corr} and an increase in the i_{corr} compared with that in the sterile medium [113]. PDS was reported to study various corrosion inhibitors at different concentrations to inhibit MIC in a CO_2-containing artificial oilfield produced water [123]. A disadvantage of this technique is its destructive nature, which causes irreversible changes to surface films due to the applied high potential range [108]. Therefore, the scan should only be done once on each working electrode. More working electrodes should be prepared if more PDS tests are required. Another caution is that during the cathodic scan, corrosion inhibitor adsorption is artificially enhanced by the imposed voltage, which may lead to erroneous anodic scan behavior. Thus, separate electrodes are recommended for the two scans in corrosion inhibitor studies sometimes.

Chapter 3: Objectives

3.1 Research Objectives

3.1.1 NRB MIC mechanism

Nitrate is often injected to reservoirs in the oil and gas industry to promote NRB growth that can inhibit SRB growth. This leads to biogenic H_2S souring inhibition. However, NRB may cause severe corrosion on carbon steel [47]. A nitrate reducing *P. aeruginosa* biofilm that does not have H_2S complication was evaluated to prove the biocatalytic role of microbes in MIC. An organic carbon starvation test was conducted to confirm the BCNR theory. Electrochemical methods such as LPR and EIS were used to provide transient corrosion data.

3.1.2 MIC caused by a sulfate reducing archaeon *Archaeoglobus fulgidus*

BCSR is capable of explaining MIC caused by corrosive bacteria SRB. However, the theories have not been expanded to cover sulfate reducing archaea due to lack of experimental data. There are lots of data on MIC at mild temperatures such as 37^{o}C. However, in a deep reservoir, much higher temperatures (e.g., 80^{o}C) are encountered. The corrosion caused by an SRA at 80^{o}C was investigated.

3.1.3 Ferrous ion concentration effect on SRB MIC of carbon steel

Ferrous ion (Fe^{2+}) concentration was found to be an important parameter in SRB growth and MIC of carbon steel by SRB. The impacts of Fe^{2+} on SRB MIC of carbon steel are complex and often confusing. It is also extremely important to have a good understanding due to the importance of SRB MIC. It warrants further studies. A causal-relationship experiment was designed to prove a hypothesis that the Fe^{2+} acceleration of

SRB MIC of carbon steel is primarily attributed to reduced H_2S toxicity that leads to a higher sessile cell count, rather than an elevated $[H_2S]$ during incubation.

3.1.4 Accelerated MIC due to microbial growth promotion by an EOR polymer and its mitigation

Seawater is usually injected with some additives such as polymers in EOR. The polymers increase the viscosity of injection water that is needed the push out viscous crude oil. However, seawater brings in nutrients and microbes downhole. Sulfate combined with other nutrients in the seawater result in biogenic souring and MIC pitting against the downhole tubing. EOR polymers may be utilized by microbes as an organic carbon source. This promotes microbial growth downhole. EOR polymers need to be tested to see whether it could be utilized by microbes.

Periodical biocide dosing is often used to mitigate souring and MIC. Unfortunately, prolonged biocide dosing leads to biocide resistance by microbes, which leads to escalated biocide dosage over time. D-amino acids can be used as biocide enhancers. The enhanced biocide application should be compatible with other EOR chemicals such as polymers, surfactants, corrosion inhibitors, and scale inhibitors.

3.1.5 Enhanced biocide treatment against corrosive biofilms using a nature-inspired anti-biofilm peptide

Biofilms will form on almost any surface in the marine environment. Sea anemones produce proteins on their surfaces to prevent biofilm adhesion. This observation inspired the finding of an anti-biofilm peptide (labeled as Peptide A) used in this work. The efficacy of THPS combined with the low concentration Peptide A was

investigated against a tough oilfield biofilm consortium. Electrochemical techniques were applied to help assess the biocide treatment outcome.

3.2 Hypotheses

- Accelerated carbon steel corrosion by nitrate reducing *P. aeruginosa* biofilm under carbon source starvation can be demonstrated from increased weight loss and pit depth data, which can be corroborated by electrochemical data. (Such data will support the electron utilization theory for EET-MIC. This NRB system does not have the complication of H_2S.)
- SRA can cause considerable corrosion on carbon steel at high temperatures. (Accelerated SRA corrosion of carbon steel under carbon source starvation will expand that EET-MIC mechanism from SRB to SRA.)
- A higher Fe^{2+} concentration in the culture medium can counter the toxic effects of H_2S to promote SRB planktonic and sessile cell growth with increased dissolved $[H_2S]$. (A previous work [76] already demonstrated that lower $[H_2S]$ due to H_2S escape to a larger headspace led to accelerated corrosion because of better sessile cell growth. The combination of this with the Fe^{2+} work provides conclusive evidence that H_2S is not the primary contributing factor in carbon steel MIC by SRB because in these two accelerated corrosion cases, dissolved $[H_2S]$ trends were opposite.)
- Large organic molecules such as EOR polymers can be utilized by field microbes as an organic carbon source, which leads to better growth and accelerates carbon steel corrosion. (Data from this can help the selection of EOR polymers and decision for biocide treatment.)

- THPS and D-amino acids as an enhanced biocide system is compatible with other EOR chemicals. (This makes oilfield single-batch chemical treatment possible.)
- The anti-biofilm peptide A inspired by nature is a biocide enhancer for biofilm treatment and MIC mitigation at a very low concentration (ppb level). (This will be a new biocide enhancer system.)

Chapter 4: Electrochemical Analyses of MIC Caused by Nitrate-reducing *P. aeruginosa* Biofilm on C1018 Carbon Steel

4.1 Introduction

The BCSR theory, which is based on SRB bioenergetics, was proposed to explain the SRB MIC. A pre-established SRB biofilm was shown to be more corrosive under organic carbon starvation [64]. Because iron oxidation coupled with nitrate reduction is thermodynamically favorable (i.e., energy releasing), the BCSR theory has been expanded to BCNR for NRB corrosion as shown in Section 2.3.1.

Nitrate is sometimes injected into oil reservoirs to increase NRB growth that can compete with SRB growth to suppress biogenic H_2S production which causes pipeline corrosion and reservoir souring [45]. NRB can also cause severe corrosion on carbon steel. It was found a nitrate reducing *B. licheniformis* biofilm was more corrosive than a sulfate reducing *D. vulgaris* biofilm on C1018 carbon steel [47]. Thus, it is necessary to investigate the NRB MIC mechanism further by studying a different NRB species.

Pseudomonas species are widely distributed in nature [99]. They are facultative bacteria. They can use nitrate as electron acceptor for anaerobic respiration. It is important to show that a pre-established NRB biofilm will switch from organic carbon to Fe(0) as electron donor under organic carbon starvation. This will explain when and why NRB MIC happens. Yang found that the pre-grown *P. aeruginosa* (PA) biofilms became more corrosive under organic carbon starvation with weight loss data and SEM pitting images [124]. These methods require cumulative time to observe the starvation effect. In comparison, electrochemical methods such as LPR and EIS can provide transient corrosion data. Thus, it is beneficial to study carbon steel corrosion by nitrate reducing

PA using electrochemical methods. The data presented in this chapter have been published in Corrosion Science [125]. Copyright permissions for the tables and figures used in this chapter have been obtained from Elsevier.

4.2 Materials and Methods

A wild-type PA from Professor Daniel J. Hassett of University of Cincinnati was used in this work. The bacterium was anaerobically cultured in a modified Luria-Bertani (LB) medium supplemented with KNO_3 (LB-NO_3 medium). The culture medium composition was listed in Table 1. C1018 carbon steel coupons were used. Detailed information about coupon preparation, chemicals used in this work, sterilization, and deoxygenation are described in Appendix A. L-cysteine at 100 ppm (w/w) was added to culture medium as an oxygen scavenger after filtered nitrogen sparging.

In each 125 mL anaerobic vial, 5 coupons, 100 mL de-oxygenated medium (with 100 ppm L-cysteine) and 2 mL PA seed culture were added. The initial planktonic cell amount was about 10^5−10^6 cells/mL. The initial pH values in the medium were 7.0. Biofilms first grew on the coupon surface for 2 days to achieve maturity. Then, the medium in the vial was pipetted out. The coupon in the vial was rinsed with a pH 7.4 phosphate buffered saline (PBS) solution for 3 times. After that, fresh media containing different amounts of organic carbon were poured into the anaerobic vials containing pre-grown biofilms on coupons. Only tryptone and yeast exact in the medium were adjusted to achieve different carbon levels with 100% being the levels in the full-strength LB-NO_3 medium. Different carbon source strengths are shown in Table 1. After refilling, all vials were sealed again in the anaerobic chamber and then incubated at 37^{o}C for additional 7 days.

Table 1. Test matrix for *P. aeruginosa* starvation test

Parameter	Condition
P. aeruginosa	PAO1 strain
Temperature	37°C
Culture medium with 100% carbon source	Tryptone 10 g Yeast extract 5 g NaCl 5 g KNO_3 10 g Deionized water 1,000 mL
Oxygen scavenger	100 ppm L-cysteine
Carbon source strengths	0% carbon source reduction (control) 90% carbon source reduction 100% carbon source reduction
Initial pH (adjusted with NaOH)	7.0 ± 0.1
Biofilm pre-growth	2 days in 100% carbon source medium
Incubation with different carbon source levels	7 days
Coupon material	C1018 carbon steel

During the 7-day incubation, planktonic cells were enumerated every day using a hemocytometer [126]. A set of vials were used for planktonic cell count only. Each time only 0.3 mL was retrieved from each vial using a syringe through the rubber septum of each vial. After the 7-day incubation, coupons were taken out for sessile cell count using the hemocytometer. The biofilm removal from a coupon surface procedure is described in Appendix A. Weight loss and culture medium pH were measured after the 2-day pre-growth and after the additional 7-day incubation. The detailed coupon preparation for weight loss is described in Appendix A. Electrochemical tests including OCP, LPR, EIS, and PDS were performed to monitor the corrosion process during the additional 7-day incubation (i.e., starvation test period). Detailed procedures for electrochemical tests are described in Appendix A.

4.3 Results and Discussion

4.3.1 PA planktonic and sessile cell counts

The planktonic cell counts of samples with different organic carbon reductions during the additional 7-day incubation are shown in Figure 9. For the control (i.e., 0% carbon source reduction), there was an increase in the planktonic cell amount and then decreased on day 4 during the 7-day incubation. The planktonic cell count in the vial with 90% carbon source reduction was lower than that in the vial with 0% carbon source reduction. The lowest planktonic cell count was in the vial with 100% carbon source reduction. The results show that planktonic cell amount depended on the organic carbon amount in the medium as expected.

The average *P. aeruginosa* sessile cell counts after the 2-day pre-growth, and after the 7-day incubation with 0% carbon source reduction, 90% carbon source reduction, and 100% carbon source reduction are 1.1×10^9 cells/cm^2, 2.9×10^8 cells/cm^2, 2.1×10^8 cells/cm^2, and 1.6×10^8 cells/cm^2, respectively as shown in Figure 10. The average sessile cell count was a combination of newly obtained data and previously pubilshed data from Yang [124]. It should be noted that dead cells and exopolymers in biofilms can be used as nutrients by starving cells [27]. Thus, for the 100% carbon source reduction, sessile cells did not suffer from a complete lack of organic carbon.

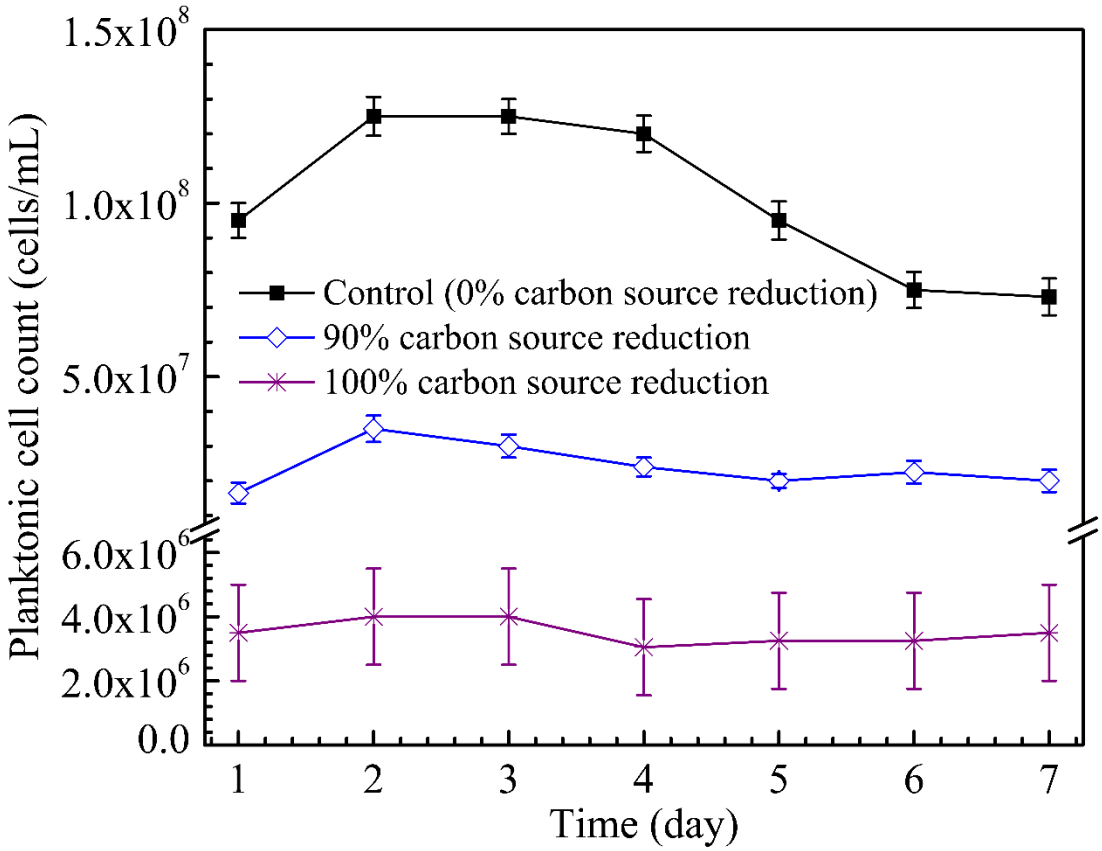

Figure 9. Planktonic cell counts in vials with different organic carbon reductions during the 7-day incubation (following a 2-day pre-growth period). (The standard deviation calculated from 4 independent samples from 4 different vials in 4 different experimental batches.)

4.3.2 PA starvation test weight loss

Figure 11 shows the weight loss data after the 2-day pre-growth and after the additional 7-day incubation with different organic carbon reductions. After the 2-day pre-growth, the average carbon steel weight loss was 1.2 mg/cm^2. The average weight losses after the additional 7-day incubation with 0% carbon source reduction, 90% carbon source reduction, and 100% carbon source reduction were 2.6 mg/cm^2, 3.4 mg/cm^2, and

4.4 mg/cm^2, respectively. The weight losses for the 90% carbon source reduction and 100% carbon source reduction were significantly different from the 0% carbon source reduction ($p = 0.01$, $p < 0.01$, respectively). Thus, the net weight losses during the 7-day starvation test were 1.4 mg/cm^2, 2.2 mg/cm^2, and 3.2 mg/cm^2, respectively after subtracting the weight loss (1.2 mg/cm^2) that occurred during the 2-day pre-growth period. The average weight loss data were a combination of newly obtained data and previously pubilshed data from Yang [124]. These weight loss data are consistent with those obtained by Yang [124]. It is clear that more carbon source reduction leads to more corrosion. The coupon weight loss in the vial with 100% carbon source reduction condition was 2.3 times compared with that in the control vial (0% carbon source reduction). This happened despite Figure 10 showing that the sessile cell count on the coupon incubated with 100% carbon source reduction lost 45% compared with that in the control vial. This showed that with a shortage of organic carbon in the medium, sessile cells switched from organic carbon to elemental iron as electron donor to harvest energy to maintain their survival, leading to accelerated carbon steel weight loss despite a loss in sessile cell count.

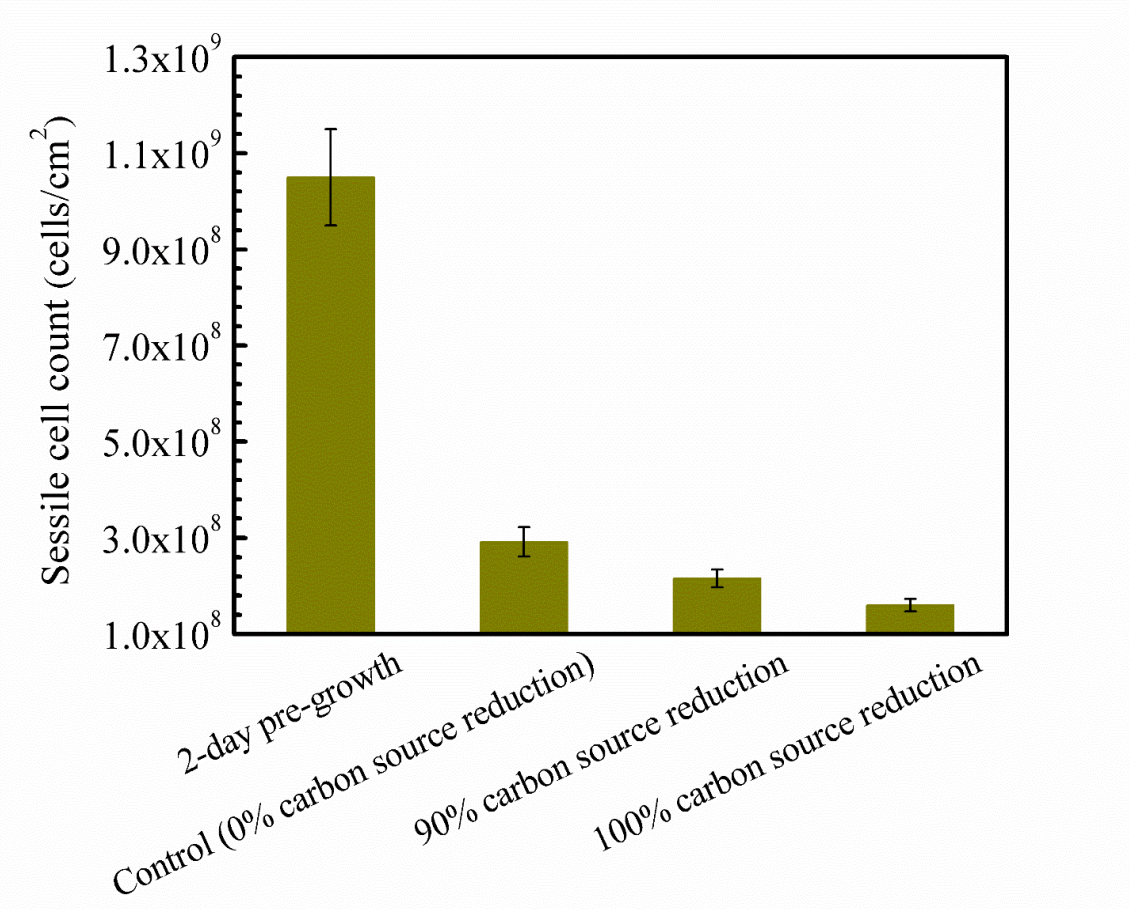

Figure 10. Sessile cell counts with different organic carbon reductions after the 7-day incubation (following a 2-day pre-growth period). (The standard deviation calculated from 4 independent samples from 4 different vials in 4 different experimental batches.)

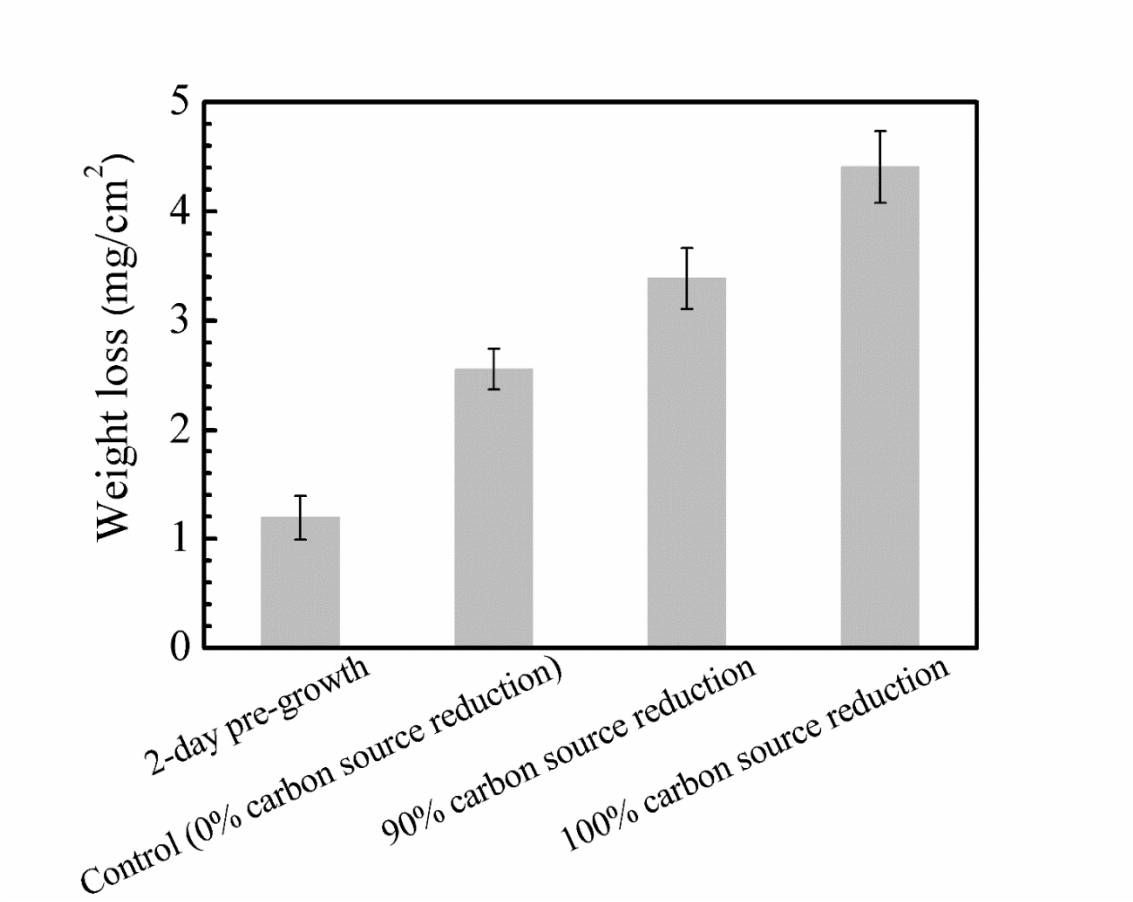

Figure 11. Weight loss data after the 2-day pre-growth and after additional 7-day incubation with different organic carbon reductions. (The standard deviation calculated from 9 independent samples from 3 different vials in 3 different experimental batches.)

The culture medium pH after the 2-day pre-growth and after the additional 7-day incubation with different organic carbon reductions are all above 8.5 as shown in Figure 12. The average pH value was a combination of newly obtained data and previously pubilshed data from Yang [124]. This indicates that PA is not an APB. Acid corrosion could not be a contributing factor in corrosion in this work.

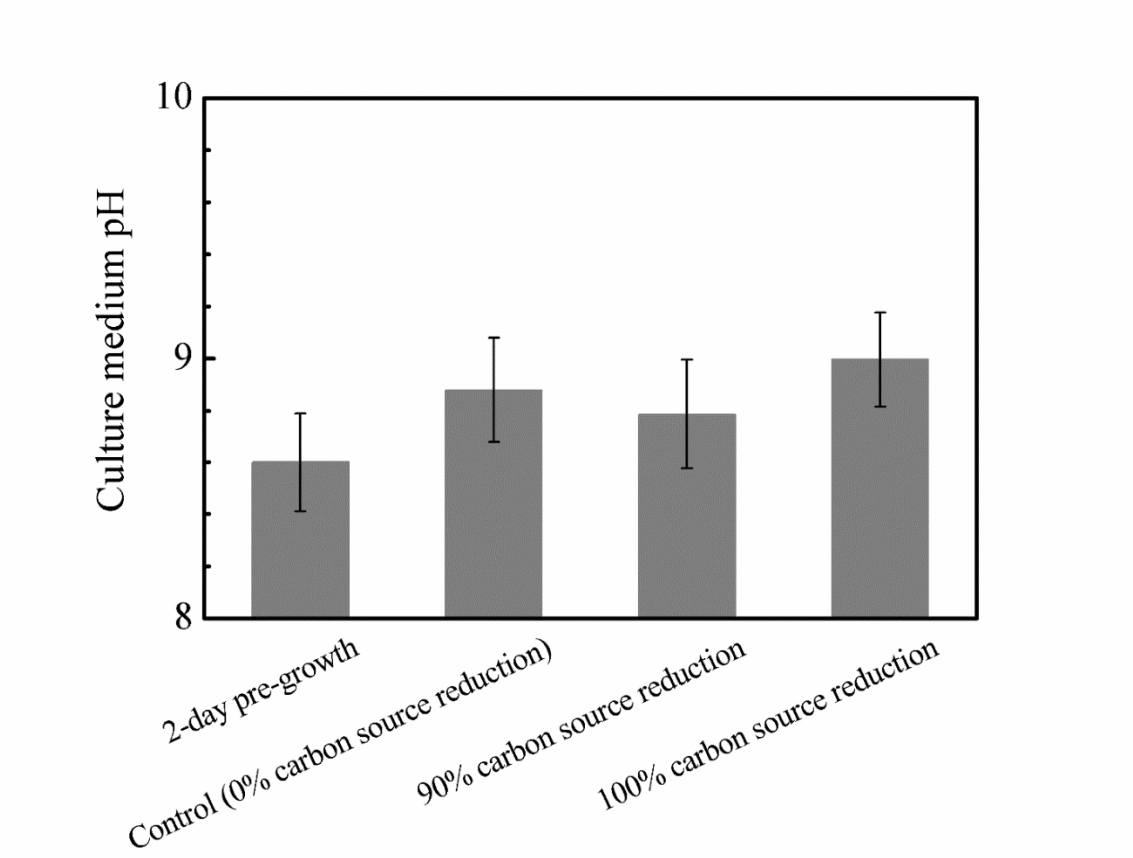

Figure 12. pH values of culture medium after the 2-day pre-growth and after additional 7-day incubation with different organic carbon reductions (initial pH before 2-day pre-growth 7.0). (The standard deviation calculated from 4 independent samples from 4 different vials in 4 different experimental batches.)

In the SRB MIC starvation test, SRB sessile cells were also found to switch from organic carbon to elemental iron as electron donor under organic carbon starvation [64]. The finding in NRB MIC starvation (Figure 13) is very helpful to support the starvation test for SRB. This is because in SRB starvation test, the more corrosion could be due to reduced FeS production that may have less passivation. This may complicate the SRB

starvation argument. However, in NRB system, there is no such complication because FeS passivation does not exist.

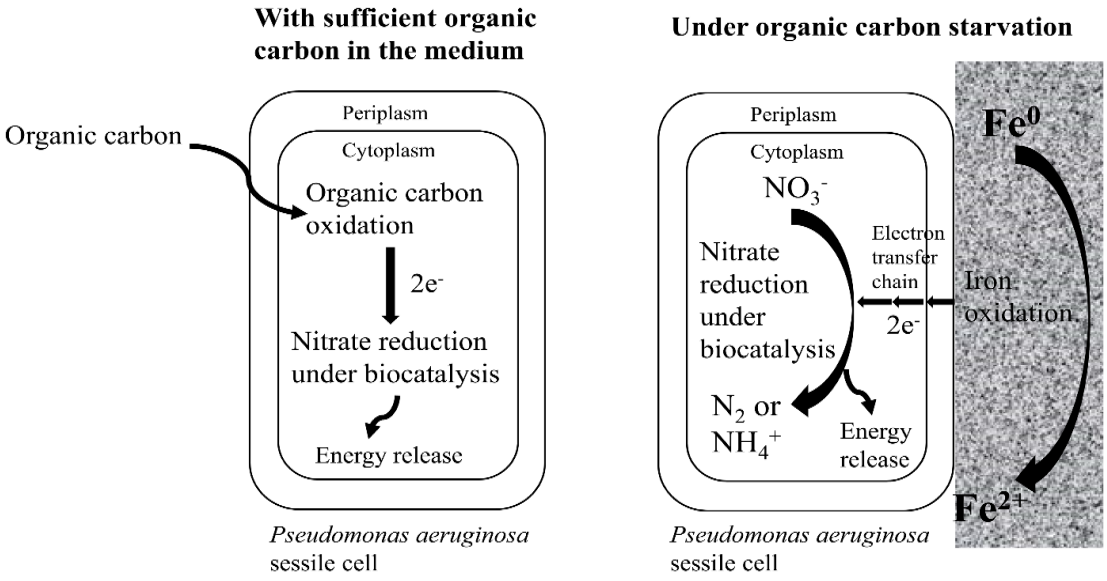

Figure 13. Schematic drawings of *P. aeruginosa* using organic carbon or iron as electron donor for nitrate respiration.

4.3.3 Electrochemical measurements of PA starvation test

Figure 14A shows the OCP of the C1018 electrode versus time during the 7-day incubation with different carbon source reductions. OCP values of the sample with 0% carbon source reduction slightly shifted to the negative direction. OCP values of the sample with 90% carbon source reduction slightly shifted to the positive direction. OCP values of the sample with 100% carbon source reduction kept steady during the 7-day incubation. A more negative OCP suggests a higher thermodynamic tendency for C1018 to lose electrons. Here, OCP results did not show the expected trend (i.e., less organic carbon for more negative OCP). This is not surprising. This is because OCP only

provides a thermodynamic tendency. The actual corrosion rate depends on kinetics. This can be seen from the Butler-Volmer equation in Equation (12) in Section 2.3.3. Current density for charge transfer depends on the exchange current density (analogous to rate constant in chemical reaction) in addition to the thermodynamic driving force (i.e., the potential difference term, $E - E_e$). This is why kinetic electrochemical tests are often needed in addition to OCP data.

Polarization resistance (R_p) versus time during the 7-day incubation with different carbon source reductions following a 2-day pre-growth period in 450 mL electrochemical glass cells filled with 350 mL medium is shown in Figure 14B. All curves shifted to a positive direction during the 7-day incubation indicating an increased corrosion resistance during the incubation period. A lower polarization resistance was observed in the vial with reduced carbon source compared with that incubated in the control medium (full strength), suggesting increased corrosion under starvation. LPR results corroborate weight loss data in Figure 11. This indicates that LPR can be qualitatively used for MIC assessment. EIS was measured on days 1, 4 and 7 during the 7-day incubation with different carbon source reductions. In the Nyquist plots in Figure 15, the working electrodes incubated with reduced levels of carbon source have smaller semi-circle diameters, suggesting more corrosion. EIS data confirm LPR data above suggesting increased corrosion under carbon source starvation.

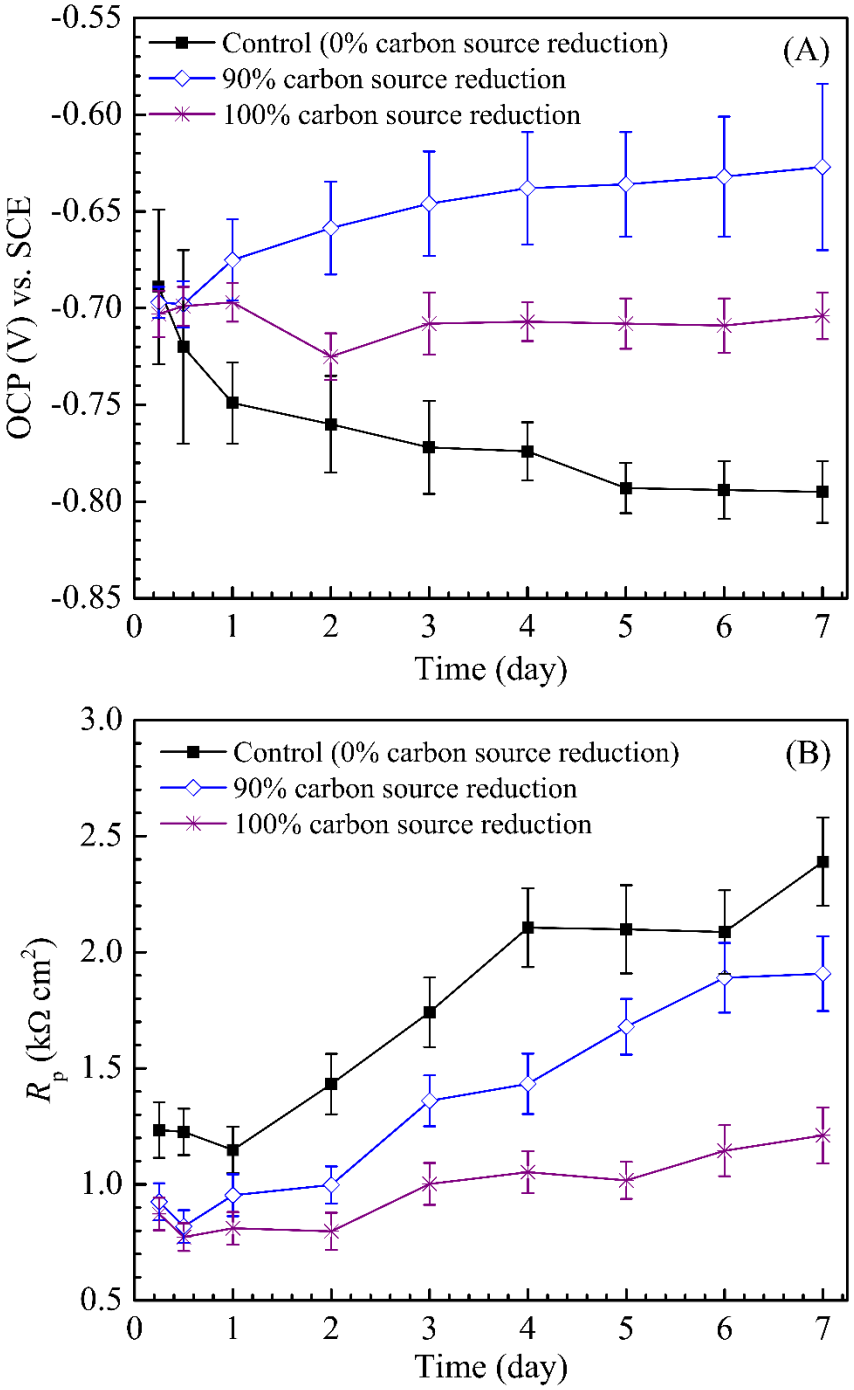

Figure 14. OCP (A) and LPR (B) versus time during the 7-day incubation with different organic carbon reductions following a 2-day pre-growth period in electrochemical glass cells. (The standard deviation calculated from 3 independent samples from 3 different vials in 3 different experimental batches.)

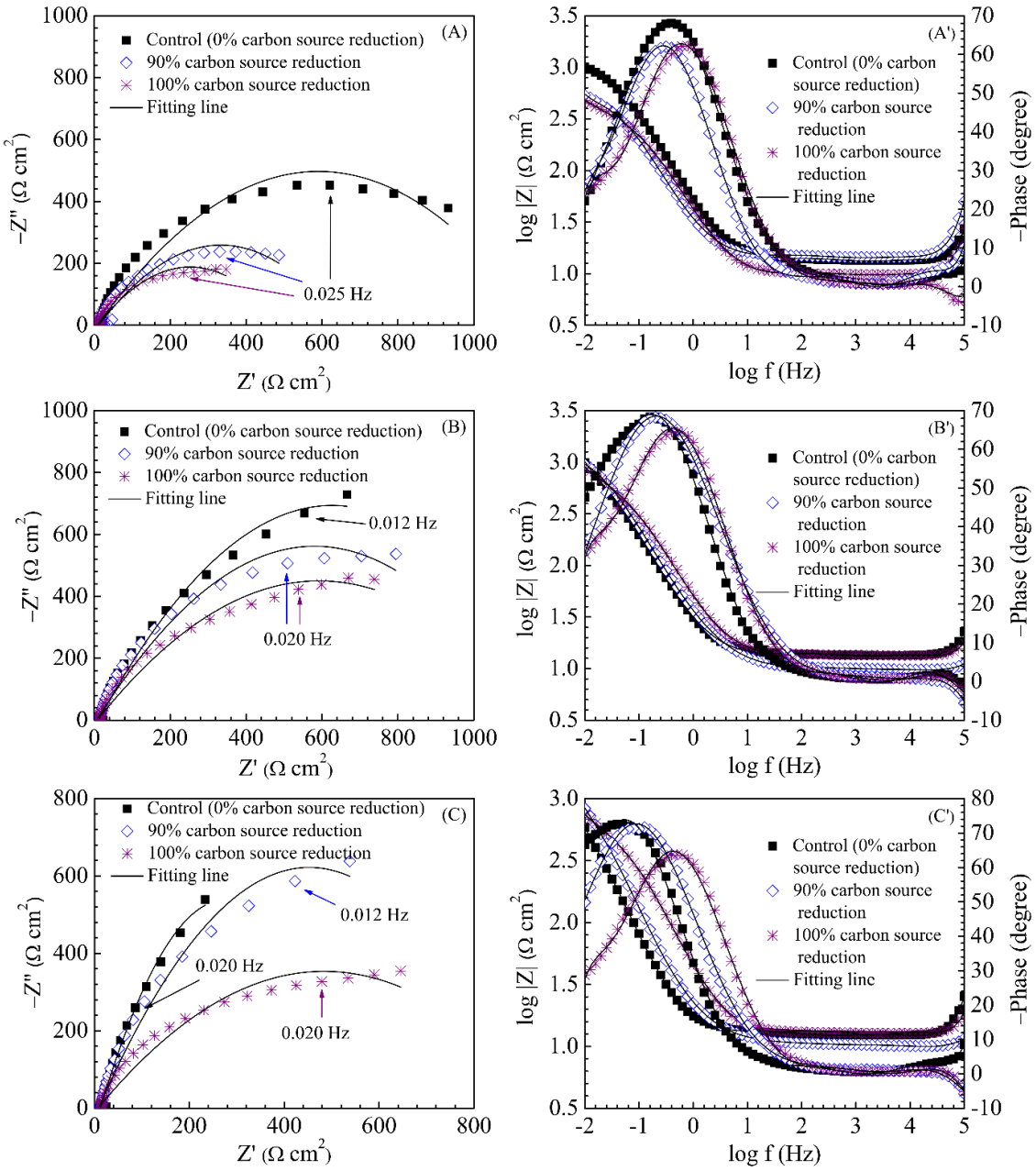

Figure 15. Nyquist and Bode plots for C1018 working electrodes incubated in electrochemical glass cells with different levels of organic carbon source during the additional 7-day incubation on day 1 (A, A′), day 4 (B, B′), and day 7 (C, C′) following a 2-day pre-growth period. (EIS was conducted under stable OCP between 10^{-2} and 10^{5} Hz with a sinusoidal voltage signal (10 mV amplitude).)

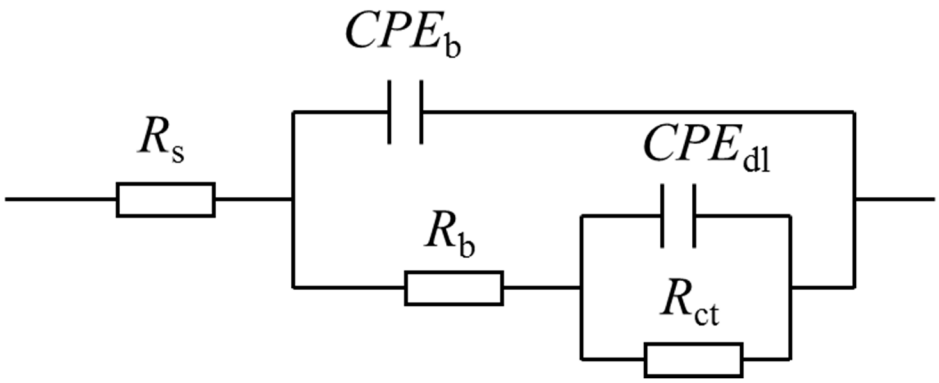

Figure 16. The equivalent circuit used for simulating the EIS data.

A two-time constant model shown in Figure 16 was used to analyze the EIS spectra. The impedance spectra fitted well with this two-time constant model (Figure 15). The electrochemical parameters from the fitting results are shown in Table 2. R_b, R_s, and R_{ct} stand for the resistance of the corrosion product film or the biofilm (or the mixture of the two), the solution resistance, and the charge transfer resistance, respectively. The impedance of constant phase element (CPE) was expressed below,

$$Z_{CPE} = Y_0^{-1}(j\omega)^{-n} \quad (20)$$

In which n and Y_0 are CPE parameters. When n equals to −1, 0 and 1, CPE is a pure inductor, pure resistor and pure capacitor, respectively. When n is 0.5, CPE is Warburg impedance element. ω is the angular frequency (rad/s). CPE_b is the admittance of the corrosion product film or the biofilm. CPE_{dl} is the admittance of the electrical double layer.

Table 2 shows that R_{ct} values are much larger than R_b, suggesting that charge transfer resistance on the metal surface is far more important than mass transfer resistance. Figure 17 shows the variation of $R_b + R_{ct}$ versus time. This combination of film resistance and charge transfer resistance represents corrosion resistance. Thus, its

inverse is proportional to corrosion rate. Figure 17 shows that the corrosion resistance for the working electrode incubated with 0% carbon source reduction was higher than the ones incubated with 90% or 100% organic carbon source reduction. The smallest corrosion resistance went to the working electrode incubated with 100% organic carbon source reduction, indicating most severe corrosion under extreme carbon starvation.

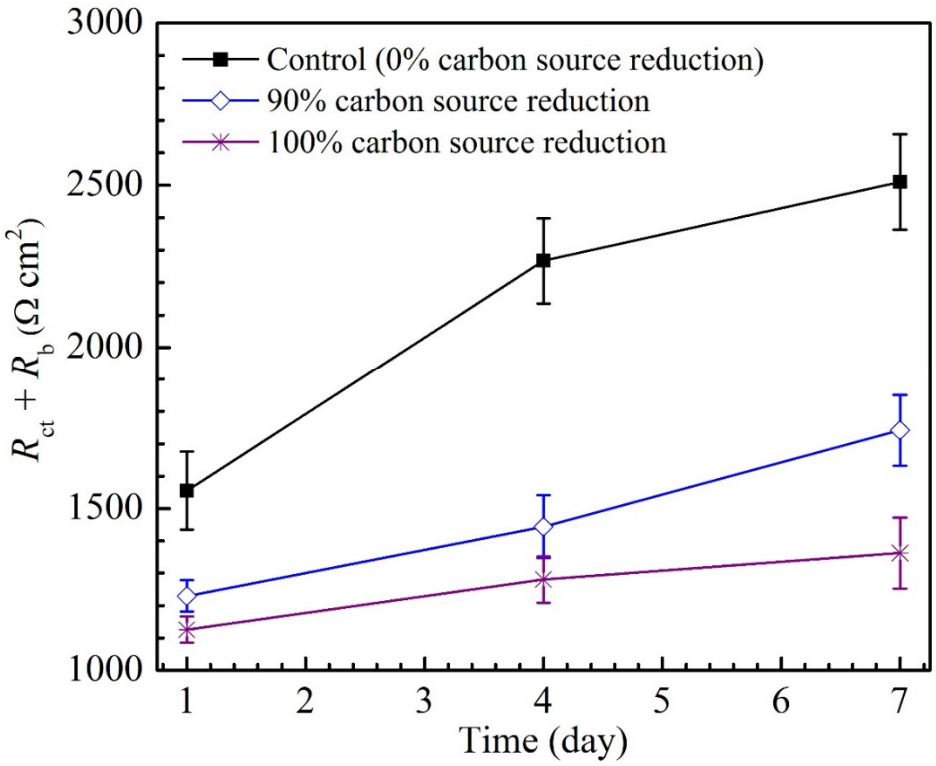

Figure 17. $R_{ct} + R_b$ vs. time during the 7-day incubation with different organic carbon reductions. (The standard deviation calculated from 3 independent samples from 3 different vials in 3 different experimental batches.)

Table 2. Fitted EIS parameters of samples with different organic carbon reductions during the 7-day incubation (The standard deviation calculated from 3 independent samples from 3 different vials in 3 different experimental batches.)

Duration (d)	R_s (Ω cm^2)	Y_b (Ω^{-1} cm^{-2} s^n)	n_b	R_b (Ω cm^2)	Y_{dl} (Ω^{-1} cm^{-2} s^n)	n_{dl}	R_{ct} (Ω cm^2)
Control (0% carbon source reduction)							
1	15 ± 3	0.00232 ± 0.00012	0.93 ± 0.04	56 ± 15	0.00174 ± 0.00052	0.76 ± 0.05	1529 ± 157
4	14 ± 3	0.00732 ± 0.00027	0.89 ± 0.03	75 ± 26	0.00737 ± 0.00156	0.79 ± 0.04	2195 ± 125
7	14 ± 2	0.00951 ± 0.00172	0.96 ± 0.02	41 ± 12	0.00706 ± 0.00124	0.78 ± 0.04	2458 ± 146
90% carbon source reduction							
1	11 ± 3	0.00647 ± 0.00117	0.97 ± 0.02	50 ± 12	0.01097 ± 0.00443	0.74 ± 0.02	1180 ± 37
4	10 ± 1	0.00505 ± 0.00031	0.83 ± 0.05	39 ± 14	0.00127 ± 0.00072	0.93 ± 0.03	1405 ± 105
7	10 ± 2	0.00712 ± 0.00053	0.87 ± 0.03	22 ± 8	0.00458 ± 0.00177	0.92 ± 0.02	1676 ± 96
100% carbon source reduction							
1	12 ± 2	0.00351 ± 0.00028	0.96 ± 0.03	46 ± 10	0.00402 ± 0.00212	0.76 ± 0.06	1090 ± 41
4	14 ± 3	0.00398 ± 0.00102	0.87 ± 0.03	33 ± 12	0.01098 ± 0.00337	0.73 ± 0.04	1248 ± 67
7	13 ± 2	0.00332 ± 0.00107	0.89 ± 0.02	20 ± 6	0.00564 ± 0.00147	0.72 ± 0.02	1343 ± 89

Figure 18 shows PDS conducted at the end of the 7-day incubation for samples incubated with different carbon source reductions. PDS was scanned only once for a single working electrode because a wide range of potential applied in PDS could damage the biofilm. The fitted Tafel parameters are listed in Table 3. The i_{corr} values for the samples incubated with reduced carbon source were higher than that in the medium with 0% carbon source reduction (control). The PDS results are consistent with LPR and EIS measurements.

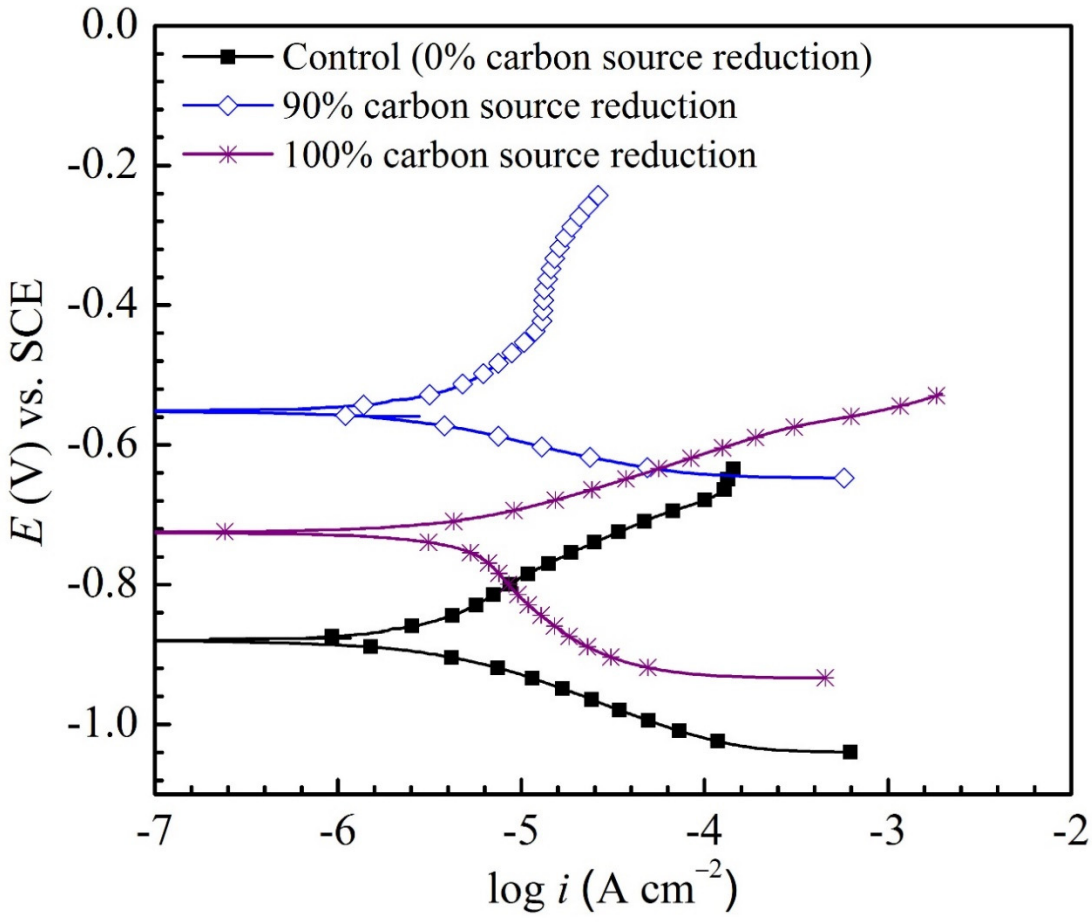

Figure 18. PDS measurements of samples with different organic carbon reductions at the end of the 7-day incubation.

Table 3. Electrochemical parameters fitted from PA starvation PDS (The standard deviation calculated from 3 independent samples from 3 different vials in 3 different experimental batches.)

	i_{corr} ($\mu A/cm^2$)	E_{corr} (V) vs. SCE	β_a (V/dec)	β_c (V/dec)
Control (0% carbon source reduction)	0.38 ± 0.04	−0.86 ± 0.05	0.08 ± 0.02	0.07 ± 0.01
90% carbon source reduction	2.72 ± 0.12	−0.55 ± 0.07	0.29 ± 0.05	0.06 ± 0.02
100% carbon source reduction	3.59 ± 0.23	−0.72 ± 0.03	0.07 ± 0.02	0.19 ± 0.04

4.4 Summary

P. aeruginosa grown as an NRB was corrosive to carbon steel. The carbon source starvation test conducted in this work supported the BCNR theory. It showed that starved sessile cells switched from organic carbon to elemental iron as electron donor, leading to more severe corrosion. The accelerated corrosion happened even though in the starvation progress, planktonic and sessile cell counts dropped. The BCNR corrosion mechanism based on bioenergetics explained when and why NRB MIC happens.

The results measured from electrochemical tests were consistent with the weight loss data obtained by Yang [124]. This indicates that properly conducted electrochemical measurements such as LPR, EIS and PDS are able to assess mechanistic MIC studies. These tests provide transient behaviors that are not shown by weight loss data, which are cumulative data.

Chapter 5: Mechanistic Study of Carbon Steel Biocorrosion at 80°C by A Thermophilic Sulfate Reducing Archaeon Biofilm

5.1 Introduction

Previously, archaea were only considered existing in extreme environments. However, in recent decades they have been found abundant in much more diverse environments in nature [54,127]. Thermophilic SRA were found abundant in marine hydrothermal systems in many places including Alaskan oil reservoirs and North Sea [61,62]. Deaerated seawater is usually injected into reservoirs to increase pressure [128]. Water injection brings nutrients and sulfate downhole that can promote SRB and SRA growth. Like SRB, SRA can utilize sulfate as electron acceptor during their respiration. Therefore, SRA can generate biogenic H_2S that leads to souring in oil wells [57,60]. SRA may also cause corrosion to pipes. Most MIC studies focused on the corrosion caused by bacteria, especially SRB. The investigations of corrosion caused by archaea are limited. The corrosion mechanism of SRA MIC has not been elucidated. This chapter is devoted to the understanding of the mechanism at a reservoir temperature. The experimental data presented in this chapter were obtained by this investigation. They have recently been published in Corrosion Science [129]. Copyright permissions for the tables and figures used in this chapter have been obtained from Elsevier.

5.2 Materials and Methods

SRA used in this work is *Archaeoglobus fulgidus* (ATCC 49558). The thermophilic extremophile was grown at 80°C as recommended by ATCC [62]. It is also a prevailing downhole reservoir temperature. The medium used to culture this archaeon was an enriched artificial seawater medium. The composition of the enriched artificial

seawater medium (g/L) is $NaHCO_3$ 0.192, Na_2SO_4 3.917, $SrCl_2 \cdot 6H_2O$ 0.040, tri-sodium citrate 0.5, KBr 0.096, $CaCl_2 \cdot 2H_2O$ 1.469, yeast extract 1, KCl 0.664, $MgCl_2 \cdot 6H_2O$ 10.610, NaCl 23.476, sodium lactate 3.5, $MgSO_4 \cdot H_2O$ 0.4, NH_4Cl 0.1, H_3BO_3 0.026, $Fe(NH_4)_2(SO_4)_2$ 1, $CaSO_4 \cdot 2H_2O$ 0.1, K_2HPO_4 0.05 [128]. C1018 carbon steel coupons were used. Detailed information about coupon preparation, chemicals used in this work, sterilization, and deoxygenation are described in Appendix A.

In each 125 mL anaerobic vial, 5 coupons, 100 mL medium and 2 mL *A. fulgidus* seed culture were added. The initial planktonic cell amount was about 10^5−10^6 cells/mL. The initial pH values in the medium were 7.0. Biofilms first grew on the coupons for 3 days to achieve maturity. After that, the medium in the vial was pipetted out. The coupon in the vial was rinsed with a pH 7.4 PBS solution for 3 times. After that, fresh media containing different amounts of organic carbon (0% carbon source reduction, 90% carbon source reduction, and 100% carbon source reduction) were transferred to the vials containing pre-grown biofilms on coupons. Only sodium lactate and yeast extract in the full-strength medium were adjusted. Citrate in the ATCC 1249 medium serves as a chelator to make Fe^{2+} more available for SRB enzymes to counter the effect of FeS precipitation. It is not used by *D. vulgaris* as an organic carbon. After refilling, all vials were sealed again in the anaerobic chamber and then incubated in an 80ºC oven for additional 7 days.

During the 7-day incubation for starvation testing, planktonic cells were enumerated every day using a hemocytometer. A set of vials were specifically used for planktonic cell count. Each time only 0.3 mL broth was retrieved from each vial. After the 7-day incubation, coupons were taken out for sessile cell count using the

hemocytometer. The biofilm removal from a coupon surface for sessile cell counting is described in Appendix A. Live and dead cells in biofilms were detected under confocal laser scanning microscopy (CLSM) (LSM 510, Carl Zeiss, Jena, Germany). The detailed cell staining procedure is described in Appendix A.

Weight loss and culture medium pH were measured after the 3-day pre-growth and after the additional 7-day incubation. The detailed coupon preparation for weight loss is described in Appendix A. After biofilms and corrosion products were removed using Clarke's solution, scanning electron microscopy (SEM) (Model JSM-6390, JEOL, Tokyo, Japan) was used to examine pit morphology for coupons incubated in media with different organic carbon levels. Infinite focus microscopy (IFM) (Model ALC13, Alicona Imaging GmbH, Graz, Austria) was used to measure the maximum pit depth. The abiotic control was incubated without any inoculation.

Electrochemical tests in this work were conducted in 500 mL glass bottles filled with 400 mL enriched artificial seawater medium. Biofilms were pre-grown anaerobically for 3 days to achieve maturity and then switched to fresh media with different organic carbon sources to incubate for another 7 days. LPR and PDS were conducted to monitor the corrosion process during the additional 7-day incubation. Detailed procedures are described in Appendix A. The potential range applied in PDS was from −150 mV to +150 mV. A Luggin capillary filled with saturated KCl solution was placed near the working electrode with a Vycor tip. The top side was sealed with silicone. The glass bottles were incubated in an 80^{o}C oven without shaking. During the electrochemical tests, glass bottles were taken out and placed in an 80^{o}C water bath. The reference electrode was then connected with the Luggin capillary after removing the

silicone to start electrochemical measurements [130]. The reference electrode was removed after measurements before the incubation resumed.

5.3 Results and Discussion

5.3.1 SRA cell enumerations, biofilm and corrosion product examination

The planktonic cell counts for different organic carbon source levels during the additional 7-day incubation are shown in Figure 19. For the control (i.e., 0% carbon source reduction), there was an increase in the planktonic cell amount and then kept steady on day 4 during the 7-day incubation. The planktonic cell count in the vial with 90% carbon source reduction was lower than that in the vial with 0% carbon source reduction. It increased during the first 2 days and then decreased during the 7-day incubation. The lowest planktonic cell count was in the vial with 100% carbon source reduction. It continuously decreased during the 7-day incubation. The decrease was due to depleting organic carbon in the medium.

The SRA sessile cell counts after the 3-day pre-growth and after the additional 7-day incubation with different organic carbon levels are shown in Figure 20. The SRA sessile cell count after the 3-day pre-growth was 2.2×10^6 cells/cm^2. The average SRA sessile cell counts after the 7-day incubation with 0% carbon source reduction, 90% carbon source reduction, and 100% carbon source reduction were 4.1×10^6 cells/cm^2, 6.0×10^6 cells/cm^2, and 3.1×10^6 cells/cm^2, respectively. It is interesting to see that the sessile cell count under 90% carbon source reduction was slightly higher than that incubated with biotic control (0% carbon source reduction) ($p = 0.03$). Their differences were not big because microbial growth is often expressed exponentially. It also showed that planktonic cells would like to convert to sessile cells under an organic carbon

starvation condition [125]. The sessile cell count for the biotic control (0% carbon source reduction) was not significantly different from the 100% carbon source reduction ($p = 0.10$). It is known that biofilm formation is a self-preservation approach by microbes [25].

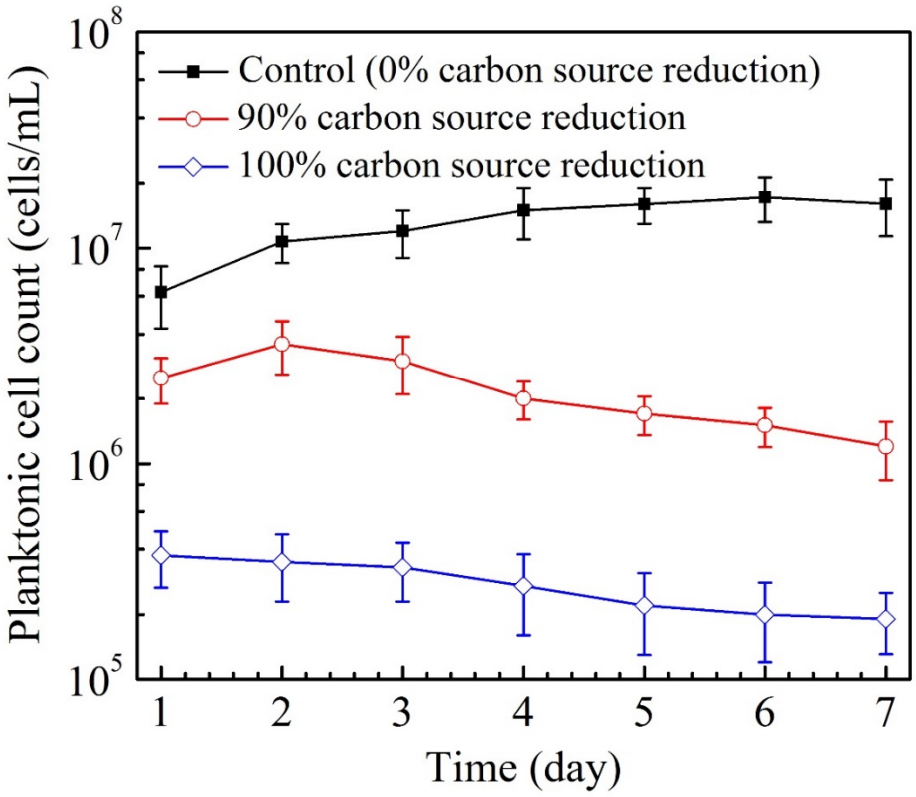

Figure 19. SRA planktonic cell counts incubated with different organic carbon source levels during the additional 7-day incubation. (The standard deviation calculated from 4 independent samples from 4 different vials in 4 different experimental batches.)

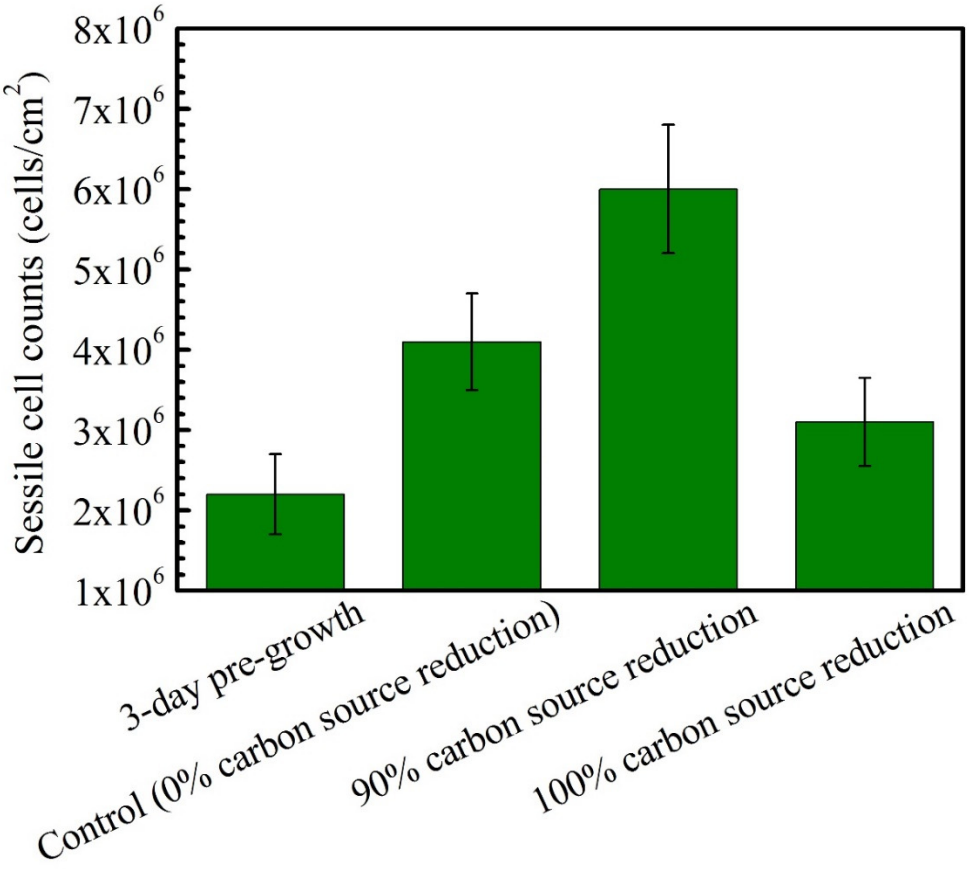

Figure 20. SRA Sessile cell counts incubated with different organic carbon source levels after the additional 7-day incubation. (The standard deviation calculated from 4 independent samples from 4 different vials in 4 different experimental batches.)

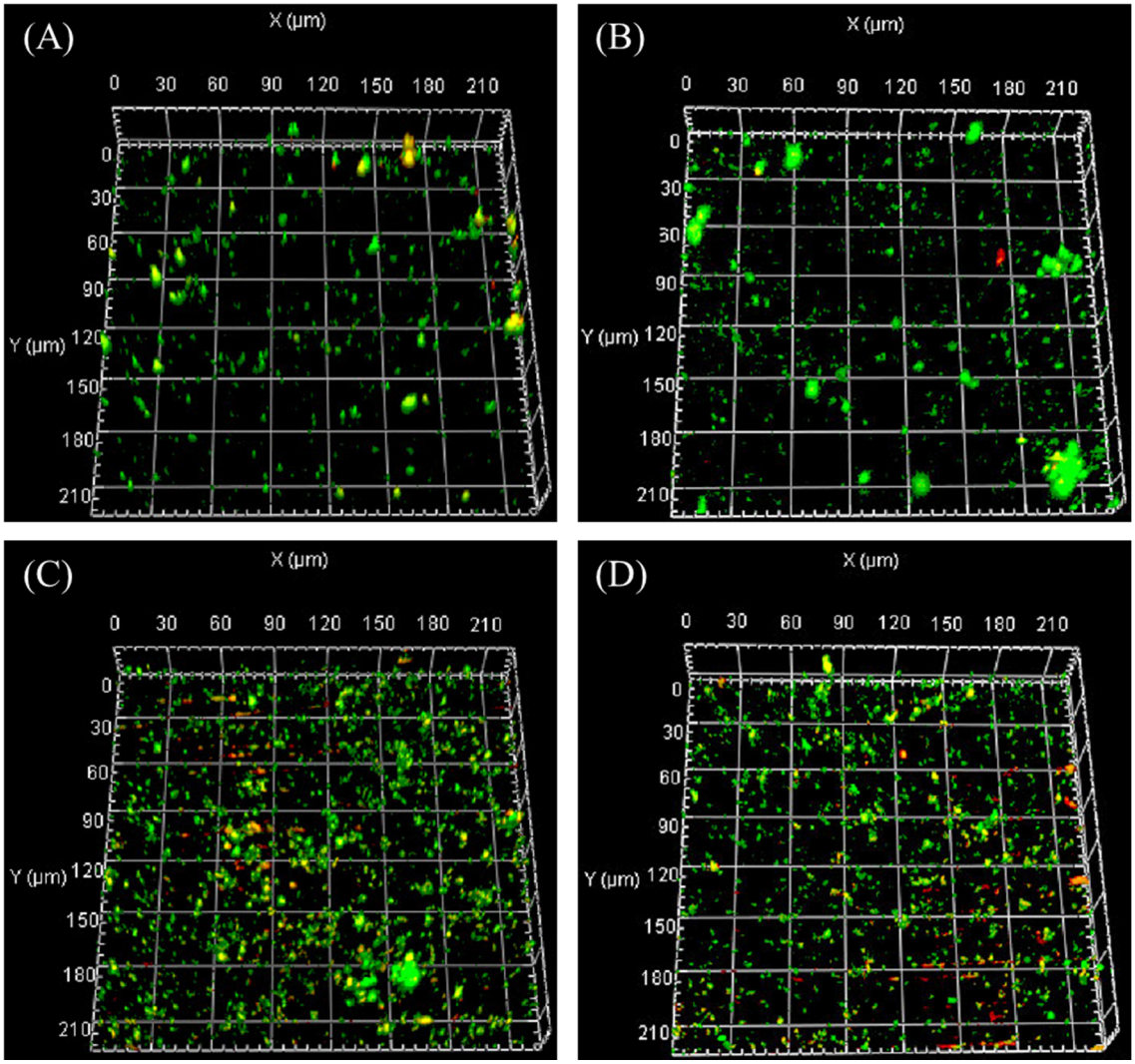

Figure 21. CLSM images of coupons after the 3-day pre-growth (A), and incubated with different organic carbon source levels after the additional 7-day incubation: 0% carbon source reduction (control) (B), 90% carbon source reduction (C), and 100% carbon source reduction (D).

3D CLSM images are shown in Figure 21 for samples after the 3-day pre-growth and incubated with different carbon source levels after the additional 7-day incubation. Figure 21(C, D) shows some dead cells (red dots). This was due to organic carbon

reduction in the fresh medium. Figure 21C also confirms that under 90% carbon source reduction the sessile cell count was the highest (Figure 20).

5.3.2 SRA corrosion analyses

Figure 22 shows the weight loss data for SRA after the 3-day pre-growth and after the additional 7-day incubation with different organic carbon reductions. After the 3-day pre-growth, the average carbon steel weight loss was 0.5 mg/cm^2. The average weight losses after the (3+7)-day incubation with 0% carbon source reduction, 90% carbon source reduction, and 100% carbon source reduction were 1.4 mg/cm^2, 2.5 mg/cm^2, and 1.9 mg/cm^2, respectively. Thus, the net weight losses during the 7-day starvation test were 0.9 mg/cm^2, 2.0 mg/cm^2, and 1.4 mg/cm^2, respectively. It is clear that more carbon source reduction led to more corrosion. The coupon weight loss in the vial with 90% carbon source reduction condition had a 122% increase in net weight loss compared with that in the control vial. The sessile cells on the coupon incubated with 90% carbon source reduction had a 46% increase compared with that in the control vial. The coupon weight loss in the vial with 100% carbon source reduction condition had a 55% increase in net weight loss compared with that in the control vial. However, the sessile cell count had a 24% decrease than that in the control vial (Figure 20). The ratio of weight losses per sessile cell were 1.0:1.5:2.0 for 0% carbon source reduction vs. 90% carbon source reduction vs. 100% carbon source reduction. The weight loss was very small for the abiotic control, suggesting chemicals at pH 7 had negligible corrosion under anaerobic and abiotic conditions. The small 0.3 mg/cm^2 abiotic weight loss could be attributed to Clarke's solution cleaning and the readability (0.1 mg) of the electronic balance used for weighing.

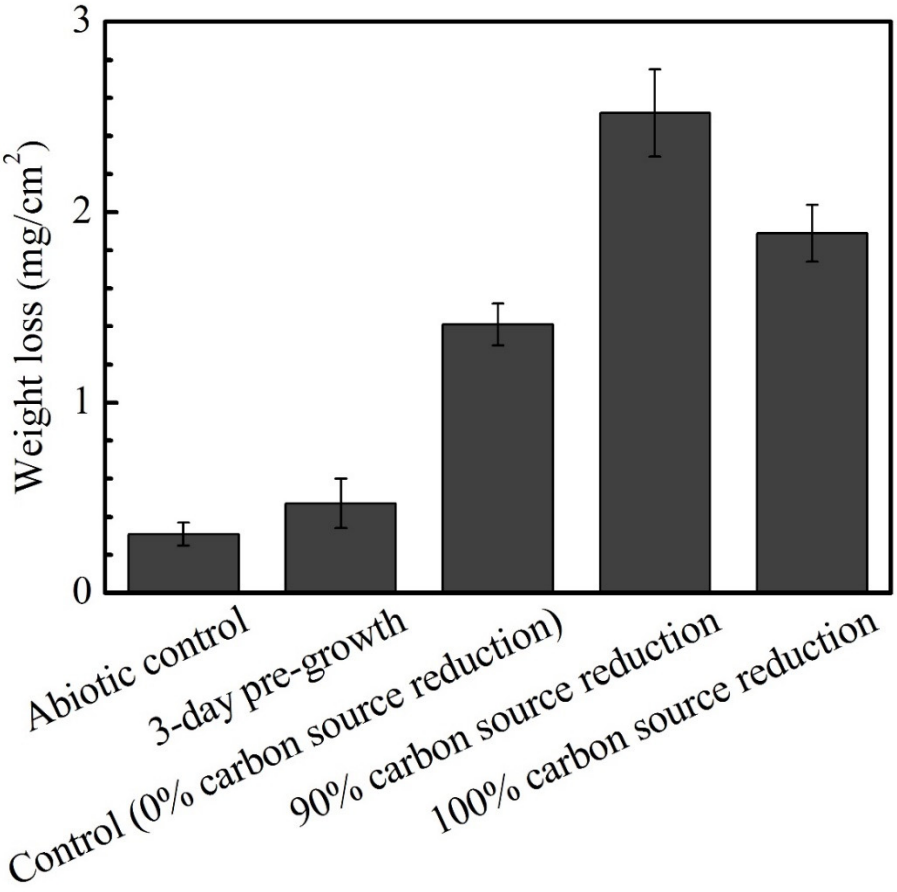

Figure 22. Weight losses of coupons: abiotic control incubated for 10 days, the 3-day pre-growth, and incubated with different organic carbon source reductions after the additional 7-day incubation. (The standard deviation calculated from 9 independent samples from 3 different vials in 3 different experimental batches.)

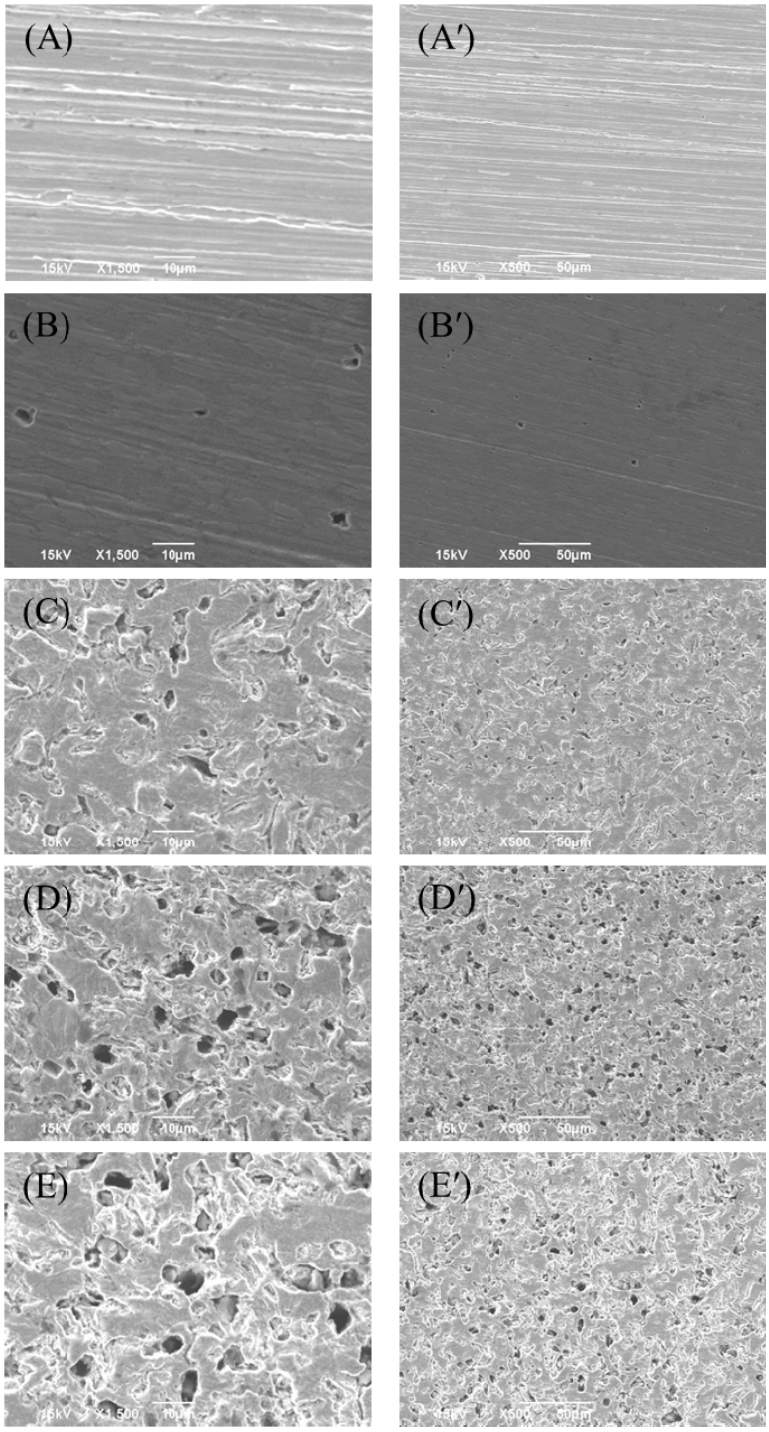

Figure 23. SEM pit morphologies of coupons: abiotic control incubated for 10 days (A, A′), the 3-day pre-growth (B, B′), and incubated with 0% carbon source reduction (C, C′), 90% carbon source reduction (D, D′) and 100% carbon source reduction (E, E′) after the additional 7-day incubation.

The culture medium pH values after the 3-day pre-growth and after the additional 7-day incubation with 0% carbon source reduction, 90% carbon source reduction and 100% carbon source reduction were 6.8 ± 0.1, 6.7 ± 0.2, 6.7 ± 0.1 and 6.7 ± 0.1, respectively. With this kind of near-neutral medium pH, acid attack could not be a significant factor in the corrosion process.

SEM was used to examine pit morphologies on the coupon surface after the biofilm and corrosion products were removed by Clarke's solution. The abiotic control coupon surface morphology had negligible corrosion after the combined 10 days of incubation as shown in Figure 23(A, A′). This corroborates the abiotic weight loss data in Figure 22. After the 3-day pre-growth, some pits show up on the carbon steel coupon surface as indicated in Figure 23(B, B′). This shows that the thermophilic SRA was corrosive and it commenced MIC in a short time (3 days). After the additional 7-day incubation, many pits are seen on the coupon surface that incubated with 0% carbon source reduction in Figure 23(C, C′). More and bigger pits are seen on coupons incubated with 90% in Figure 23(D, D′) and 100% in Figure 23(E, E′) carbon source reductions. The SEM pitting images in Figure 23 corroborate the weight loss data in Figure 22.

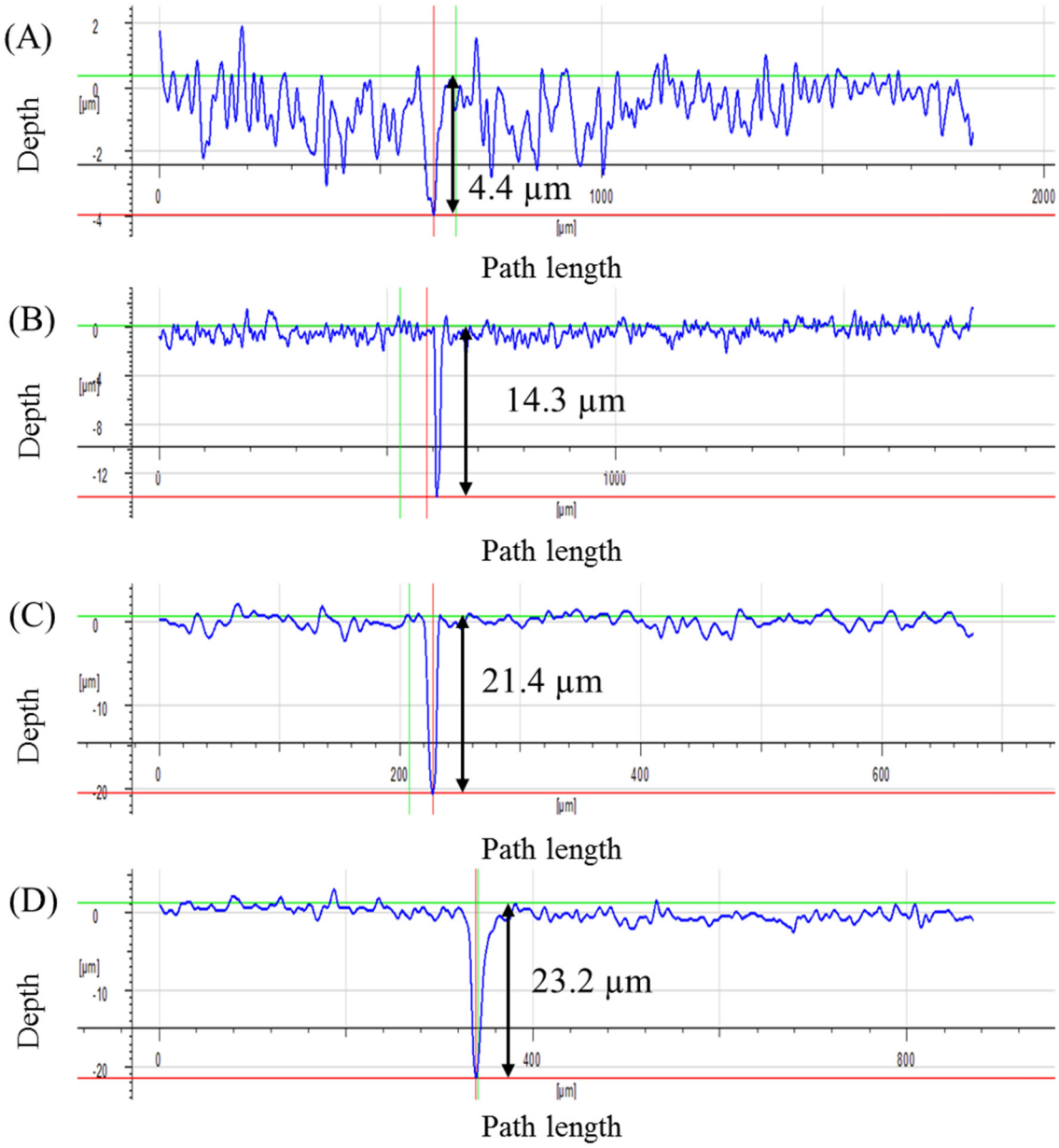

Figure 24. Maximum pit depths on corroded coupons: after 3-day pre-growth (A), and after the additional 7-day incubation with 0% carbon source reduction (B), 90% carbon source reduction (C), and 100% carbon source reduction (D).

Figure 24 shows the maximum pit depth data after the 3-day pre-growth and after the additional 7-day incubation with different organic carbon levels. After the 3-day pre-

growth, the maximum pit depth was 4.4 μm (Figure 24A). After the (3+7)-day incubation, the maximum pit depths for the incubation with 0% carbon source reduction, 90% carbon source reduction, and 100% carbon source reduction were 14.3 μm, 21.4 μm and 23.2 μm, respectively. Thus, the net maximum pit depths during the 7-day starvation test period were 9.9 μm, 17.0 μm and 18.8 μm, respectively after deducting the 3-day pre-growth pit depth. Deeper pitting was caused by SRA sessile cells under more severe starvation. This means that sessile cells attacked carbon steel more aggressively for survival when the carbon source was limited in the medium. It should be noted that manual operation was required in IFM to find the deepest pit. It was possible that the operator might miss the deepest one [131]. The IFM results in Figure 24 are consistent with SEM pitting data in Figure 23.

In the SRB MIC starvation test, SRB sessile cells were found to switch from organic carbon to elemental iron as electron donor under organic carbon starvation [64]. Jia et al. found that a larger anaerobic vial with a larger headspace led to a lower dissolved H_2S concentration in the medium, which caused more sessile SRB cell growth that resulted in more corrosion [76]. It was concluded that biogenic H_2S is not the main factor in SRB MIC. This shows SRB MIC is EET-MIC rather than M-MIC. The data here show that with limited or no organic carbon in the bulk fluid, SRA sessile cells became more corrosive and utilized extracellular electrons released from iron oxidation to harvest energy to maintain their survival. The sulfate reducing *A. fulgidus* starvation results supported the bioenergetics of MIC by SRB. *A. fulgidus* was reported to possess cellular electron transport systems [132]. Thus, the results here show that SRA are capable of EET, which means the bioenergetics theory for SRB can be expanded to SRA.

The abiotic control results confirm that a biocatalysis is required to use electrons from iron oxidation for sulfate reduction.

5.3.3 Electrochemical measurements of SRA starvation test

R_p versus time during the 7-day incubation with different carbon source levels are shown in Figure 25. LPR was scanned once a day. The abiotic control had a very large resistance and kept steady during the 7-day incubation, suggesting negligible corrosion. For the biotic samples, the resistances shifted to the positive direction during the 7-day incubation indicating an increased resistance. For all biotic samples, the control with 0% carbon source reduction had the highest resistance while the lowest was observed on samples incubated with 90% carbon source reduction. The corrosion rate in the glass cell with reduced carbon source was higher compared with that incubated in the full-strength medium. This qualitatively matched the weight loss data in Figure 22. This means that LPR can be used qualitatively to monitor corrosion caused by a sulfate reducer.

Figure 26 shows the PDS conducted at the end of the 7-day incubation for samples incubated with different carbon source levels. It was scanned only once due to a wide range of potential (−150 mV to +150 mV) applied that could damage the biofilm. The fitted Tafel parameters (i.e., E_{corr}, i_{corr}, β_α and β_c) are listed in Table 4. The i_{corr} for the samples incubated with reduced levels of carbon source were higher than that in the medium with 0% carbon source reduction, indicating more severe MIC under starvation. The PDS results are consistent with the LPR measurements.

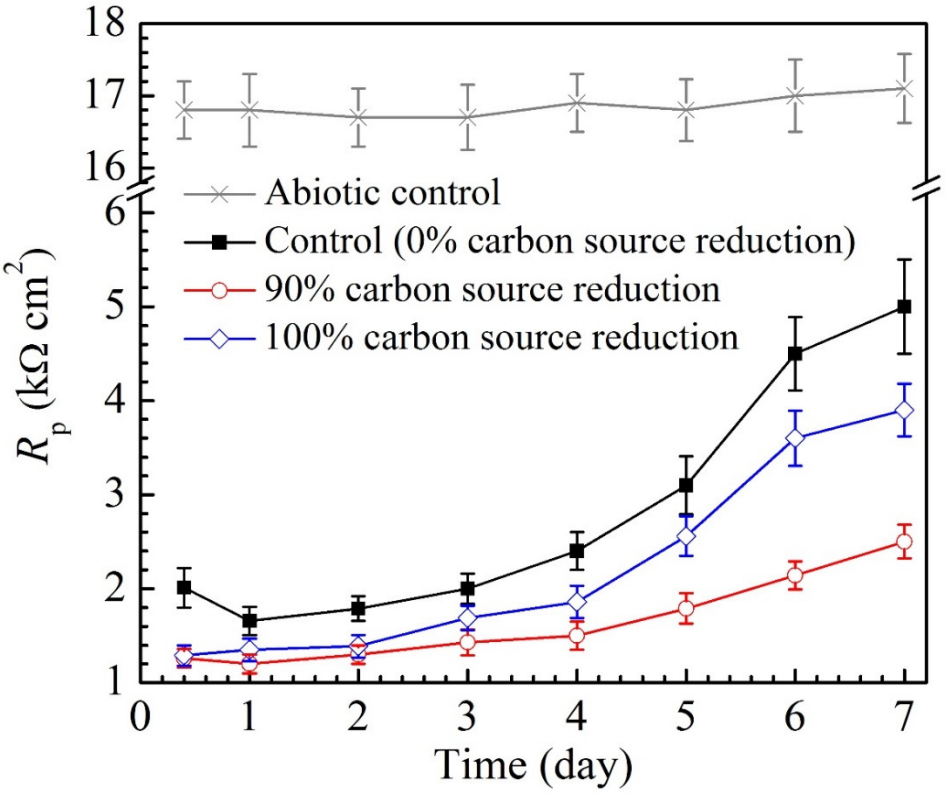

Figure 25. Polarization resistance versus time for coupons incubated in the abiotic full-strength medium and incubated in media with different organic carbon source levels after the additional 7-day incubation. (The standard deviation calculated from 3 independent samples from 3 different vials in 3 different experimental batches.)

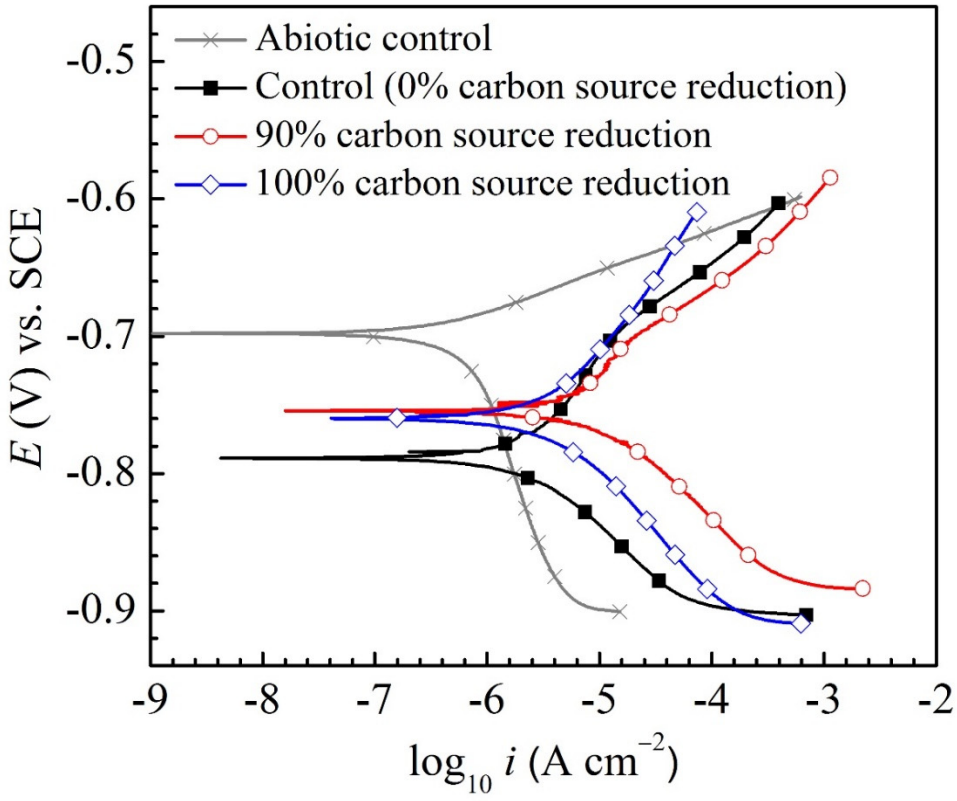

Figure 26. PDS measurements of coupons incubated in the abiotic full-strength medium and incubated in media with different organic carbon source levels at the end of the 7-day incubation.

Table 4. Fitted electrochemical parameters after the PDS (The standard deviation calculated from 3 independent samples from 3 different vials in 3 different experimental batches.)

	i_{corr} ($\mu A/cm^2$)	E_{corr} (V) vs. SCE	β_a (mV/dec)	β_c (mV/dec)
Abiotic control	0.6 ± 0.2	−0.68 ± 0.02	39 ± 5	210 ± 16
Control (0% carbon source reduction)	2.9 ± 0.6	−0.79 ± 0.04	91 ± 8	69 ± 7
90% carbon source reduction	7.2 ± 0.9	−0.75 ± 0.03	82 ± 7	67 ± 6
100% carbon source reduction	4.3 ± 0.7	−0.76 ± 0.04	107 ± 11	85 ± 9

5.4 Summary

Experimental data showed that *A. fulgidus*, a thermophilic sulfate reducing archaeon, was corrosive against C1018 carbon steel at 80ºC. It was found that under organic carbon source starvation, the SRA became more corrosive. Under carbon source starvation, the *A. fulgidus* planktonic cells decreased during the additional 7-day incubation. Under a 90% carbon source reduction, the sessile cell amount increased by 46% while the net weight loss increased by 122% compared with the control (incubated in the full-strength medium). Under a 100% carbon source reduction, the sessile cell amount increased by 24% while the net weight loss increased by 55% compared with the control. Under carbon source reductions, more severe pitting corrosion occurred compared with the control. The corrosion results extended the bioenergetics theory for SRB to SRA. LPR and PDS results supported the weight loss and pitting corrosion trends.

Chapter 6: Effects of Ferrous Ion Concentration on MIC of Carbon Steel by Sulfate Reducing *Desulfovibrio vulgaris* Biofilm

6.1 Introduction

Ferrous ion (Fe^{2+}) concentration was found to be an important parameter in SRB growth and MIC of carbon steel by SRB. Previous reports focused on the effect of iron sulfide (FeS) film on SRB MIC. For example, Lee et al. reported an increased corrosion rate with more Fe^{2+} added to the culture medium [133]. They concluded that the FeS film formed at a low Fe^{2+} concentration was protective. King et al. considered that an increased $[Fe^{2+}]$ led to the FeS film breakdown that caused more corrosion [134]. SEM observations of cracks in relatively thick FeS films can be misleading because cracks can develop during the coupon surface dehydration step, which is required for SEM. Because an increased $[Fe^{2+}]$ can lead to more corrosion, some people even label FeS as a corrosive agent [135]. However, Fe and S in FeS do not have any vacancy for electrons, which means that FeS is not an oxidant. Thus, unlike sulfate, FeS is not an oxidant (electron acceptor). It has been suggested that an uneven FeS film on a carbon steel surface provides an increased overall cathodic surface area for electron harvesting through this semi-conductive mineral film by the SRB sessile cells on and embedded in the film [136]. The accelerated cathodic reaction increased anodic iron oxidation on spots that are unpassivated or less passivated.

In SRB respiration using sulfate, sulfate reduction produces bisulfide (HS^-) as shown in Reaction (2). HS^- can combine with a proton to form hydrogen sulfide (H_2S) in Reaction (21) or to loss a proton to become sulfide ion in Reaction (22) [137]. HS^- can react with Fe^{2+} to form FeS in Reaction (23) [138]. When [FeS] reaches supersaturation,

some FeS is precipitated, which gives the characteristic ink-black color indicative of the presence of FeS produced from sulfate reduction by SRB [76].

$$HS^- + H^+ \leftrightharpoons H_2S \quad (21)$$

$$HS^- \leftrightharpoons H^+ + S^{2-} \quad (22)$$

$$Fe^{2+} + HS^- \leftrightharpoons FeS + H^+ \quad (23)$$

H_2S is toxic to most life forms. It inhibits SRB growth [139]. However, the mechanism of sulfide inhibition of SRB growth is not fully understood [139]. Postgate speculated that FeS precipitation reduces the availability of Fe ion that is needed for ferredoxin and cytochrome *c* enzymes to function. These enzymes are critical in the SRB electron transport chain for sulfate respiration [139,140].

It was recently demonstrated that biogenic H_2S is not a major contributor to SRB MIC of carbon steel in anaerobic vials with broth pH near 7, while EET-MIC is the underlining mechanism [76]. By fixing the culture medium liquid volume while varying the headspace volume, it was found that a larger headspace volume yielded a lower concentration of $[H_2S]$ in the liquid phase because more H_2S escaped to the headspace. This led to a higher sessile cell count due to alleviated H_2S toxicity and a thinner iron sulfide corrosion product film layer. As a result, weight loss and pit depth increased [76].

The effects of Fe^{2+} on SRB MIC of carbon steel are complex and often confusing. However, it is also extremely important to have a good understanding due to the importance of SRB MIC of carbon steel. It warrants further studies to pinpoint the exact reason for increased corrosion with increased $[Fe^{2+}]$. Here, a causal-relationship experiment was designed to prove a hypothesis that the Fe^{2+} acceleration of SRB MIC of

carbon steel is primarily attributed to reduced H_2S toxicity that leads to a higher sessile cell count at an elevated *[*H_2S*]* during incubation.

6.2 Materials and Methods

The metal used in this study was C1018 carbon steel. The bacterium used in this work was *D. vulgaris* (ATCC 7757). It was cultured in ATCC 1249 medium [76]. Detailed information about coupon preparation, chemicals used in this work, sterilization, and deoxygenation are described in Appendix A.

Anaerobic vials (125 mL) were each filled with 100 mL modified ATCC 1249 medium with an adjusted Fe^{2+} concentration (20 ppm, 50 ppm, 100 ppm or 200 ppm by mass). Five replicate coupons were added to each vial before inoculation. Vials were inoculated with a *D. vulgaris* seed culture and incubated anaerobically at 37^{o}C for 7 days. During the 7-day incubation, a set of vials were dedicated to planktonic cell counting. Another set of anaerobic vials were used only for H_2S measurements. The third set of vials were opened for biofilm examinations and corrosion analyses after the 7-day incubation. The experiment was repeated thrice for reproducibility. Figure 27 shows anaerobic vials with different initial Fe^{2+} concentrations after the 7-day incubation.

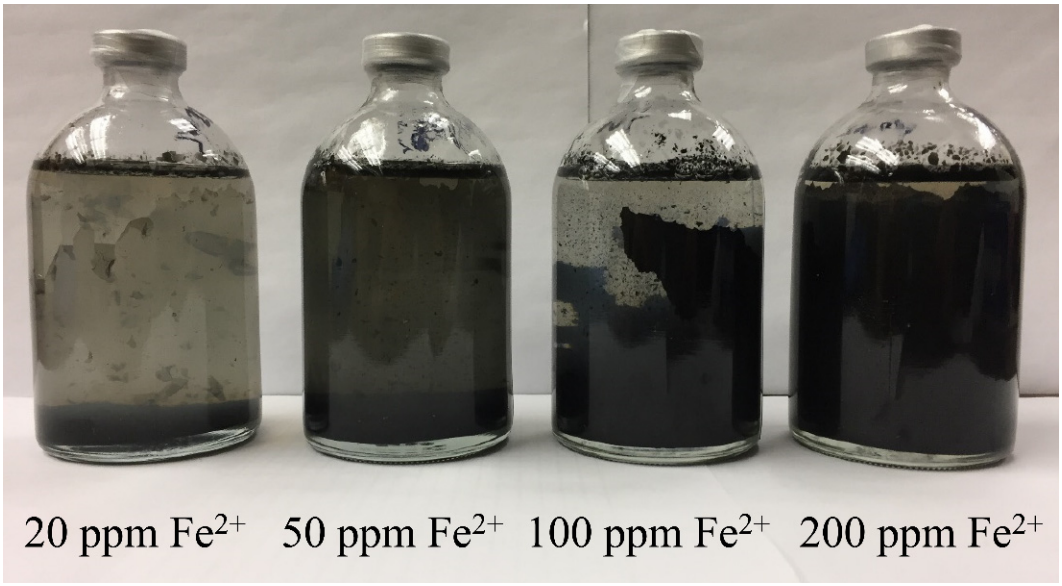

Figure 27. Anaerobic vials with different initial Fe^{2+} concentrations after the 7-day incubation.

The H_2S concentration in the gas phase in each anaerobic vial was measured using a micro-gas chromatography (micro-GC) instrument (Agilent 490, Agilent Technologies, Palo Alto, CA, USA) every other day during the 7-day incubation. Micro-GC operating parameters [76] and the H_2S equilibrium calculations based on Henry's law (a solubility constant *K* value of 0.0737 at 37°C for H_2S was used) were reported in a previous work [141]. Planktonic and sessile cell counts were enumerated with a hemocytometer under an optical microscope at 400× magnification. The details for planktonic cell count are described in Section 5.2. The planktonic cell counts on days 0, 1, 3, 5 and 7 during the 7-day incubation were assayed. Sessile cell counts were checked only once at the end of the 7-day incubation. The procedure for sessile cell counting is described in Appendix A. Biofilm observation was conducted with CLSM. The detailed CLSM staining procedures are described in Appendix A.

After the biofilm and corrosion products were removed in accordance with ASTM G1−03 using a fresh Clarke's solution, weight loss was obtained. The detailed coupon cleaning method for weight loss is described in Appendix A. Then, corrosion pits were examined under SEM using the same coupons. The pit depth was measured with IFM.

Electrochemical tests were conducted in several 450 mL glass cells with three electrodes submerged in 360 mL culture medium. The headspace volume to the liquid volume was the same as in the 125 mL vials. Each glass cell contained the ATCC 1249 culture medium with an adjusted Fe^{2+} concentration. Each glass cell was inoculated with 3.6 mL *D. vulgaris* seed culture in the anaerobic chamber. LPR was conducted once every day near the end of the day with a scan rate of 0.167 mV/s between −10 mV and +10 mV vs. the stable OCP. EIS was performed near the end of days 1, 4 and 7 under the stable OCP in the 10^{-2} to 10^{5} Hz frequency range with a 10 mV sinusoidal signal. PDS was obtained only once for each working electrode at the end of the 7-day incubation with a scan rate of 0.167 mV/s between −200 mV and +200 mV versus the OCP. More details for the procedures are described in Appendix A.

6.3 Results and Discussion

6.3.1 Dissolved H_2S concentration, SRB cell count and coupon weight loss

Figure 28 shows planktonic cell counts in anaerobic vials with different initial Fe^{2+} concentrations during the 7-day incubation. Note that the full-strength ATCC 1249 medium has 200 ppm $[Fe^{2+}]$. The initial planktonic cell amount in all cases was around 10^{6} cells/mL right after inoculation. More planktonic SRB cells were observed in the medium with a higher initial $[Fe^{2+}]$. The planktonic cell count in the medium with 200 ppm initial Fe^{2+} concentration was about 2-3 times of that in the medium with 20 ppm

initial Fe^{2+} concentration. This kind of relatively small difference may not be detectable using less accurate MPN enumeration.

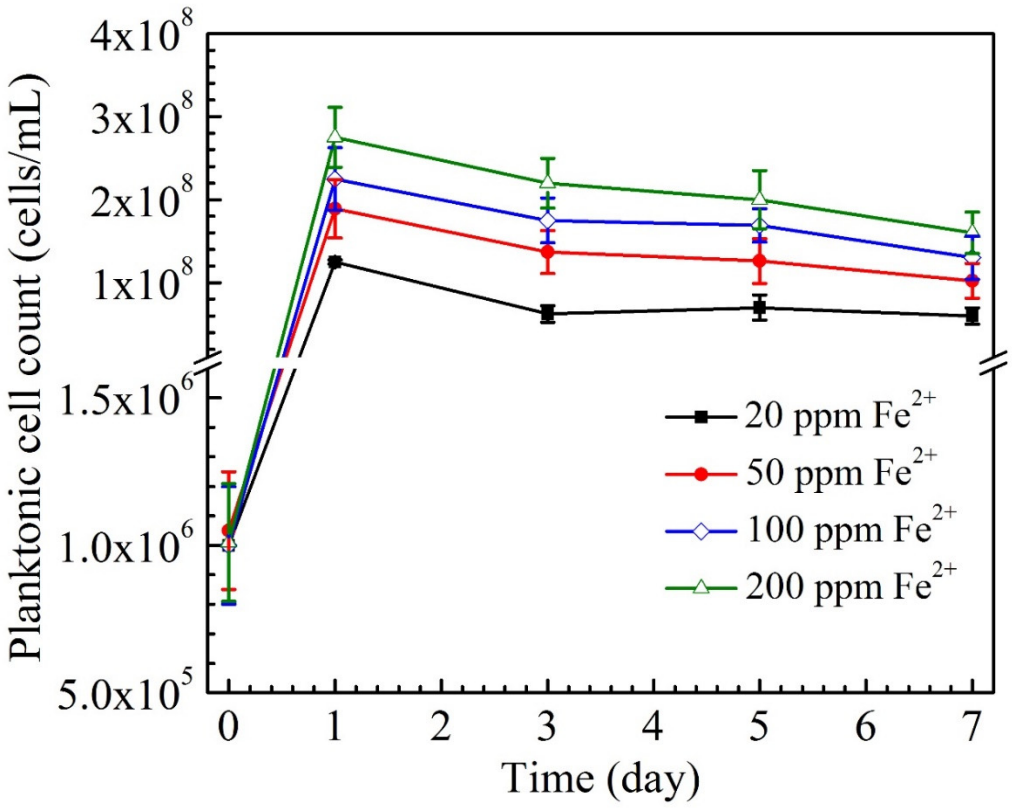

Figure 28. Planktonic cell counts from hemocytometer readings during the 7-day incubation in vials with different initial Fe^{2+} concentrations. (The standard deviation calculated from 3 independent samples from 3 different vials in 3 different experimental batches.)

The dissolved $[H_2S]$ for each initial Fe^{2+} concentration during the 7-day incubation is shown in Figure 29. It shows that a higher initial Fe^{2+} concentration led to a higher dissolved $[H_2S]$, obviously due to better SRB growth as indicated by Figure 28. In all cases, the dissolved $[H_2S]$ increased with incubation time as expected. The culture medium pH values after the 7-day incubation were 6.8 ± 0.1, 6.7 ± 0.1, 6.6 ± 0.1 and 6.6 ± 0.1 for vials with initial Fe^{2+} concentrations of 20 ppm, 50 ppm, 100 ppm and 200 ppm, respectively. These near neutral pH values indicate that acid corrosion was unlikely a contributing factor to corrosion weight loss.

Figure 30 lists the sessile cell count and weight loss data after the 7-day incubation in anaerobic vials with different initial Fe^{2+} concentrations. The average sessile cell counts were 4.3×10^7 cells/cm^2, 8.7×10^7 cells/cm^2, 1.4×10^8 cells/cm^2 and 2.0×10^8 cells/cm^2 for vials with initial Fe^{2+} concentrations of 20 ppm, 50 ppm, 100 ppm and 200 ppm, respectively. The sessile cell count was higher in anaerobic vials with a higher initial Fe^{2+} concentration, similar to the planktonic cell count trend. The sessile cell count in the medium with 200 ppm initial Fe^{2+} concentration was 4.7 times of that in the medium with 20 ppm initial Fe^{2+} concentration. The average weight losses were 0.9 mg/cm^2, 2.2 mg/cm^2, 3.1 mg/cm^2 and 4.5 mg/cm^2 for initial Fe^{2+} concentrations of 20 ppm, 50 ppm, 100 ppm and 200 ppm, respectively. The weight loss for 200 ppm is 5 times of that for 20 ppm initial Fe^{2+} concentration. Figure 30 shows that weight loss trend coincides with the sessile cell count trend. With more sessile cells, more electrons were harvested by sessile SRB cells. Thus, the observation here supports the BCSR theory.

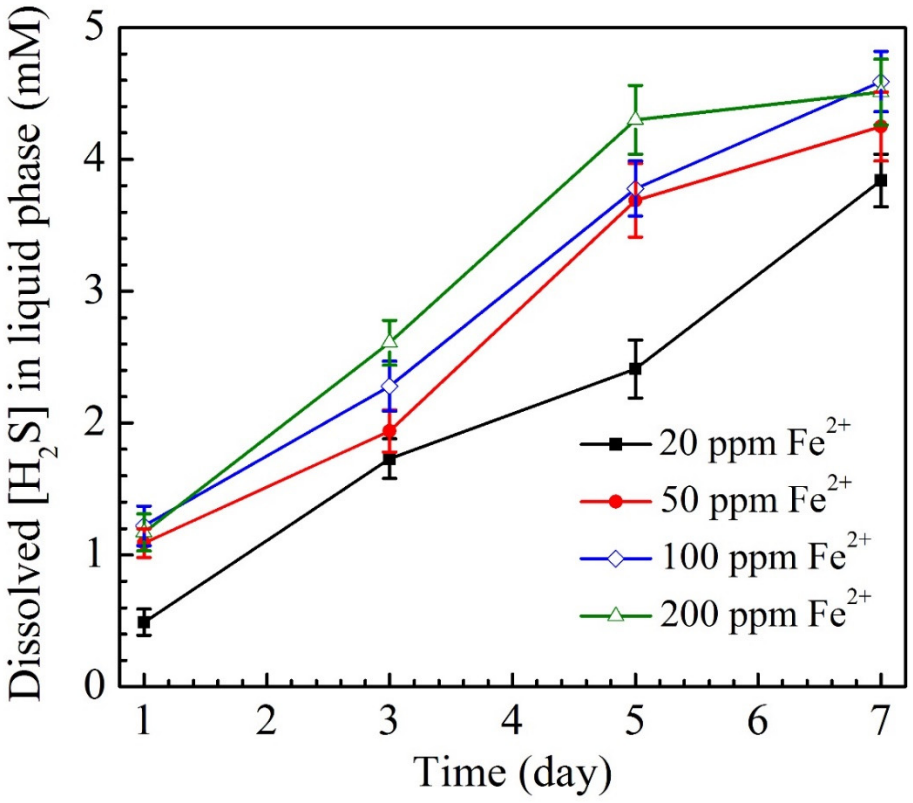

Figure 29. Dissolved H_2S concentrations in SRB broths with different initial Fe^{2+} concentrations during the 7-day incubation. (The standard deviation calculated from 3 independent samples from 3 different vials in 3 different experimental batches.)

6.3.2 Biofilm observation

The 3D CLSM images of biofilms on coupons retrieved from the anaerobic vials after the 7-day incubation are shown in Figure 31. The biofilm thickness increased with an increased initial Fe^{2+} concentration, which is consistent with the sessile cell count trend. The biofilm thickness values fall in a narrow range of 40-68 μm in Figure 31. This means the increase in the sessile cell count was mostly through volumetric density increase rather than through thickness increase.

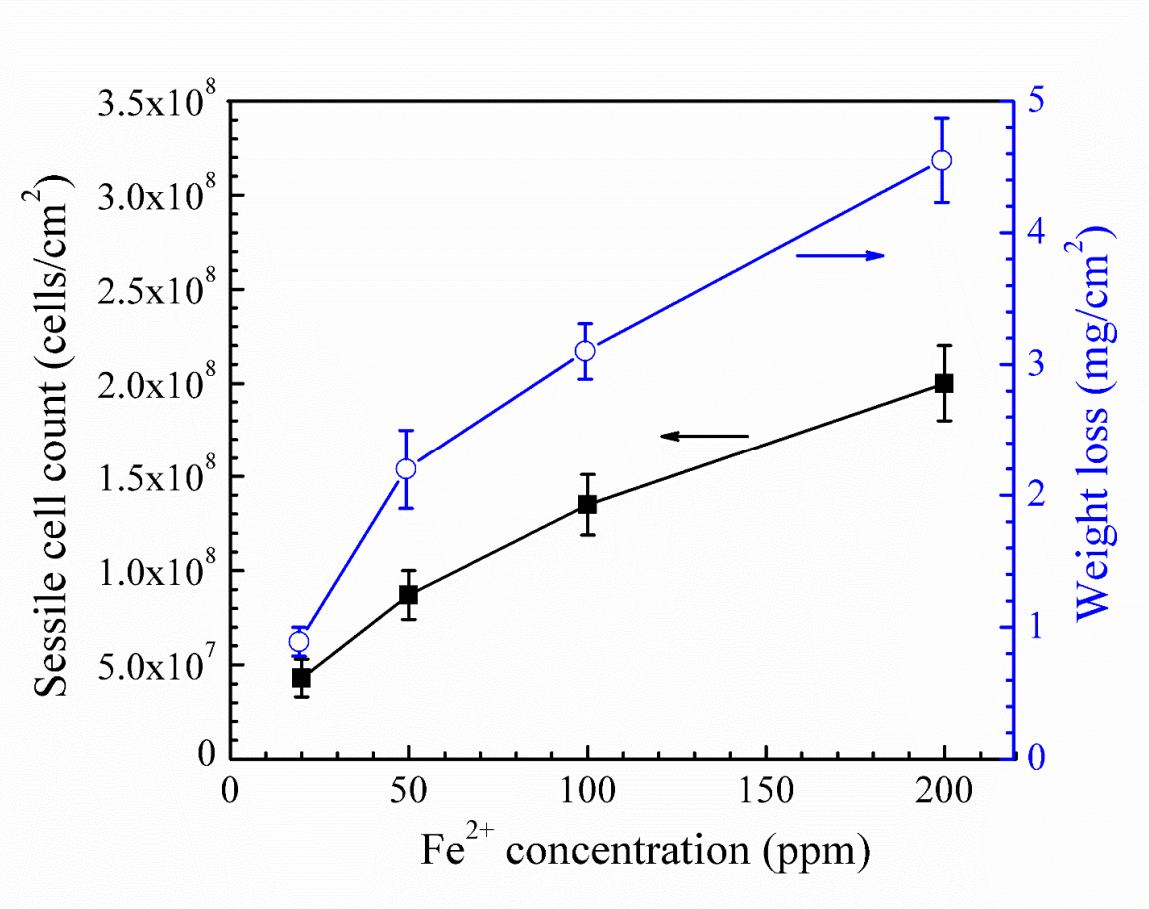

Figure 30. Sessile cell counts (squares) and weight losses of coupons (circles) after the 7-day incubation in vials with different initial Fe^{2+} concentrations. (The standard deviation calculated from 3 independent samples from 3 different vials in 3 different experimental batches.)

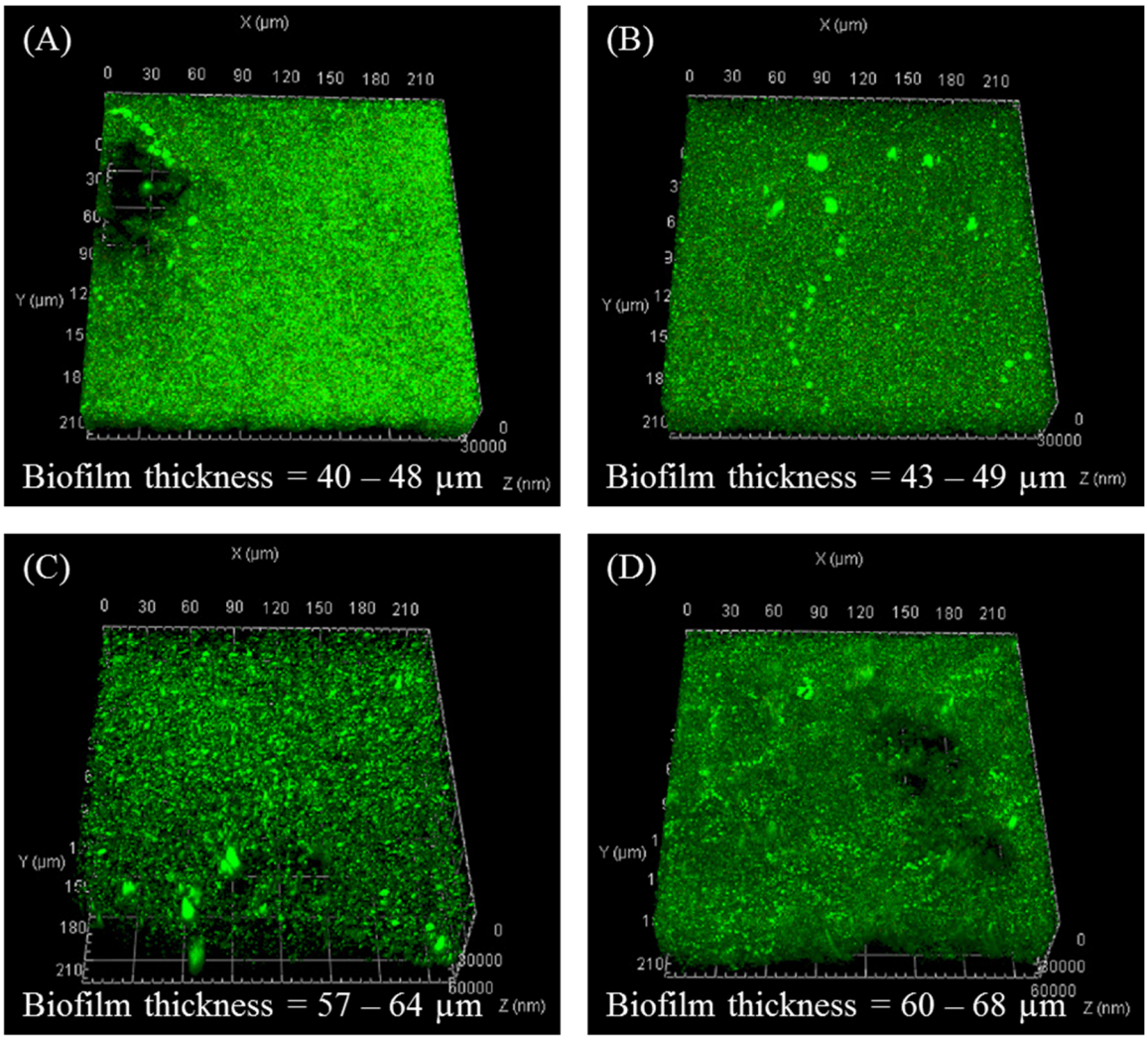

Figure 31. CLSM images of the carbon steel coupon surfaces after the 7-day incubation with different initial Fe^{2+} concentrations: 20 ppm (A), 50 ppm (B), 100 ppm (C), and 200 ppm (D).

6.3.3 Corrosion pit examination

Figure 32 shows the SEM images of coupon surfaces after biofilms and corrosion products were removed. After the 7-day incubation, pitting corrosion was found in Figure 32(B,C,D). The average maximum pit depths on the coupon incubated with initial Fe^{2+} concentrations of 20 ppm, 50 ppm, 100 ppm and 200 ppm were 7 μm, 12 μm, 19 μm and

29 μm, respectively (Figure 33). Each average maximum pit depth was calculated from 3 independent samples in 3 different experimental runs. The average maximum pit depth data in Figure 33 corroborate the SEM pit images in Figure 32 and the weight loss data trend in Figure 30.

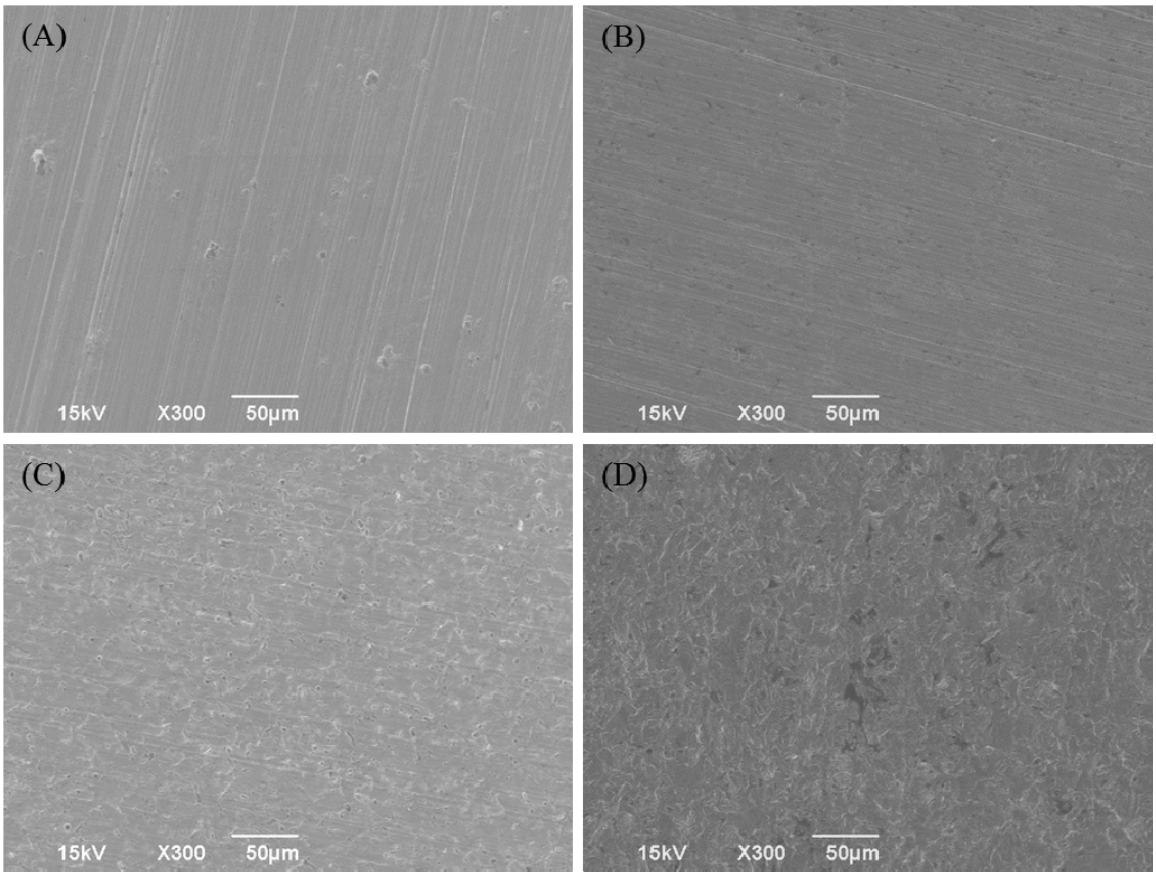

Figure 32. SEM images of the coupons (with biofilms and corrosion products removed) after the 7-day incubation with different initial Fe^{2+} concentrations: 20 ppm (A), 50 ppm (B), 100 ppm (C), and 200 ppm (D).

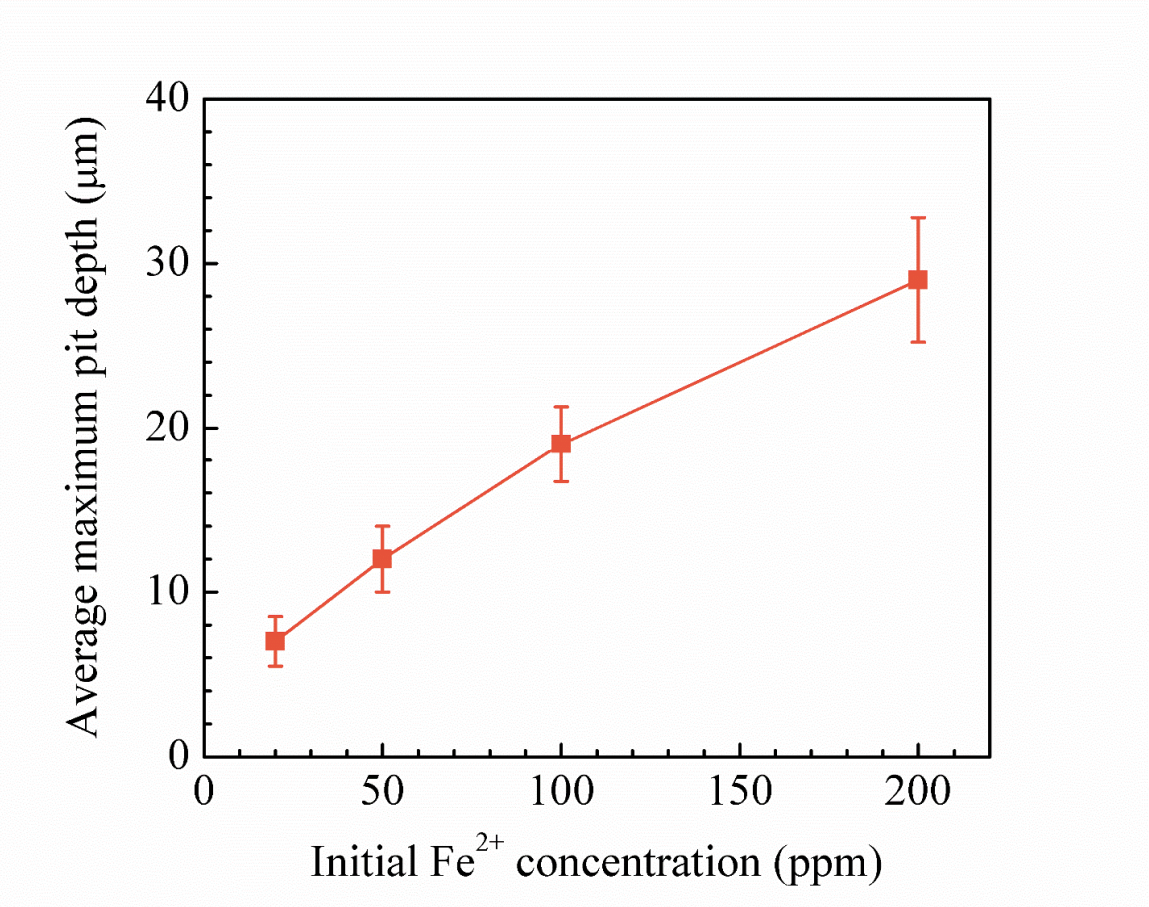

Figure 33. Average maximum pit depths on the coupons after the 7-day incubation with different initial Fe^{2+} concentrations: 20 ppm, 50 ppm, 100 ppm and 200 ppm. (The standard deviation calculated from 3 independent samples from 3 different vials in 3 different experimental batches.)

6.3.4 Electrochemical measurements

The variations of OCP with time for tests with different initial Fe^{2+} concentrations during the 7-day incubation are shown in Figure 34. The OCP of the coupon incubated with 20 ppm initial Fe^{2+} concentration slightly shifted to the negative direction during the 7-day incubation. For the coupons incubated in the medium with 50 ppm, 100 ppm and 200 ppm initial Fe^{2+} concentrations, the OCP values shifted to the positive direction

during the 7-day incubation. At the end of the 7th day, all the 3 OCP values were close and they were much higher than that for 20 ppm. A more negative OCP indicates a higher thermodynamic tendency to lose electrons. However, the actual corrosion rate depends on corrosion kinetics [128]. The higher thermodynamic tendency for the 20 ppm Fe^{2+} coupon corresponding to a lower corrosion weight loss is interesting, but not uncommon [125]. The kinetic electrochemical data below are more useful in explaining corrosion weight loss.

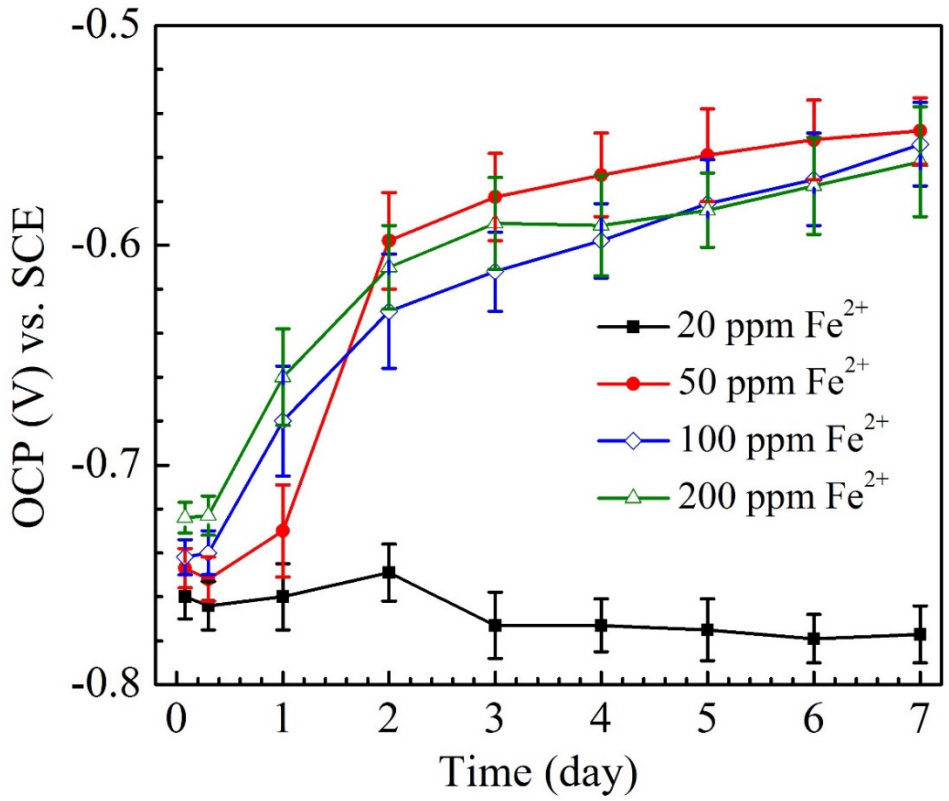

Figure 34. Variations of OCP versus time during the 7-day incubation with different initial Fe^{2+} concentrations. (The standard deviation calculated from 3 independent samples from 3 different vials in 3 different experimental batches.)

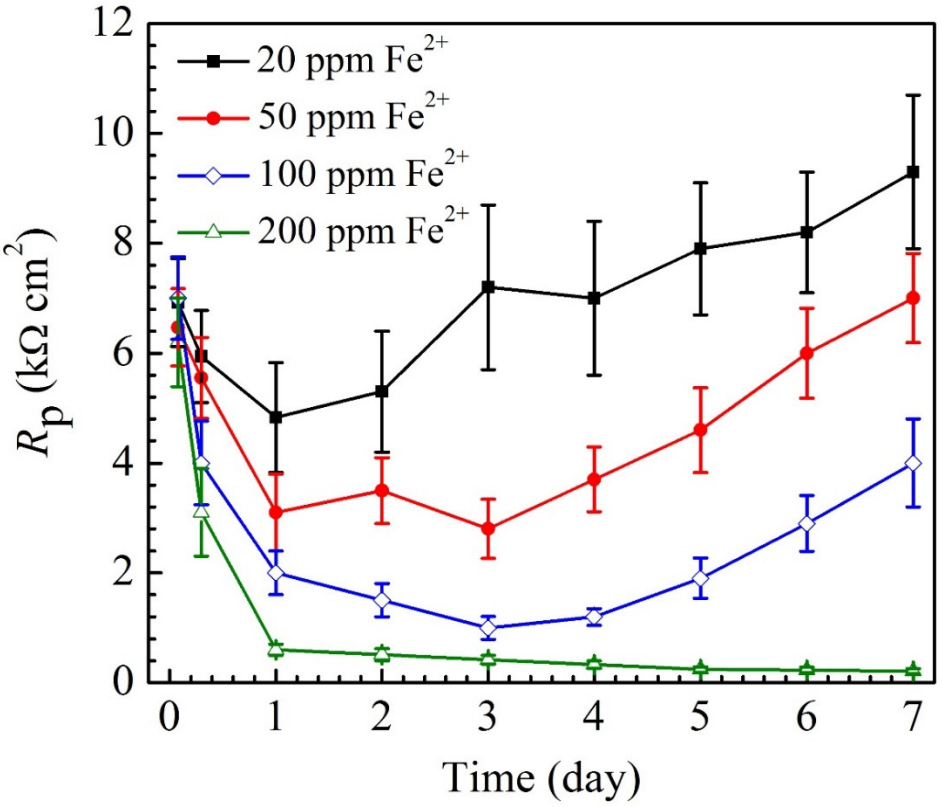

Figure 35. Variations of LPR versus time during the 7-day incubation with different initial Fe^{2+} concentrations. (The standard deviation calculated from 3 independent samples from 3 different vials in 3 different experimental batches.)

The corrosion resistance (R_p) values calculated from LPR measurements in Figure 35 show time-dependent inverse corrosion rate trend of coupons during the 7-day incubation. The lowest R_p was found for 200 ppm initial Fe^{2+} concentrations, corresponding to the highest corrosion rate. Unlike the one-shot weight loss data at the end of the 7-day incubation, R_p provided a transient corrosion kinetic behavior. The R_p values for 20 ppm, 50 ppm and 100 ppm initial Fe^{2+} concentrations first decreased and

then increased during the 7-day incubation. The R_p for 200 ppm initial Fe^{2+} concentration decreased and then kept relatively steady during the 7-day incubation.

EIS was performed on days 1, 4 and 7 for glass cells with different initial Fe^{2+} concentrations during the 7-day incubation. Figure 36 shows the Nyquist and Bode plots. The Nyquist plot diameter of the coupon incubated in the medium with a lower initial Fe^{2+} concentration is larger, which means a higher impedance or a lower corrosion rate. The equivalent electrical circuit in Figure 16 is used to fit the impedance spectra in Figure 36.

Table 5 shows the fitted electrochemical parameters from the EIS spectra in Figure 36. In Table 5, it is clear that R_{ct} is much larger than R_b, suggesting that charge transfer resistance was much larger than mass transfer resistance. This is common in electrochemical systems in which EET is often a bottleneck. Theoretically, the sum of $R_{ct} + R_b$ is comparable to R_p in LPR analysis [142]. Figure 37 shows that the $R_{ct} + R_b$ trends of different initial Fe^{2+} concentrations are similar to those for R_p in Fig. 35. Qualitatively, both R_p and $R_{ct} + R_b$ trends in this work corroborate the weight loss data, confirming that an increased initial Fe^{2+} concentration led to more severe corrosion.

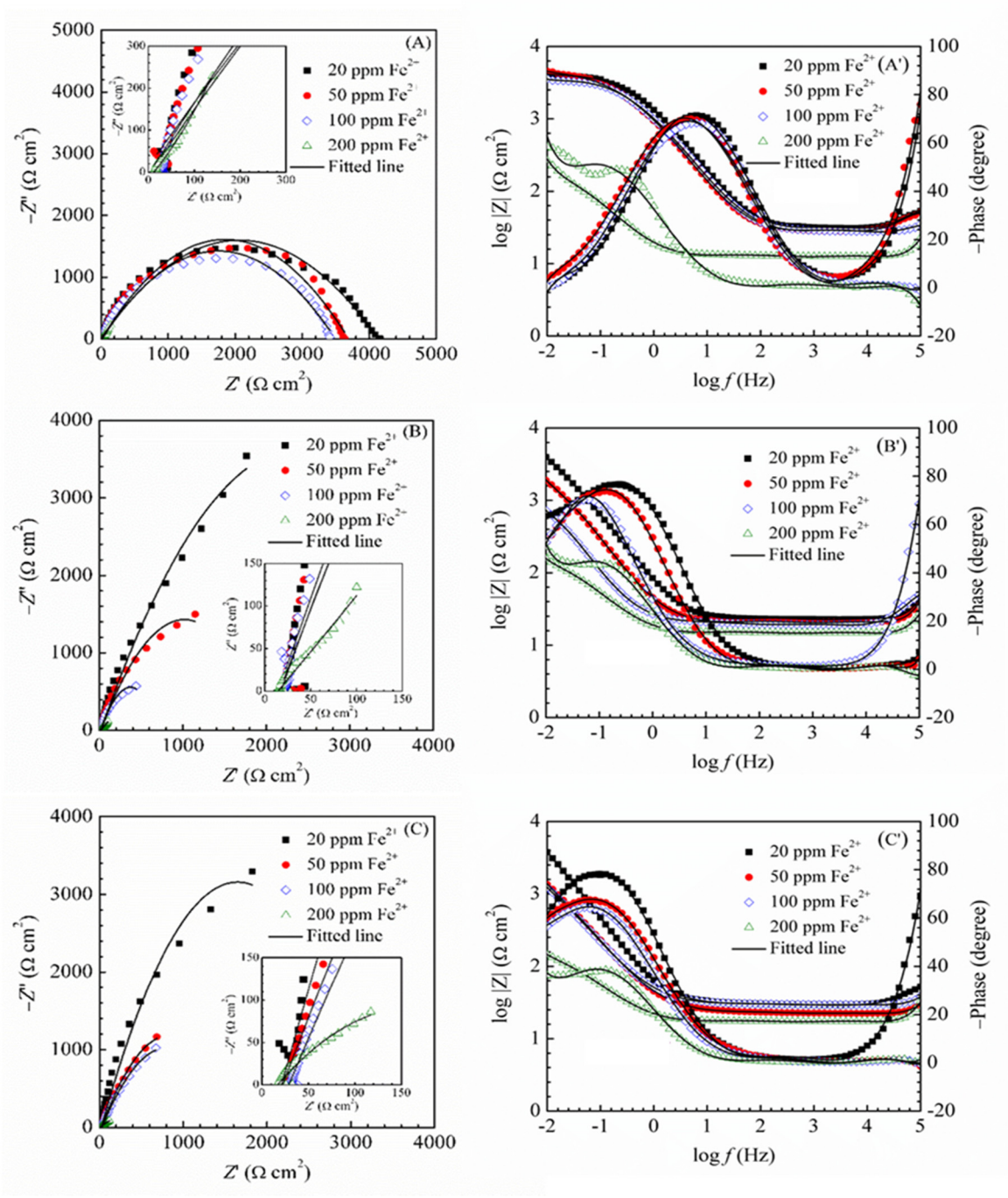

Figure 36. Nyquist and Bode plots for the coupons during the 7-day incubation with different initial Fe^{2+} concentrations: (A, A′) 1st day, (B, B′) 4th day, and (C, C′) 7th day. (EIS was conducted under stable OCP between 10^{-2} and 10^{5} Hz with a sinusoidal voltage signal (10 mV amplitude).)

PDS was conducted at the end of the 7-day incubation (Figure 38) only once for each working electrode as a common practice because the wide voltage range could damage the biotic coupon surface. The fitted electrochemical parameters containing corrosion potential (E_{corr}), anodic and cathodic Tafel slopes (β_α and β_c), and corrosion current density (i_{corr}) are shown in Table 6. Theoretically, i_{corr} is directly proportional to corrosion rate. The i_{corr} data here once again show that a higher initial Fe^{2+} concentration led to a higher corrosion rate. All the three electrochemical techniques above provided the same corrosion trend that corroborates the weight loss data.

Table 5. Fitted electrochemical parameters from the EIS spectra in Figure 36

Duration (d)	R_s (Ω cm^2)	Y_b (Ω^{-1} cm^{-2} s^n)	n_b	R_b (Ω cm^2)	Y_{dl} (Ω^{-1} cm^{-2} s^n)	n_{dl}	R_{ct} (Ω cm^2)
20 ppm Fe^{2+}							
1	14	0.0008	0.98	40	0.0005	0.91	4160
4	20	0.0007	0.83	36	0.0012	0.97	5941
7	16	0.0005	0.95	35	0.0031	0.95	8742
50 ppm Fe^{2+}							
1	21	0.0031	0.91	39	0.0037	0.89	3521
4	18	0.0076	0.96	75	0.0029	0.75	3766
7	17	0.0110	0.98	95	0.0027	0.88	6859
100 ppm Fe^{2+}							
1	28	0.0006	0.91	62	0.0004	0.92	2484
4	27	0.0019	0.81	47	0.0112	0.98	1416
7	21	0.0054	0.92	30	0.0141	0.97	3614
200 ppm Fe^{2+}							
1	14	0.0154	0.93	87	0.0312	0.87	712
4	15	0.0212	0.95	51	0.0436	0.86	408
7	18	0.0170	0.98	13	0.0231	0.81	372

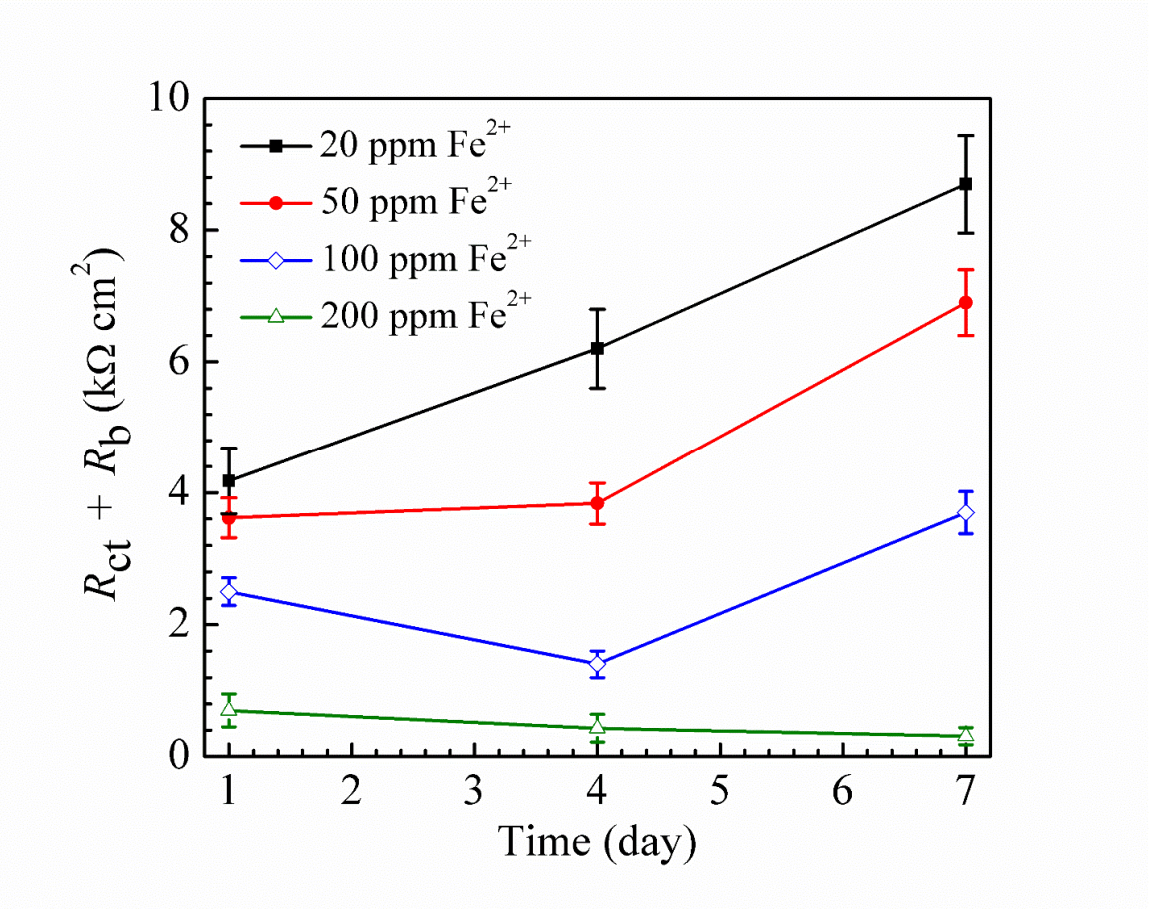

Figure 37. $R_{ct} + R_b$ vs. time during the 7-day incubation with different initial Fe^{2+} concentrations. (The standard deviation calculated from 3 independent samples from 3 different vials in 3 different experimental batches.)

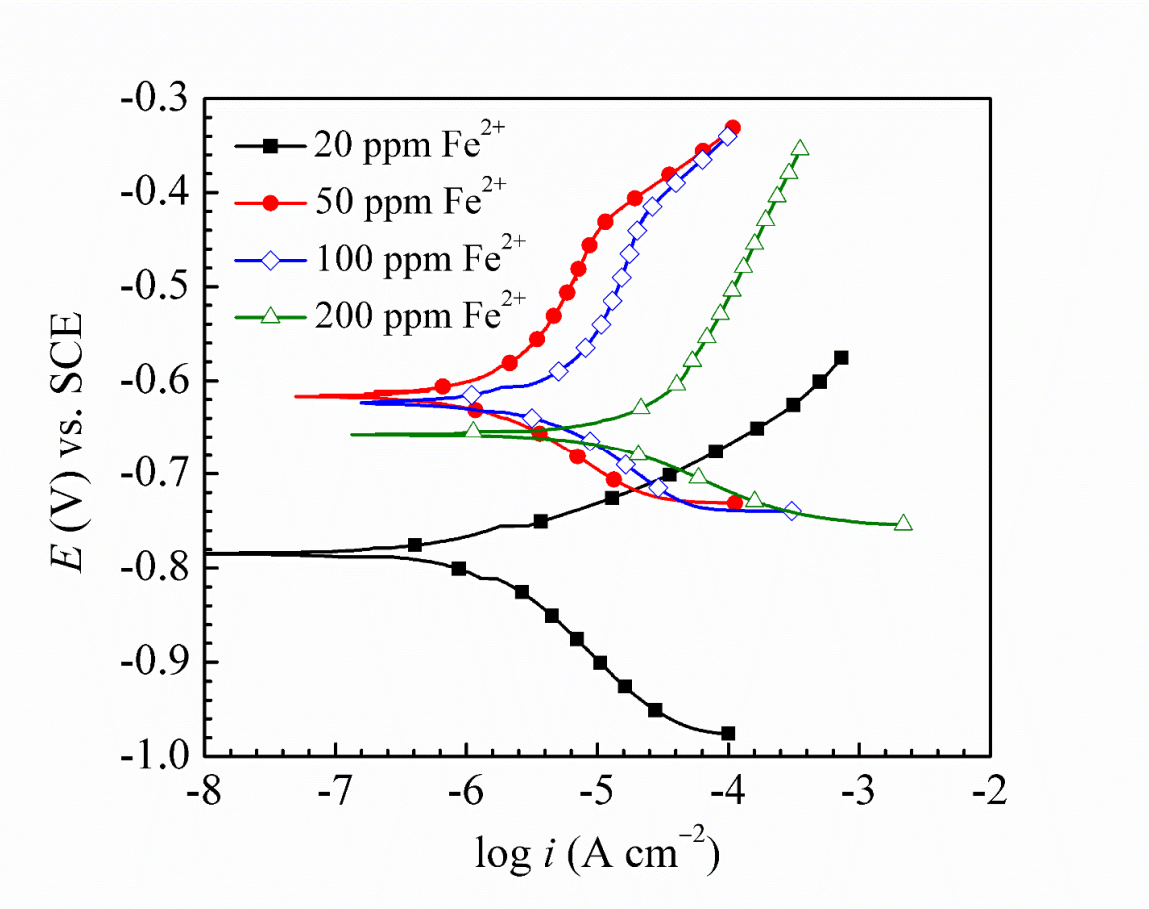

Figure 38. PDS for coupons at the end of the 7-day incubation with different initial Fe^{2+} concentrations.

Table 6. Electrochemical parameters calculated from PDS obtained at the end of the 7-day incubation (The standard deviation calculated from 3 independent samples from 3 different vials in 3 different experimental batches.)

Fe^{2+} concentration	E_{corr} (mV) vs. SCE	β_a (mV/dec)	β_c (mV/dec)	i_{corr} ($\mu A/cm^2$)
20 ppm	−775 ± 21	66 ± 5	131 ± 14	1.4 ± 0.2
50 ppm	−616 ± 17	218 ± 12	94 ± 11	2.1 ± 0.3
100 ppm	−624 ± 15	314 ± 17	125 ± 13	6.4 ± 0.7
200 ppm	−663 ± 18	258 ± 15	78 ± 9	20.3 ± 2.6

Although an increased initial Fe^{2+} concentration took out more sulfide through FeS precipitation as seen in Figure 27, the dissolved *[*H_2S*]* remained higher (Figure 29) because there were more planktonic and sessile cells producing more H_2S (Figures 28 and 30). Thus, the better SRB growth was obviously not because of a lower dissolved *[*H_2S*]* as in a previous work using a larger headspace volume to allow H_2S to escape. One speculated mechanism for H_2S toxicity toward SRB cells is that the precipitation of FeS by H_2S makes Fe^{2+} less available for the functioning of ferredoxin and cytochrome *c* enzymes [139,140]. Therefore, increasing the Fe^{2+} concentration in the culture medium helped counter the cytotoxicity of H_2S by maintaining the supply of Fe^{2+} for growth, which resulted in more planktonic and sessile SRB cells as shown in Figures 28 and 30. Citrate is actually used in ATCC 1249 culture medium for SRB not as organic carbon, but as a chelator to help counter the loss of Fe^{2+} to FeS precipitation [143,144]. Because SRB MIC of carbon steel belongs to EET-MIC [48,76] and ferredoxin and cytochrome *c* mediate the electron transport chain, there was also a possibility that increased Fe^{2+} could help maintain the electron transport chain, leading to more uptake of electrons from elemental iron.

After the 7-day incubation, the weight loss for 200 ppm initial Fe^{2+} concentration was 5 times of that for 20 ppm initial Fe^{2+} concentration (Figure 30). This ratio is much closer to the corresponding sessile cell count ratio of 4.7 (Figure 30) than the corresponding planktonic cell count ratio of 2.7 (Figure 28). This shows that sessile cells are more relevant to weight loss than planktonic cells. Furthermore, planktonic cells cannot harvest electrons from the carbon steel surface because of a liquid water gap. It is

reasonable to say that the increased sessile cell count was the primarily contributing factor for increased corrosion in this work.

Increasing the initial Fe^{2+} concentration from 100 ppm to 200 ppm, the sessile cell count increased by 43%, and this caused a weight loss increase of 45% (Fig. 4). This example demonstrates that a relatively small change in sessile cell count can cause a considerable change in weight loss. Unfortunately, in many cases, sessile cells cannot be enumerated using a hemocytometer due to low cell numbers that are below the hemocytometer detection limit (50,000 cells/mL). MPN has to be used with a much lower accuracy, sometimes down to one order of magnitude accuracy if only one roll of test tubes are used for enumeration [95]. This kind of low accuracy is incapable of revealing that increased corrosion weight losses are attributed to increased sessile cell counts as shown in this work. In the case of increased weight loss due to carbon source starvation, high-precision SRB sessile cell counting is not essential because starvation leads to much fewer (rather than much more) sessile cells [64].

It is interesting that in a previous study using the same culture medium and SRB, but with varied headspace volumes, a larger headspace reduced the dissolved $[H_2S]$ due to more H_2S escaping to the headspace, and it led to a higher sessile count and corrosion weight loss [76]. In this work, a higher initial Fe^{2+} concentration in general corresponded to a higher dissolved $[H_2S]$, but it also led to a higher sessile cell count and corrosion weight loss. In these two cases, corrosion increased but the former had a decreased $[H_2S]$ and the latter an increased $[H_2S]$. This conflicting $[H_2S]$ trend means that dissolved $[H_2S]$ could not be considered the underlining causal factor for increased corrosion weight loss. In both cases, the causal factor was the increased sessile cell count, one

owing to more H_2S escape to the headspace and the other Fe^{2+} detoxification. More sessile cells harvest more electrons, causing more weight loss. This work further strengthens the theory that H_2S corrosion is not the primary contributor to MIC of carbon steel by SRB. Rather, the electron harvest from elemental iron for energy production through EET is the main contributor [64].

6.4 Summary

In this work, the effects of initial Fe^{2+} concentration in the culture medium on dissolved biogenic *[*H_2S*]*, *D. vulgaris* planktonic and sessile cell counts, culture medium pH, corrosion weight loss and pit depth were systematically investigated. This work suggested that the initial Fe^{2+} concentration plays an important role in the MIC of carbon steel by SRB. A higher Fe^{2+} concentration in the culture medium countered the toxic effects of H_2S and promoted SRB planktonic and sessile cell growth. The increased sessile cells led to higher corrosion weight losses and deeper pits. This work confirmed that H_2S is not the primary contributing factor in carbon steel MIC by SRB. It also demonstrated that high-precision sessile cell counting is important in some mechanistic MIC investigations.

Chapter 7: Accelerated MIC of Carbon Steel Due to Growth Promotion by An Enhanced Oil Recovery Polymer

7.1 Introduction

The pressure in a reservoir decreases after many years of oil extraction. EOR is usually practiced in the oil and gas industry to increase reservoir pressure in order to sustain oil production [145]. Seawater is usually used in water flooding with other chemicals [146]. However, this practice can bring nutrients, some oxidants (e.g., sulfate) and microbes downhole [147]. This can promote microbial growth and cause MIC. A reservoir environment is originally anaerobic due to consumption of oxygen by organic matters [148]. Oxygen is usually removed from injection water to avoid corrosion to downhole tubing. Such an anaerobic environment can promote anaerobes such as sulfate reducing microbes (SRM) (i.e., SRB and SRA) to flourish since water injection brings sulfate [149]. Other microbes can also grow to form microbial communities [100,102]. SRM can produce biogenic H_2S causing reservoir souring [150]. In EOR operations, an organic polymer is often added. It is necessary to investigate if oilfield microbes can utilize polymers as a carbon source for growth thus increasing MIC [151].

Polymers are often added during water injection in EOR to increase the viscosity of injection fluid because a viscous injection water is more effective in pushing out viscous crude oil [152]. Partially hydrolyzed polyacrylamide (HPAM), which can tolerate high mechanical forces is a popular EOR polymer [153,154]. However, there is a concern that it might be used as a carbon or nitrogen source by downhole microbes [153]. It was found that the amide group in HPAM was hydrolyzed to the carboxyl group by an SRB, causing viscosity loss [155]. Some *Bacillus* spp. were found to use the HPAM's amide

group as a nitrogen source, and the carbon backbone as a carbon source [156]. It is foreseeable that a biofilm community containing multiple species can degrade HPAM more easily than pure strains [157]. Currently, there is no literature reporting the HPAM degradation on microbial growth and its impact on MIC. The data presented in this chapter have been published in Corrosion Science [111]. Copyright permissions for the tables and figures adopted in this chapter have been obtained from Elsevier.

7.2 Materials and Methods

Petronas provided a commercial HPAM-based polymer (cHPAM) tested in this work. An oilfield biofilm consortium (named Consortium II) supplied by a major oil company was used. The metagenomics data from Ecolyse, Inc. (College Station, TX, USA) are shown in Table 7. It indicates that this consortium contained SRB, fermentative and biodegradation microbes. An artificial seawater culture medium (supplemented with 100 ppm L-cysteine as an oxygen scavenger) with a composition (g/L) of $NaHCO_3$ 0.192, Na_2SO_4 3.917, $SrCl_2 \cdot 6H_2O$ 0.040, tri-sodium citrate 0.5, KBr 0.096, $CaCl_2 \cdot 2H_2O$ 1.469, KCl 0.664, $MgCl_2 \cdot 6H_2O$ 10.610, NaCl 23.476, $MgSO_4 \cdot H_2O$ 0.4, NH_4Cl 0.1, H_3BO_3 0.026, $Fe(NH_4)_2(SO_4)_2$ 0.1, $CaSO_4 \cdot 2H_2O$ 0.1, K_2HPO_4 0.05 was used to culture Consortium II. C1018 carbon steel coupons were used. Detailed information about coupon preparation, chemicals used in this work, sterilization, and deoxygenation are described in Appendix A.

Table 7. Metabolic assignments of dominant bacterial species

Species	Consortium II	Trait
Bacillus sp.	6.0%	Biosurfactant producing; Varies
Bacteroides sp.	1.4%	Fermentative bacteria
Garciella sp.	78.8%	NRB; Sulfidogen; TRB; SRB
Tepidibacter sp.	13.6%	Biodegradation (HC)

In each 125 mL anaerobic vial, 5 coupons, 100 mL medium, cHPAM and 1 mL Consortium II seed culture were added. The added cHPAM reached a final concentration of 1,000 ppm. The initial planktonic cell amount was about 10^6 cells/mL. The initial pH value in the medium was 7.0. Consortium II seed was cultured in enriched artificial seawater medium with 1 g/L yeast extract and 3.5 g/L sodium lactate. Thus the inoculation could bring a small amount of organic carbon to culture medium in the vials. Vials were sealed and incubated at 37^{o}C for 30 days anaerobically. During the 30-day incubation, a set of vials were used for obtaining planktonic cell counts. The details for planktonic cell counting are described in Section 5.2. After days 7, 14, 21 and 30, coupons were retrieved for SRB sessile cell counting using most probable number (MPN) method. Details about biofilm removal and MPN are described in Appendix A. After days 7, 14, 21 and 30, the culture medium viscosity was measured using a falling ball viscometer at 23^{o}C [158]. Biofilm observation was conducted with SEM and CLSM. The detailed SEM preparation and CLSM staining procedures are described in Appendix A.

After the 30-day incubation, corrosion products on coupons were analyzed using X-ray diffraction (XRD) (Bruker D8 Discovery, Bruker AXS GmbH, Karlsruhe, Germany). Weight loss and culture medium pH were measured after the 30-day incubation. The detailed coupon preparation for weight loss is described in Appendix A. After biofilms and corrosion products were removed using a fresh Clarke's solution,

SEM was used to examine coupon pit morphologies. IFM was used to measure the maximum pit depth after biofilms and corrosion products were removed.

Electrochemical tests in this work were conducted in 450 mL glass cells filled with 350 mL artificial seawater medium. OCP, LPR and EIS were conducted to monitor the corrosion process during the 30-day incubation. Detailed procedures are described in Appendix A.

7.3 Results and Discussion

7.3.1 Microbial growth and culture medium viscosity

The planktonic cell counts of samples incubated with and without cHPAM in the artificial seawater medium during the 30-day incubation are shown in Figure 39. For the control (0 ppm cHPAM), the planktonic cell count continuously decreased during the 30-day incubation. For the medium with 1,000 ppm cHPAM, the planktonic cell count decreased during the first 5 days. After that, the planktonic cell count started to increase. This result shows that it took some time for Consortium II to adapt to the large organic molecule. This was expected because it takes time for microbes to produce the necessary enzymes to digest a new nutrient.

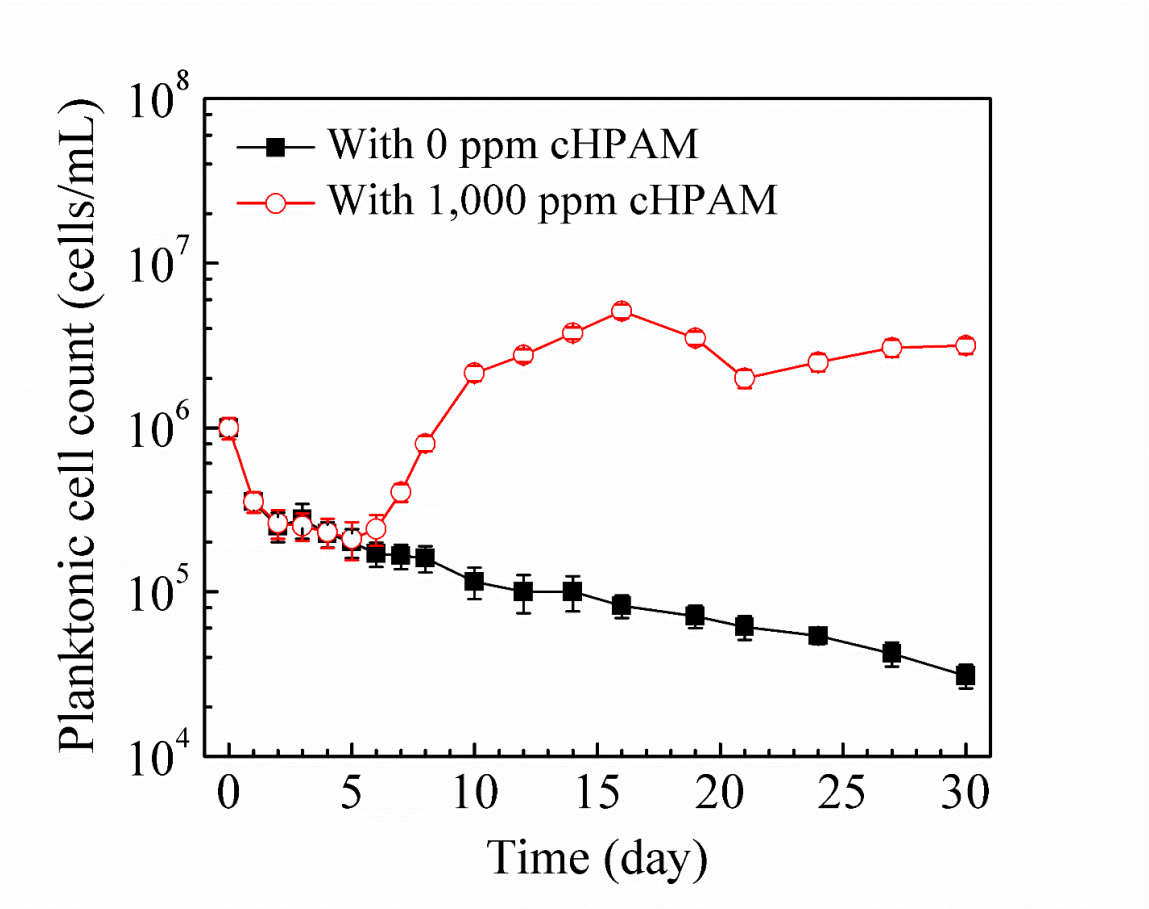

Figure 39. Planktonic cell counts incubated anaerobically at 37°C with and without cHPAM during the 30-day incubation. (The standard deviation calculated from 4 independent samples from 4 different vials in 4 different experimental batches.)

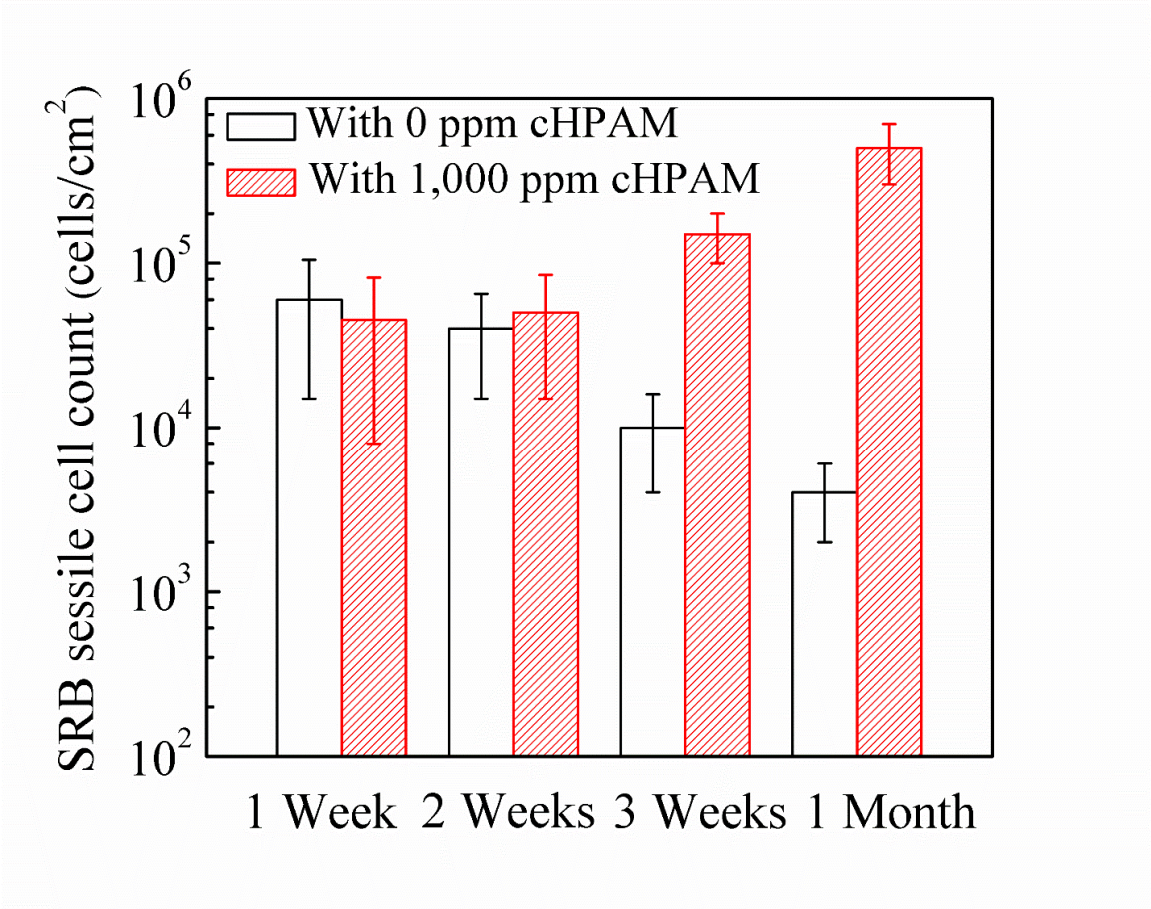

Figure 40. SRB sessile cell counts incubated anaerobically at 37°C with and without cHPAM during the 30-day incubation. (The standard deviation calculated from 4 independent samples from 4 different vials in 4 different experimental batches.)

The SRB sessile cell counts of samples incubated with and without cHPAM in the artificial seawater medium on days 7, 14, 21 and 30 are shown in Figure 40. The SRB sessile cell count of the control sample continuously decreased during the 30-day incubation. However, the SRB sessile cell count of samples incubated with cHPAM in the medium continuously increased. This showed that the SRB sessile cell growth benefited from the cHPAM utilization. In this work, only SRB in the consortium was

enumerated because SRB are the main bacteria in this consortium [100] and also SRB MIC was the primary corrosive factor [159].

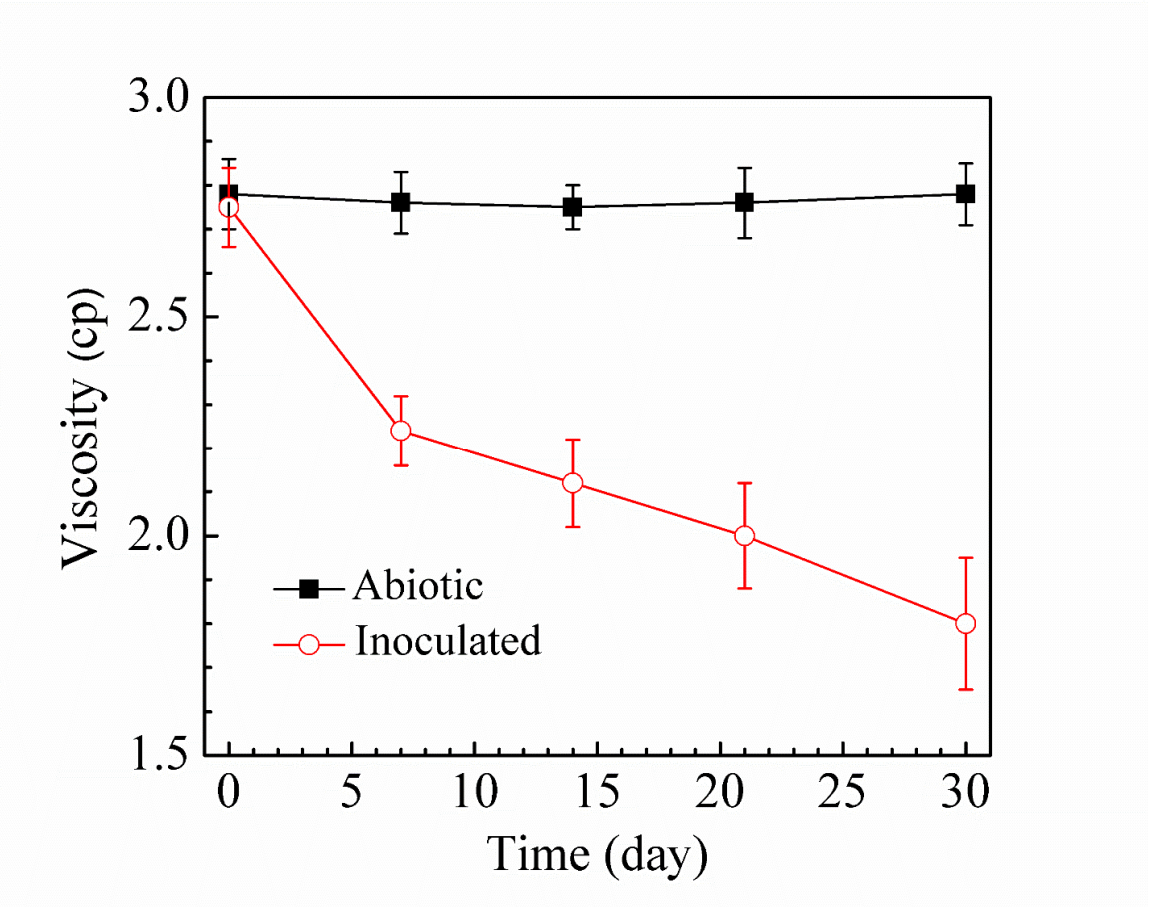

Figure 41. Viscosities of media (measured at 23°C) with and without inoculation during the 30-day incubation. (The standard deviation calculated from 3 independent samples from 3 different vials in 3 different experimental batches.)

Figure 41 shows the viscosities of samples incubated with 1,000 ppm cHPAM in the artificial seawater medium with and without inoculation during the 30-day incubation. In the control medium containing 1,000 ppm cHPAM without inoculation, the viscosity of the medium remained constant during the 30-day incubation. However, for the artificial seawater medium inoculated with Consortium II, the viscosity decreased with

time due to cHPAM consumption. After the 30-day incubation, the viscosity decreased by 34.5%. This proved the utilization of cHPAM in the medium because cHPAM degradation made the medium less viscous. Planktonic cell count and SRB sessile cell count are consistent with the viscosity loss.

7.3.2 Biofilm and corrosion product examinations

Figure 42 shows SEM images that provide visual differences. The coupon incubated in the medium with cHPAM had a FeS film covered on the surface. Biofilm SEM images of samples incubated with and without cHPAM in the inoculated artificial seawater medium after the 30-day incubation are shown in Figure 43(A, B). It confirms that the biofilm Consortium II was a mixed culture because different cell shapes are seen in SEM images. However, in both SEM images, numerous cells are seen without a clear difference between these two samples. This is because SEM images cannot tell live cells from dead cells in biofilms. 3D CLSM images are shown in Figure 43(A′, B′) for samples after the 30-day incubation. Figure 43A′ shows that sessile cells on the coupon incubated in the artificial seawater medium without cHPAM were mostly dead cells (red dots). This is due to a lack of organic carbon in the medium. In comparison, sessile cells on the coupon incubated with cHPAM in the medium were mostly live cells (green dots) as shown in Figure 43B′. The biofilm thickness of the sample incubated with cHPAM was also larger than that of the sample incubated without cHPAM as shown in Figure 43(A′, B′). CLSM images generally corroborate the SRB sessile cell count data in Figure 40.

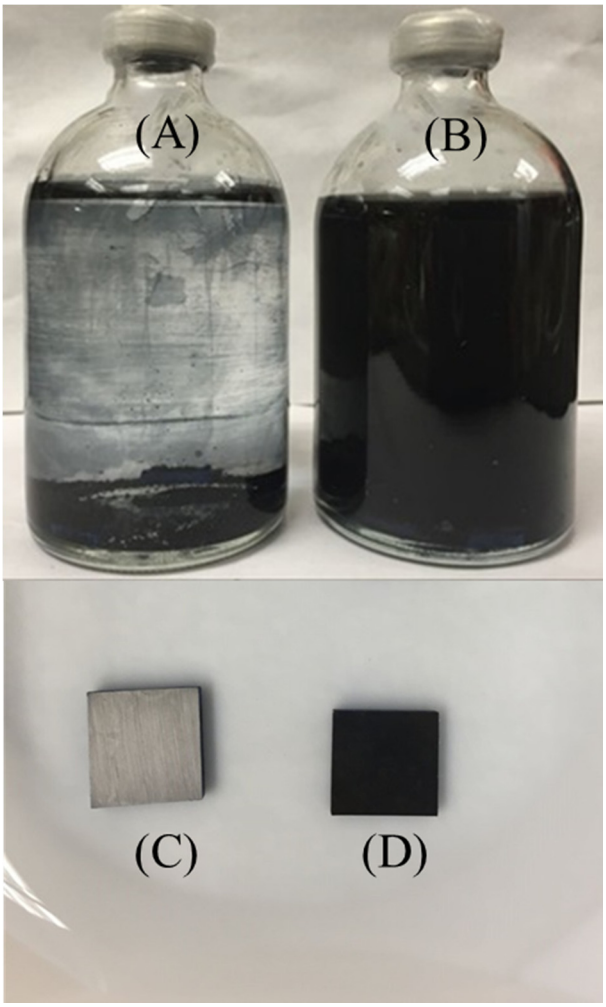

Figure 42. Images (top) of 125 mL anaerobic vials after the 30-day incubation in artificial seawater medium inoculated with Consortium II: (A) Growth without cHPAM in the medium, and (B) growth with cHPAM in the medium. Bottom images are coupons after the 30-day incubation: (C) Incubated without cHPAM in the medium, and (D) incubated with cHPAM in the medium.

The main corrosion products on coupons incubated with and without cHPAM in the inoculated artificial seawater medium after the 30-day incubation were identified as iron sulfides by XRD in Figure 44. Iron sulfides on the coupon incubated in the artificial

seawater medium without cHPAM were mackinawite (FeS) and pyrite (FeS_2). Mackinawite, pyrrhotite ($Fe_{1-x}S$, $0 \leq x \leq 0.17$) and pyrite were found among the iron sulfides on the coupon incubated in the artificial seawater medium with cHPAM. It was found in both cases that mackinawite was the main corrosion product.

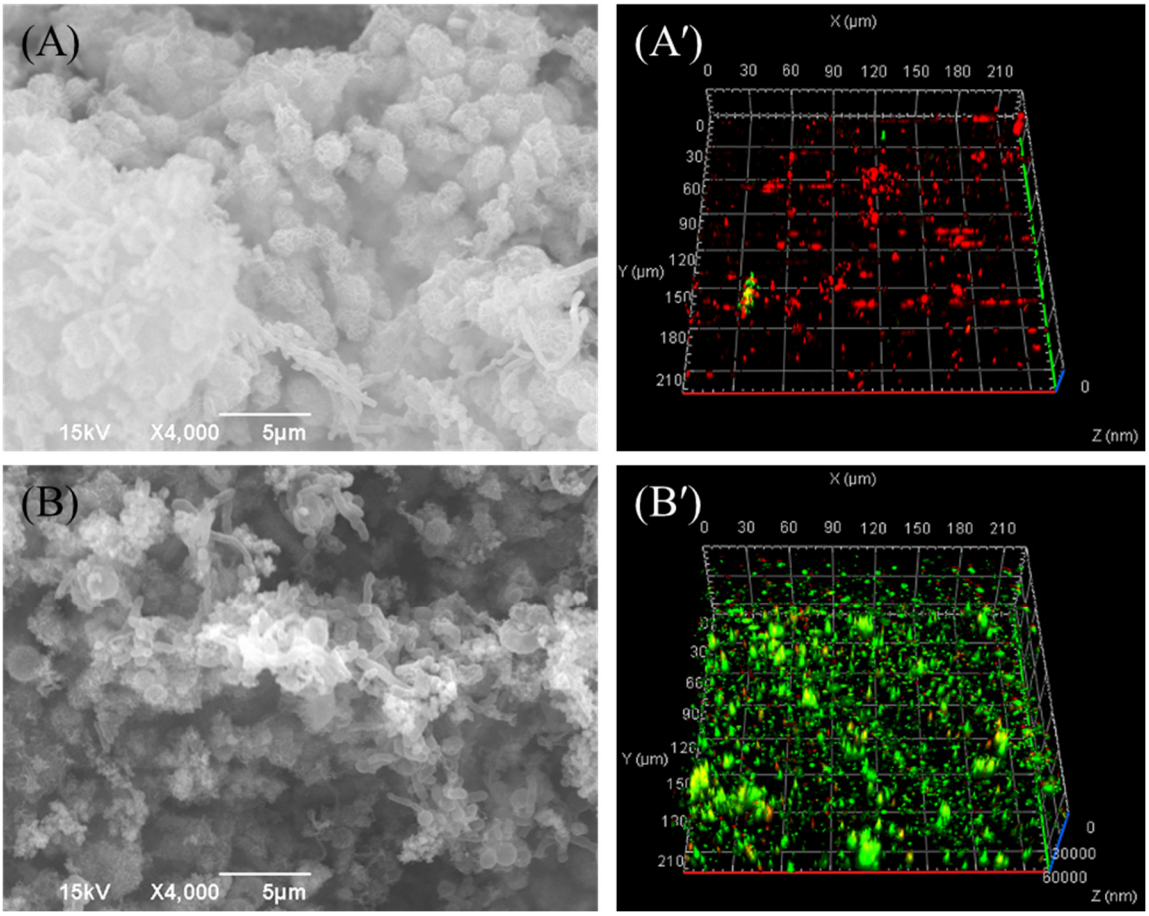

Figure 43. Biofilm SEM images on coupons incubated without (A) and with (B) cHPAM after the 30-day incubation. Biofilm CLSM images on coupons incubated without (A′) and with (B′) cHPAM after the 30-day incubation.

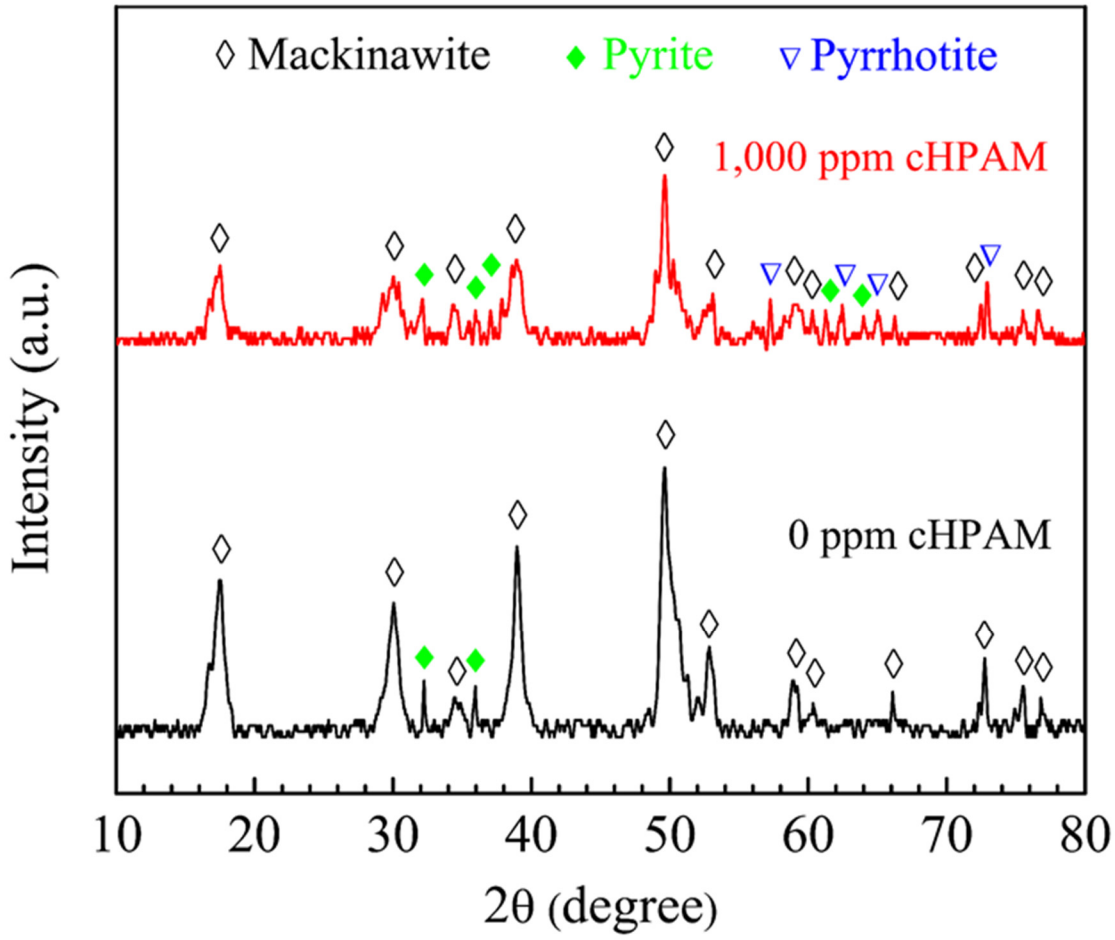

Figure 44. Corrosion products on coupons incubated with and without cHPAM after the 30-day incubation.

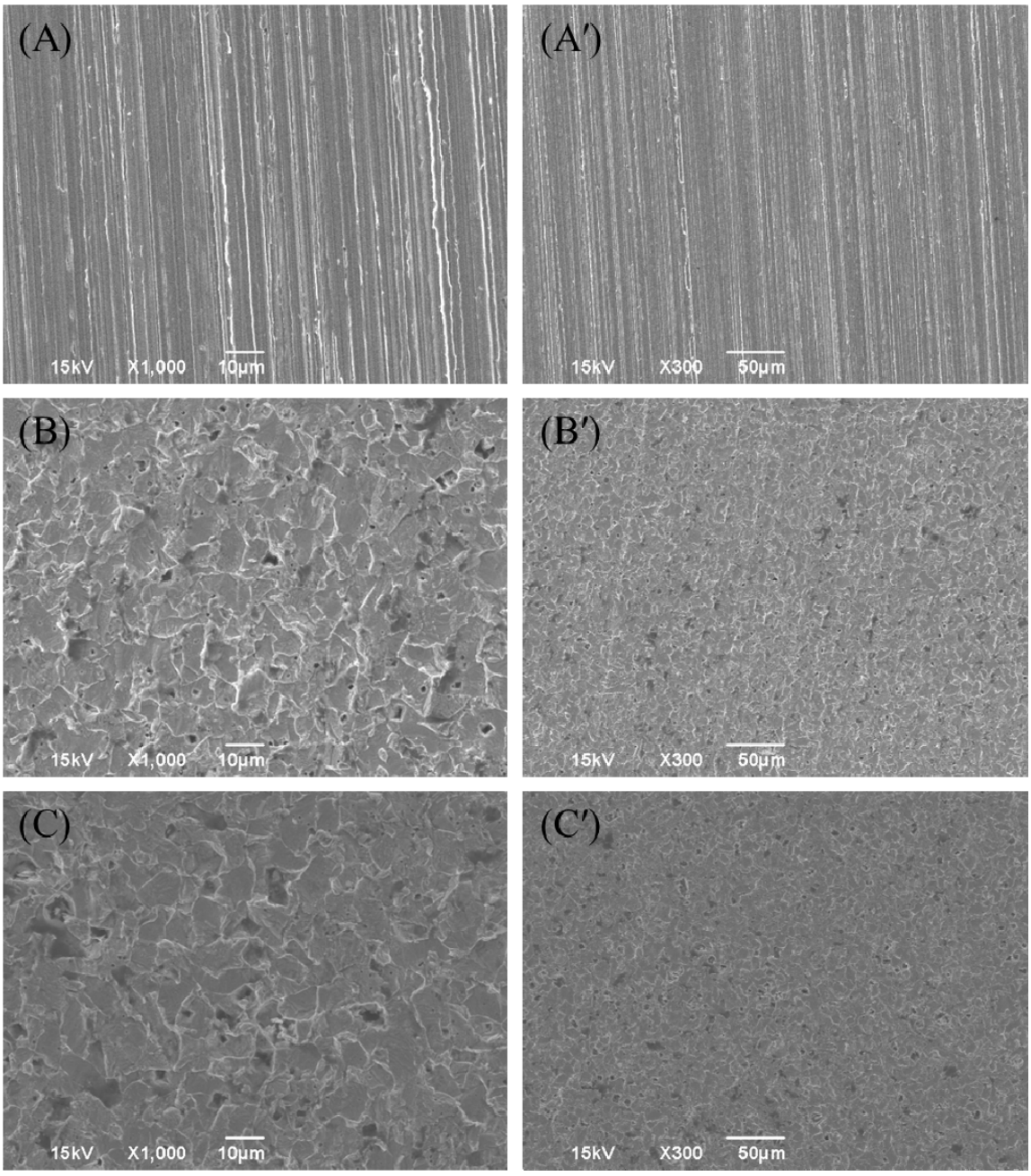

Figure 45. SEM pit morphologies for coupons incubated in abiotic medium with 1,000 ppm cHPAM (A, A′), incubated in inoculated medium without 1,000 ppm cHPAM (B, B′), and incubated in inoculated medium with 1,000 ppm cHPAM (C, C′) after the 30-day incubation.

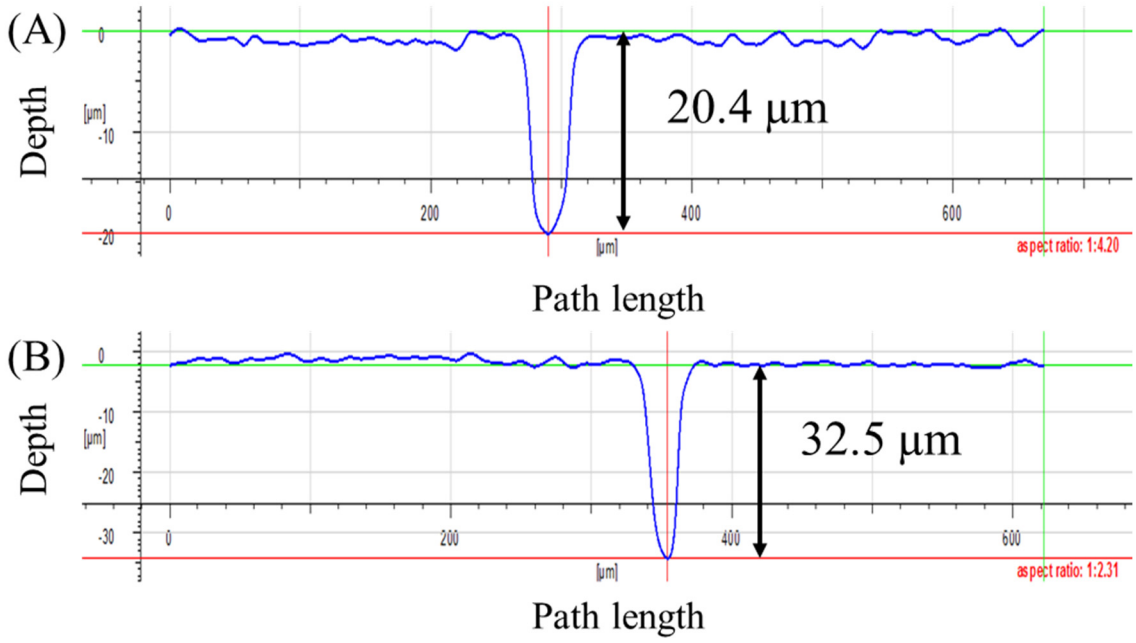

Figure 46. Maximum pit depths for coupons incubated in inoculated medium without 1,000 ppm cHPAM (A), and incubated in inoculated medium with 1,000 ppm cHPAM (B) after the 30-day incubation.

7.3.3 Corrosion analyses

The average weight losses of samples incubated in the abiotic control, inoculated without cHPAM and inoculated with cHPAM in the artificial seawater medium after the 30-day incubation were 0.3 mg/cm^2, 3.3 mg/cm^2 and 4.1 mg/cm^2, respectively. The weight loss was negligible for the abiotic control, suggesting the sterile artificial seawater at pH 7.0 was not corrosive under anaerobic condition during the 30-day incubation. The coupon weight loss in the vial with cHPAM in the medium was higher than that in the vial without cHPAM, suggesting that the cHPAM-enhanced SRB sessile cell growth led to more severe corrosion.

The culture medium pH values after the 30-day incubation without and with cHPAM in the artificial seawater medium were 7.1 ± 0.3 and 7.5 ± 0.4, respectively. With such near-neutral medium pH, acid corrosion was not a contributing factor.

SEM was used to examine pit morphologies on the coupon surface after the biofilm and corrosion products were removed using Clarke's solution. The abiotic control coupon surface morphology had negligible corrosion after 30 days of incubation as shown in Figure 45(A, A′). This corroborates the abiotic weight loss data. After the 30-day incubation, many pits are seen on the surface of the coupon that was incubated without cHPAM in the artificial seawater medium as shown in Figure 45(B, B′). More and bigger pits are seen on coupons incubated with cHPAM (Figure 45(C, C′)). The SEM pitting information in Figure 45 corroborate the weight loss data.

Figure 46 shows the maximum pit depth data after the 30-day incubation with and without cHPAM in the artificial seawater medium. After the 30-day incubation, the maximum pit depth for the incubation without cHPAM in the artificial seawater medium was 20.4 μm. The sample incubated with cHPAM in the artificial seawater medium was 32.5 μm. The pit depth data here are consistent with SEM pit morphologies in Figure 45.

In this work, the culture medium pH in the medium with and without cHPAM were more than 7 after the 30-day incubation. The weight loss data and SEM pitting data also confirm that the main corrosion cause was SRB, which utilized electrons from iron oxidation for sulfate reduction under biocatalysis as indicated in Reactions 2 and 3. The corrosion products identified from XRD were mainly iron sulfides, confirming SRB corrosion.

7.3.4 Electrochemical measurements

Figure 47A shows OCP versus time during the 30-day incubation with and without cHPAM in the inoculated artificial seawater medium. In both cases, OCP values of all samples generally shifted to the positive direction and then kept steady during the 30-day incubation. R_p versus time during the 30-day incubation with and without cHPAM in the inoculated artificial seawater medium is shown in Figure 47B. The R_p values of all samples decreased and then kept steady during the 30-day incubation. A lower polarization resistance was observed in the vial with cHPAM compared with that incubated without cHPAM in the inoculated artificial seawater medium, suggesting increased corrosion. This shows that cHPAM utilization promoted microbial growth thus causing more severe corrosion. LPR results corroborate the weight loss data trend.

EIS was measured on days 4, 7, 14, 21 and 30 during the 30-day incubation with and without cHPAM in the inoculated artificial seawater medium. Figure 48 shows the Nyquist and Bode plots. On days 7, 14, 21 and 30, the Nyquist semi-circle diameters of coupons incubated with cHPAM were smaller than those incubated without cHPAM, suggesting higher corrosion with polymer utilization. On day 4, these two were similar. This was consistent with the planktonic cell count in Figure 39 indicating that it took time for microbes to adapt to the large molecule and start to use it. After 14 days of incubation, the Nyquist plot semi-circle diameters of the coupon incubated without cHPAM did not change much, indicating small corrosion change. A similar trend was found for coupons incubated with cHPAM.

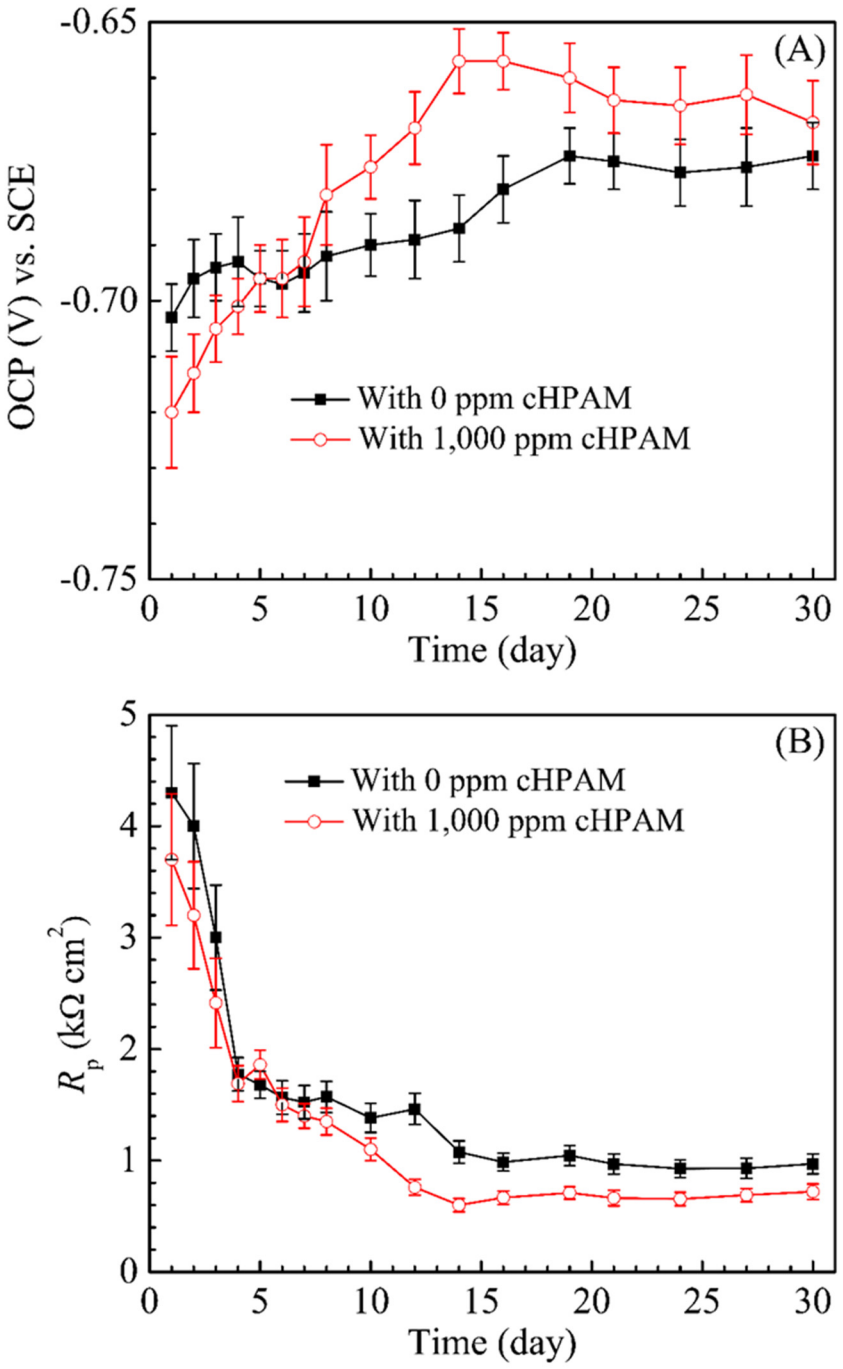

Figure 47. Variations of OCP (A) and polarization resistance (B) versus time for coupons incubated in inoculated media with and without cHPAM during the 30-day incubation. (The standard deviation calculated from 3 independent samples in 3 different experimental batches.)

The EIS data were fitted with the two-time constant model shown in Figure 16. The electrochemical parameters from the fitting are shown in Table 8. It shows that R_{ct} values were much larger than R_b values, indicating charge transfer resistance control of the corrosion process. The charge transfer resistances of coupons incubated with cHPAM were lower than those of samples incubated without cHPAM in the artificial seawater medium. The EIS results again confirm that the polymer utilization led to more corrosion.

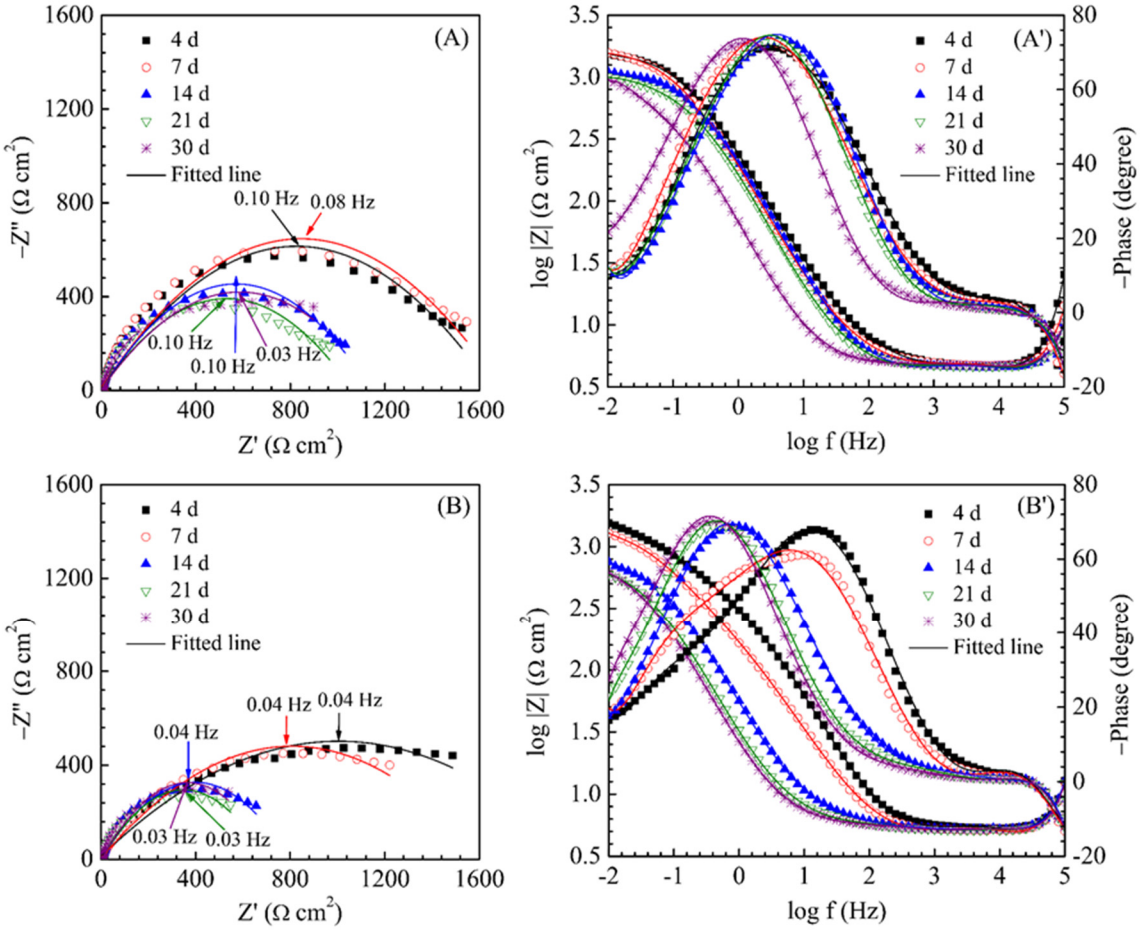

Figure 48. Nyquist and Bode plots for samples incubated in inoculated media without (A, A′) and with (B, B′) cHPAM during the 30-day incubation. (EIS was conducted under stable OCP between 10^{-2} and 10^{5} Hz with a sinusoidal voltage signal (10 mV amplitude).)

Table 8. Fitted EIS parameters of coupons incubated with and without cHPAM during the 30-day incubation. (The standard deviation calculated from 3 independent samples in 3 different experimental batches.)

Duration (day)	R_s (Ω cm^2)	Y_b (Ω^{-1} cm^{-2} s^n)	n_b	R_b (Ω cm^2)	Y_{dl} (Ω^{-1} cm^{-2} s^n)	n_{dl}	R_{ct} (Ω cm^2)
With 0 ppm cHPAM (inoculated)							
4	9 ± 1	0.00041 ± 0.00011	0.91 ± 0.08	81 ± 6	0.00052 ± 0.00013	0.71 ± 0.08	1494 ± 212
7	7 ± 2	0.00052 ± 0.00008	0.93 ± 0.05	69 ± 8	0.00061 ± 0.00015	0.76 ± 0.05	1580 ± 161
14	5 ± 1	0.00048 ± 0.00011	0.92 ± 0.06	48 ± 7	0.00066 ± 0.00014	0.67 ± 0.07	1098 ± 108
21	6 ± 1	0.00071 ± 0.00022	0.94 ± 0.03	33 ± 6	0.00069 ± 0.00019	0.63 ± 0.04	1012 ± 85
30	6 ± 1	0.00162 ± 0.00043	0.91 ± 0.07	21 ± 5	0.00151 ± 0.00051	0.53 ± 0.07	1161 ± 67
With 1,000 ppm cHPAM (inoculated)							
4	6 ± 1	0.00025 ± 0.00007	0.94 ± 0.05	41 ± 7	0.00101 ± 0.00039	0.51 ± 0.06	1862 ± 241
7	7 ± 2	0.00048 ± 0.00011	0.95 ± 0.04	38 ± 7	0.00151 ± 0.00041	0.56 ± 0.12	1322 ± 151
14	6 ± 1	0.00159 ± 0.00056	0.91 ± 0.06	28 ± 6	0.00216 ± 0.00055	0.71 ± 0.09	782 ± 81
21	6 ± 1	0.00629 ± 0.00148	0.85 ± 0.08	22 ± 5	0.00221 ± 0.00061	0.91 ± 0.07	746 ± 68
30	6 ± 1	0.00769 ± 0.00216	0.89 ± 0.09	14 ± 3	0.13976 ± 0.04395	0.92 ± 0.06	762 ± 79

7.4 Summary

This work showed that a commercial EOR polymer was degraded by an oilfield biofilm consortium in an artificial seawater medium during a 30-day incubation and this resulted in reduced viscosity by 34.5%. The utilization promoted planktonic cell growth in the bulk fluid and SRB sessile cell growth on C1018 carbon steel coupons. The better

SRB sessile cell growth led to more severe corrosion on carbon steel coupons. Electrochemical tests (LPR and EIS) corroborated the weight loss data and the pitting data trends. This corrosion study on the EOR polymer utilization on MIC will help field operators to select EOR polymers. It also points out that biocide dosing may be required.

Chapter 8: Enhanced Biocide Treatment by D-amino Acids against An Oilfield Biofilm and Its Corrosion on Carbon Steel in The Presence of Oilfield Chemicals

8.1 Introduction

Seawater injection in EOR brings water and nutrients downhole that promote microbial growth, leading to MIC. Microbes often live in a community that protects them from hazardous environments [100]. Comparing to planktonic cells, a much higher biocide concentration is needed to treat sessile cells in the field due to the protection of biofilms [160]. The repeated use of a biocide may promote persister cells that are resistant to biocide treatment. This may lead to higher biocide concentrations over time [85]. The high biocide concentrations may cause both environmental and economic issues. THPS is a commonly used biocide because this broad-spectrum biocide is considered green. High THPS dosages can also introduce a lot of sulfate that can precipitate Ba^{2+} in the drilling fluid, causing problematic scales downhole [100]. Thus, it is necessary to enhance THPS to treat problematic biofilms [14].

D-amino acids are natural products that can be found almost everywhere [90]. Recently, D-amino acids have been found to be able to disperse biofilms. For industrial biofilm consortia, a mixture of D-amino acids may be required since different microbes may have different responses to D-amino acids [100].

Glutaraldehyde is not compatible with D-amino acids because it is a cross-linking agent. During EOR, all chemicals such as polymers, surfactants, biocides, corrosion inhibitors and scale inhibitors are injected downhole in one batch. Thus, D-amino acids need to be compatible with them during the application. This work evaluated their performances as biocide enhancers in the presence of various oilfield chemicals. The data

presented in this chapter have been published in International Biodeterioration & Biodegradation [128]. Copyright permissions for the tables and figures used in this chapter have been obtained from Elsevier.

8.2 Materials and Methods

Biofilm Consortium II described in Section 7.2 was used in this work. Enriched artificial seawater (supplemented with 100 ppm L-cysteine as an oxygen scavenger) was used to culture Consortium II. The chemical composition (g/L) of the enriched artificial sweater is $NaHCO_3$ 0.192, Na_2SO_4 3.917, $SrCl_2 \cdot 6H_2O$ 0.040, tri-sodium citrate 0.5, KBr 0.096, $CaCl_2 \cdot 2H_2O$ 1.469, yeast extract 1, KCl 0.664, $MgCl_2 \cdot 6H_2O$ 10.610, NaCl 23.476, sodium lactate 3.5, $MgSO_4 \cdot H_2O$ 0.4, NH_4Cl 0.1, H_3BO_3 0.026, $Fe(NH_4)_2(SO_4)_2$ 0.5, $CaSO_4 \cdot 2H_2O$ 0.1, K_2HPO_4 0.05. cHPAM, a surfactant (alpha olefin sulfonate), a corrosion inhibitor (imidazoline salt), and a scale inhibitor (diethylene triamine penta (methylene phosphonic acid) (DTPMPA)) were provided by Petronas. An equimolar D-amino acid mixture (D-mix) of four D-amino acids containing D-tyr, D-met, D-trp, and D-leu was used. C1018 carbon steel coupons were used. Detailed information about coupon preparation, chemical suppliers, medium sterilization, deoxygenation and anaerobic manipulation are described in Appendix A.

In each 125 mL anaerobic vial, 5 coupons, 100 mL medium, and 1 mL Consortium II seed culture were added. The initial planktonic cell amount was about 10^6 cells/mL. The initial pH value in the medium was 7.0. Vials were sealed and incubated at 37^{o}C for 4 days. It was found that 4 days was enough to grow a mature biofilm on carbon steel coupons. After that, anaerobic vials were opened in an anaerobic chamber to add different chemicals to treat the mature biofilms. One thousand ppm cHPAM, 200 ppm

imidazoline salt, 5,000 ppm alpha olefin sulfonate, and 15 ppm DTPMPA were added to all vials. The biocide alone treatment vial contained 100 ppm THPS without D-amino acids for biofilm treatment. The enhanced biocide treatment vial contained 100 ppm THPS and 100 ppm D-mix. All treatment chemicals were added at the same time. Vials were sealed again and incubated at 37°C for another 7 days (Figure 49). The abiotic control contained all chemicals without inoculation.

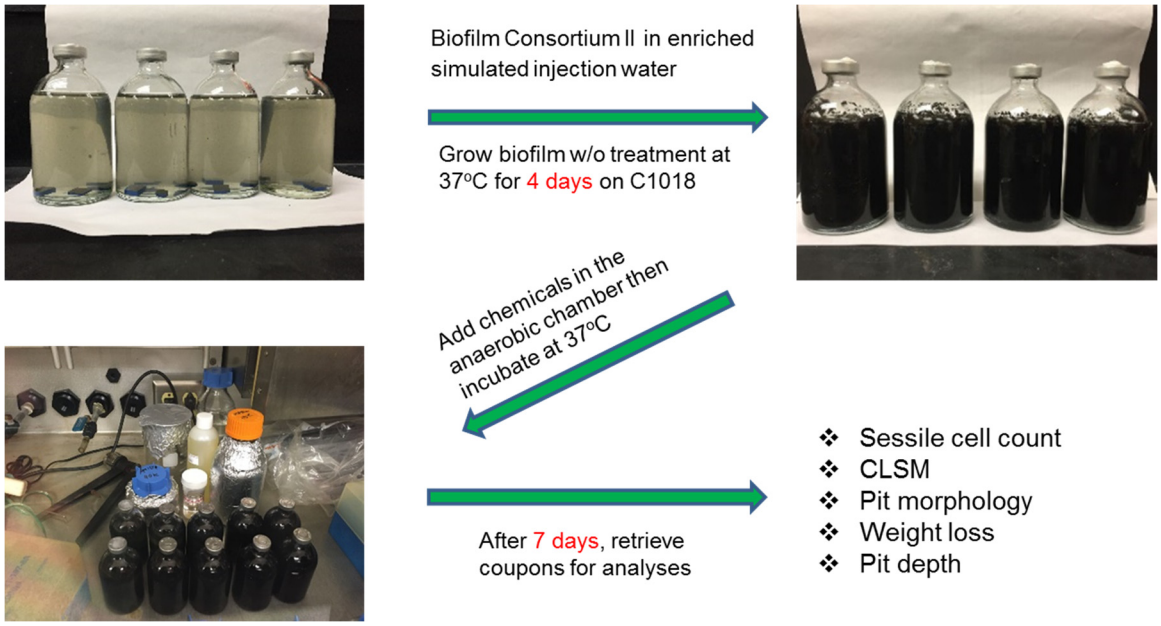

Figure 49. Experimental setup of tests conducted in anaerobic vials with different treatment chemicals.

After the 7-day incubation, coupons were retrieved for APB, general heterotrophic bacteria (GHB), and SRB sessile cell counts using MPN method. Details about biofilm removal and MPN enumeration are described in Appendix A. Biofilm observation was conducted with SEM and CLSM. The detailed SEM preparation and CLSM staining procedures are described in Appendix A.

After the 4-day pre-growth and the additional 7-day incubation periods, weight loss and culture medium pH were measured. The detailed coupon preparation procedure for weight loss is described in Appendix A. After biofilms and corrosion products were removed using Clarke's solution, SEM was used to examine pit morphology. IFM was used to find maximum pit depths.

Electrochemical tests in this work were conducted in 450 mL glass cells filled with 350 mL artificial seawater medium (supplemented with 100 ppm L-cysteine). OCP, LPR, EIS and PDS were conducted to monitor the corrosion process during the additional 7-day incubation. Detailed procedures are described in Appendix A.

8.3 Results and Discussion

8.3.1 Sessile cell count

The sessile cell counts on coupons incubated in media with and without biocide treatment after the additional 7-day incubation are shown in Figure 50. The SRB, APB and GHB sessile cell counts on the control coupons were 3.5×10^6 cells/cm^2, 1.6×10^5 cells/cm^2, and 6.7×10^5 cells/cm^2 after the 7-day incubation period. When 100 ppm THPS was added, this treatment achieved a 1-log reduction in APB and GHB sessile cell counts and a 1.5-log reduction in SRB sessile cell count compared with the no treatment control. The combination of 100 ppm THPS + 100 ppm D-mix achieved an extra 1-log reduction in APB and GHB sessile cell counts and an extra 2.5-log reduction in sessile cell count vs. the 100 ppm THPS alone treatment. Sessile cell data in Figure 50 indicate that THPS was enhanced by D-amino acids against biofilm Consortium II in the presence of oilfield chemicals. This means that D-amino acids were chemically compatible with

those oilfield chemicals tested in this study because the efficacy was comparable to those achieved in a test without oilfield chemicals [100].

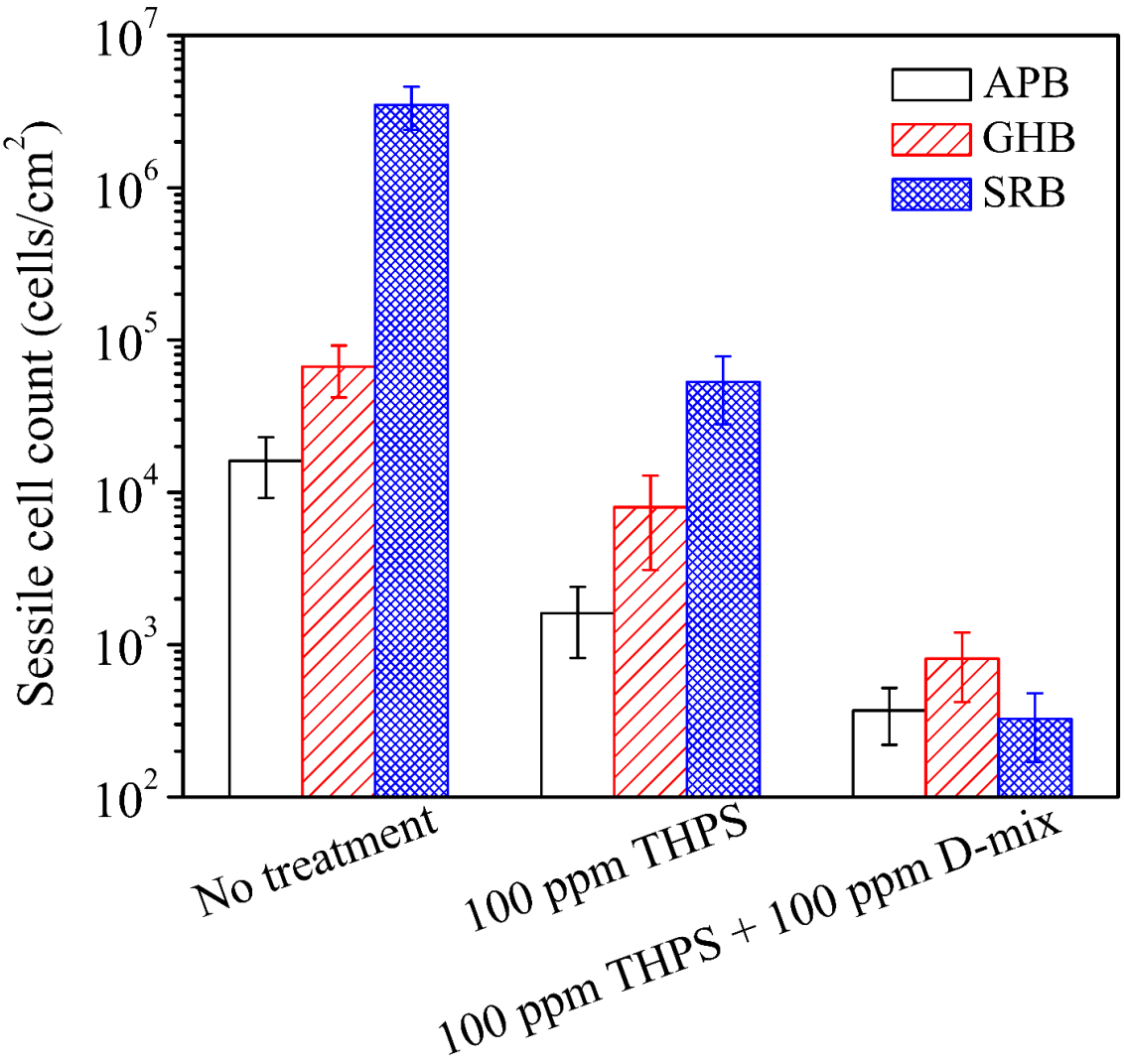

Figure 50. Sessile cell counts (APB, SRB and GHB) on coupons incubated anaerobically in media with and without biocide treatment after 7-day incubation. (The standard deviation calculated from 4 independent samples from 4 different vials in 4 different experimental batches.)

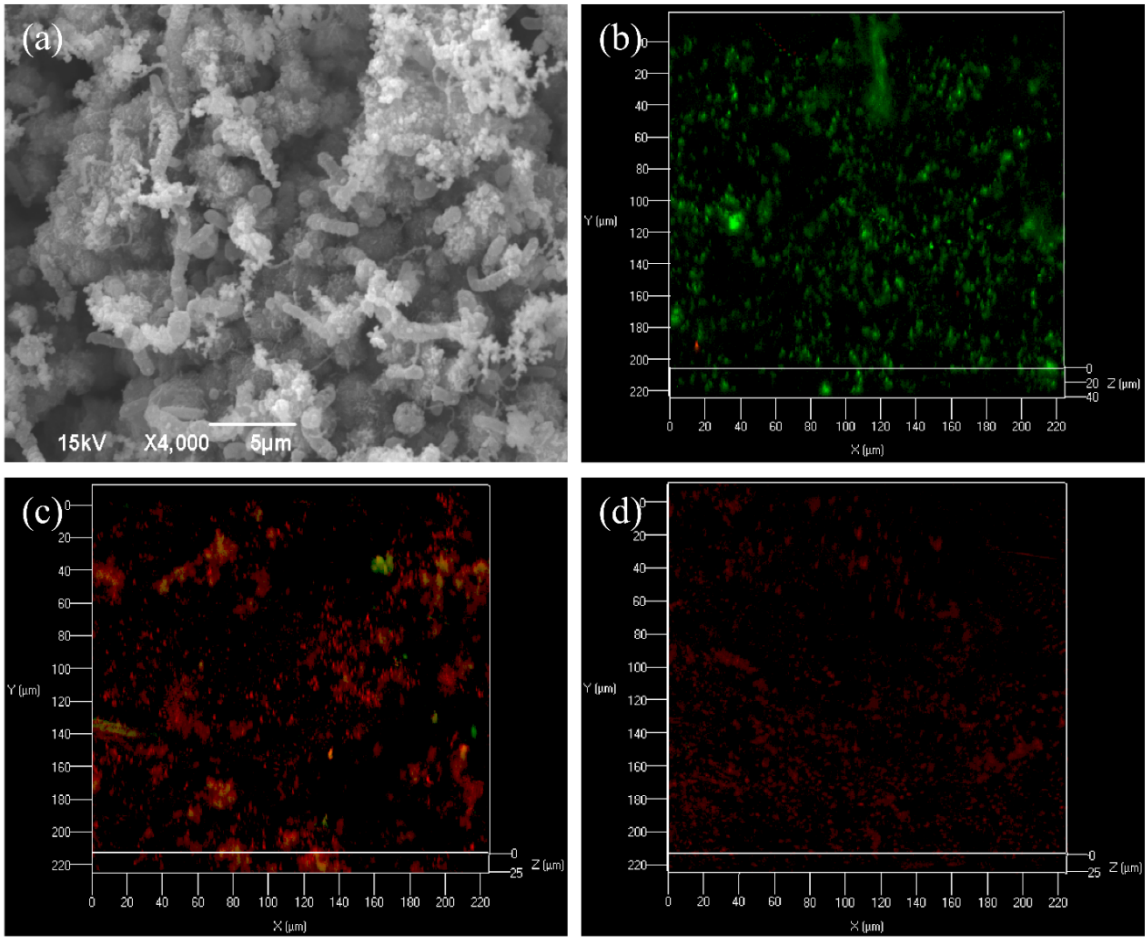

Figure 51. Biofilm SEM image of the no treatment control after the 7-day incubation test (a). Biofilm CLSM images on coupons incubated with: no treatment (control) (b), 100 ppm THPS (c), and 100 ppm THPS + 100 ppm D-mix (d) after the 7-day incubation period.

8.3.2 Biofilm observation

Biofilm SEM images of samples incubated with no treatment in the enriched artificial seawater medium after the additional 7-day incubation are shown in Figure 51a. It confirms that biofilm Consortium II was a mixed culture because different cell shapes are seen in the SEM images. The SEM images of coupons with biocide treatments are not

shown. They were all similar with abundant sessile cells on the coupon surface. This is because after biocide treatment, killed sessile cells still remain on the coupon surface without detachment. SEM biofilm images cannot tell the difference (i.e., show the difference between live and dead cells). 3D CLSM images are shown in Figure 51(b,c,d) for samples after the 7-day incubation. Figure 51b shows that sessile cells on the coupon incubated in the artificial seawater medium without treatment were mostly live cells. Many sessile cells were killed as shown in Figure 51c when 100 ppm THPS was added. It is difficult to find live cells on coupons treated with the combination of 100 ppm THPS + 100 ppm D-mix, suggesting enhanced THPS efficacy by D-amino acids. CLSM results qualitatively corroborate the sessile cell counts in Figure 50.

8.3.3 Corrosion analyses

The average weight losses for the abiotic control, 4-day pre-growth without treatment, additional 7-day incubation with no treatment control, additional 7-day incubation with 100 ppm THPS alone treatment, and additional 7-day incubation with 100 ppm THPS + 100 ppm D-mix treatment were 0.2 mg/cm^2, 1.0 mg/cm^2, 3.2 mg/cm^2, 2.4 mg/cm^2, and 1.8 mg/cm^2, respectively (Figure 52). The weight loss was negligible for the abiotic control, suggesting that the abiotic medium at pH 7.0 was not corrosive under anaerobic condition. The net weight losses for the no treatment control, 100 ppm THPS alone treatment, and 100 ppm THPS + 100 ppm D-mix treatment during the 7-day incubation were 2.2 mg/cm^2, 1.4 mg/cm^2, and 0.8 mg/cm^2, respectively, after deducting the 4-day pre-growth. The data indicate that 100 ppm THPS reduced the weight loss by 36.4% compared with the untreated control. While the combination of 100 ppm THPS + 100 ppm D-mix reduced the weight loss by 63.6% compared with the untreated control.

Weight loss results here clearly show that THPS was enhanced by D-amino acids in the mitigation of Consortium II on carbon steel. The culture medium pH of the abiotic control did not change as shown in Figure 52. The culture medium pH values after the 4-day pre-growth and after the 7-day incubation with and without biocide treatment in the enriched artificial seawater medium were all above 6.5. With such near-neutral pH, acid corrosion was not a factor.

Figure 53 shows SEM images that were used to examine pit morphologies on the coupons for abiotic control, after 4-day pre-growth without treatment, and after the additional 7-day incubation with and without treatment. The abiotic control coupon surface morphology had negligible corrosion after 11 days of incubation as shown in Figure 53b. This corroborates the abiotic weight loss data. After the 4-day pre-growth, some small pits were found on the coupon surface (Figure 53a). For the coupon incubated with no treatment (control) after the additional 7-day incubation, many large pits are seen in Figure 53c. Fewer and smaller pits are seen in Figure 53d on the coupon when treated with 100 ppm THPS alone. After the treatment with 100 ppm THPS + 100 ppm D-mix, fewer pits are seen in Figure 53e compared with 100 ppm THPS alone treatment in Figure 53d. The SEM pitting information in Figure 53 corroborates the weight loss data.

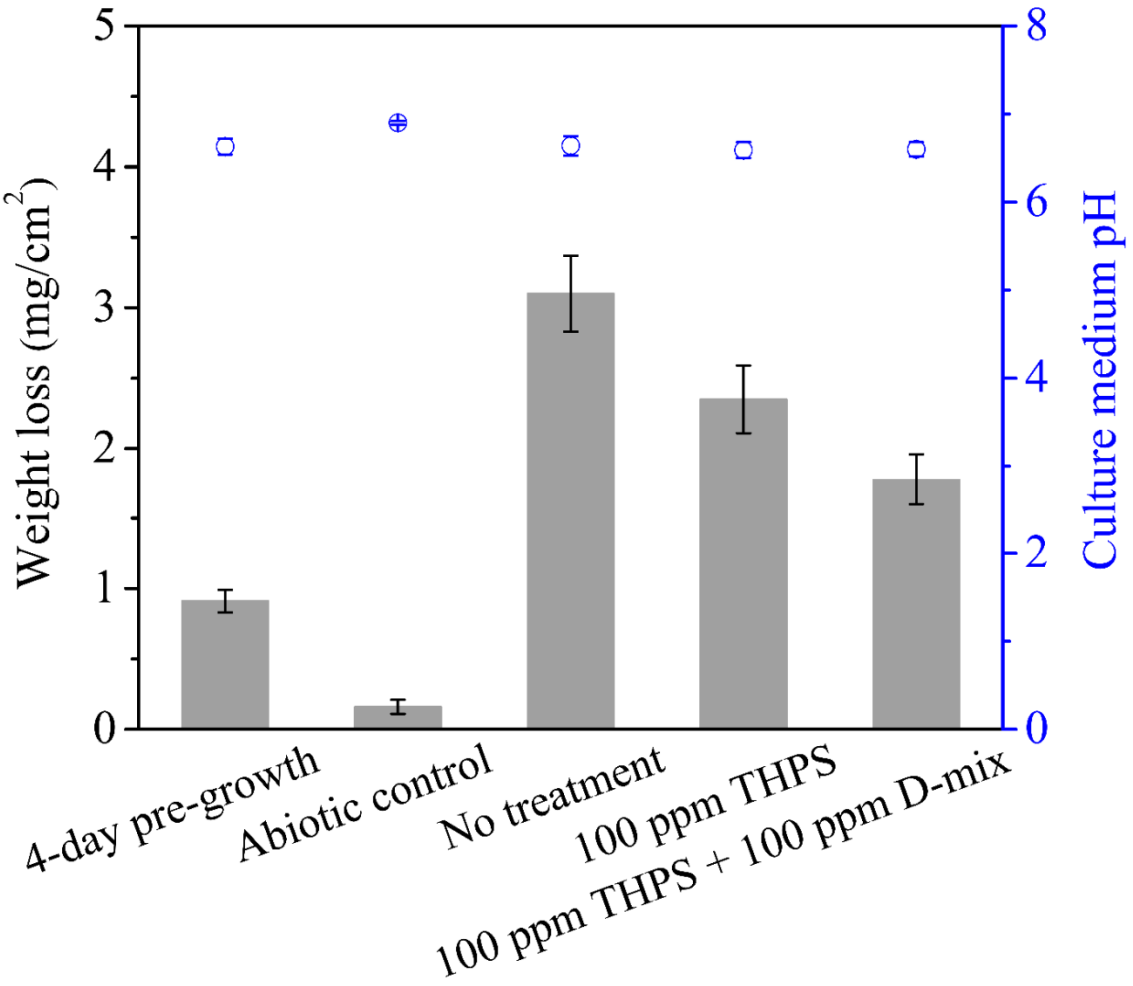

Figure 52. Weight losses of coupons (bars) and culture medium pH values (circles) after the 4-day pre-growth, and after additional 7-day incubation for abiotic control, and coupons incubated with and without treatment. (The standard deviation of weight loss calculated from 9 independent samples from 3 different vials in 3 different experimental batches. The standard deviation of pH value calculated from 3 independent samples from 3 different vials in 3 different experimental batches.)

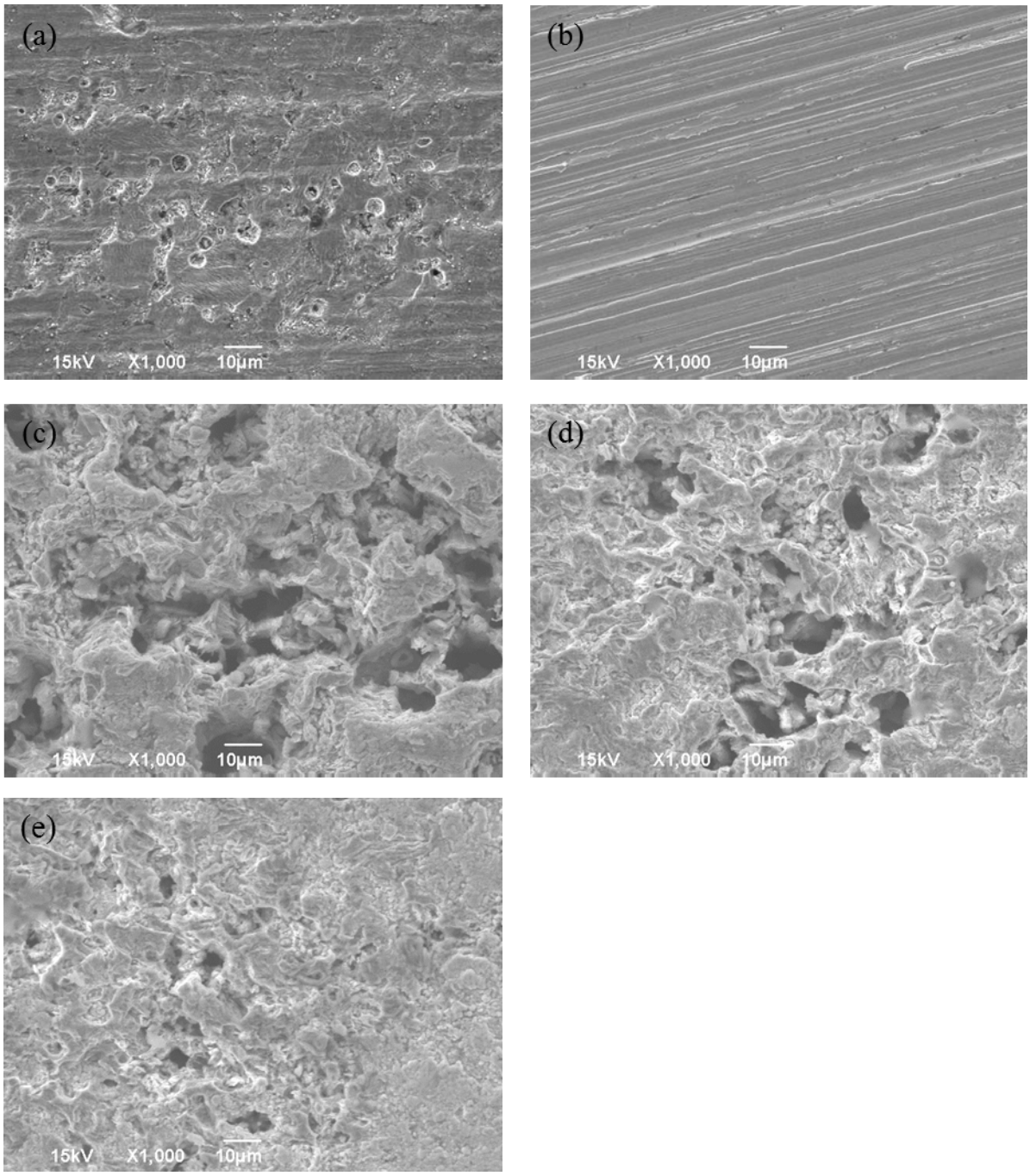

Figure 53. SEM pit images for coupons: after the 4-day pre-growth (a), after for 4 + 7 days in abiotic medium (no treatment) (b), after the 7-day incubation test with no treatment (control) (c), with 100 ppm THPS (d), and with 100 ppm THPS + 100 ppm D-mix (e).

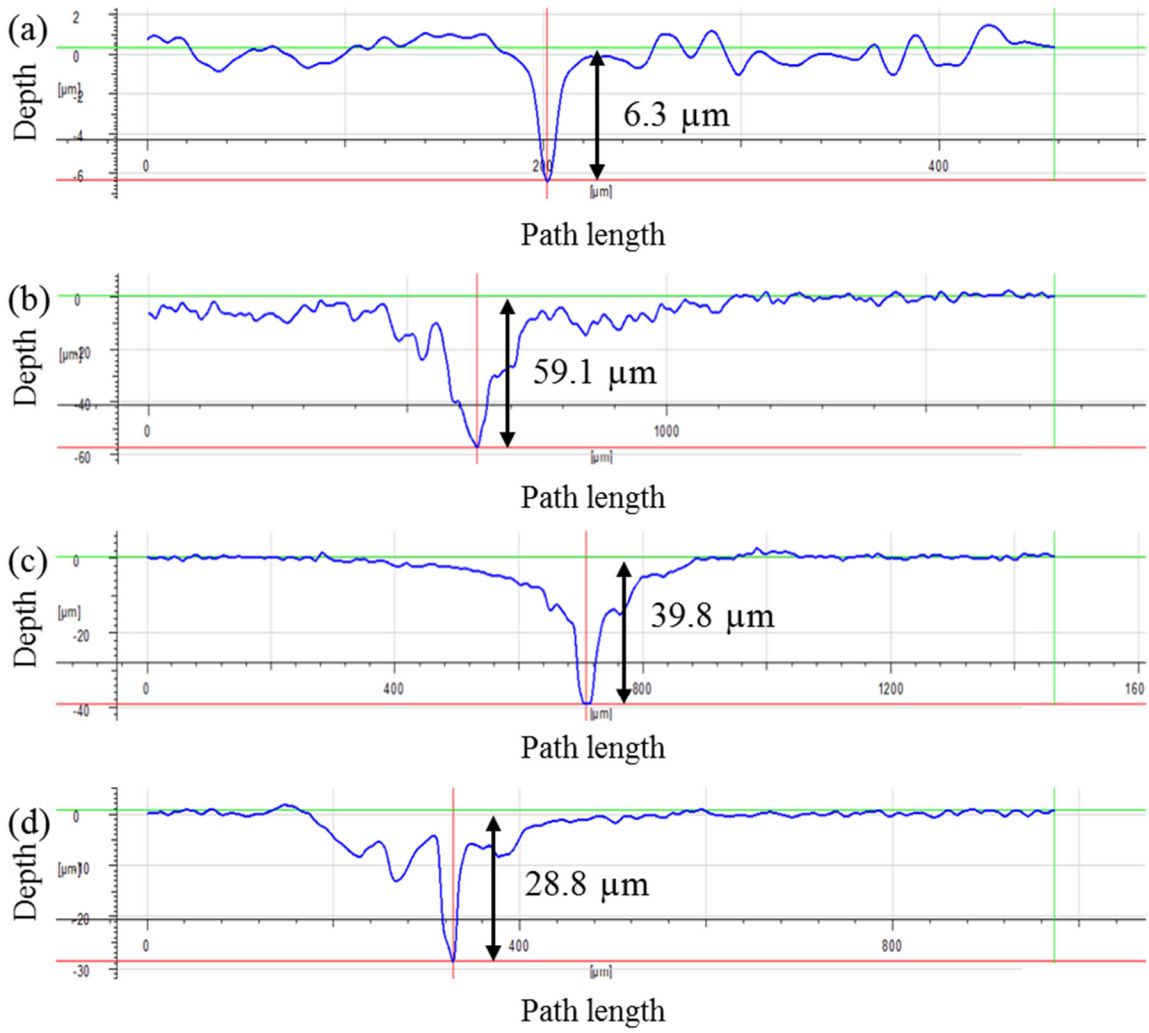

Figure 54. IFM maximum pit depths on coupons: after the 4-day pre-growth (a), and after the 7-day incubation test with no treatment (control) (b), with 100 ppm THPS (c), and with 100 ppm THPS + 100 ppm D-mix (d).

The MIC mitigation effect was also studied using maximum pit depth data. The data are useful because MIC failures are usually due to pinhole leaks [9]. Figure 54 shows the maximum pit depth data after 4-day pre-growth without treatment, and after the additional 7-day incubation with and without biocide treatment. After the 4-day pre-growth, the maximum pit depth was 6.3 µm. The maximum pit depths for the no

treatment control, 100 ppm THPS alone treatment, and 100 ppm THPS + 100 ppm D-mix treatment after additional 7-day incubation were 59.1 μm, 39.8 μm, and 28.8 μm, respectively. The net maximum pit depths after deducting the 4-day pre-growth were 52.8 μm, 33.5 μm, and 22.5 μm, respectively. This indicated that the 100 ppm THPS alone treatment and the 100 ppm THPS + 100 ppm D-mix treatment reduced the maximum pit depth by 36.6% and 57.4%, respectively, compared with the untreated control.

8.3.4 Electrochemical measurements

Figure 55a shows OCP versus time during the additional 7-day incubation with and without biocide treatment. For the no treatment control, OCP generally shifted to the negative direction during the 7-day incubation. For the 100 ppm THPS alone treatment, OCP generally shifted to the positive direction. For the 100 ppm THPS + 100 ppm D-mix treatment, OCP kept steady. OCP results here did not show any trend that could be used to explain the treatment efficacy. This is not surprising because OCP only provides thermodynamic tendency. The actual corrosion rate depends on kinetics. Thus, LPR was performed.

R_p versus time trends during the 7-day incubation with and without treatment are shown in Figure 55b. The R_p values of the no treatment control continuously decreased during the 7-day incubation. A higher R_p was observed in the vial treated with 100 ppm THPS alone compared with the no treatment control, suggesting decreased corrosion. When 100 ppm THPS + 100 ppm D-mix was used, R_p was higher than that treated with the 100 ppm THPS alone. This shows that D-amino acids enhanced THPS against biofilm Consortium II, leading to reduced corrosion. LPR results corroborate the weight loss data

and the pitting data trends. This also means that LPR, when conducted properly, can be used in biocide assessments.

EIS was measured on days 1, 4 and 7 during the 7-day incubation with and without treatment. Figure 56 shows the Nyquist and Bode plots. The Nyquist plots showed that the semi-circle diameter for the no treatment control was much smaller than those treated with biocides. This indicated a reduced corrosion after biocide treatment. The Nyquist semi-circle diameter of the 100 ppm THPS + 100 ppm D-mix treatment was larger than that of the 100 ppm THPS alone treatment, suggesting that the D-amino acids enhanced THPS mitigation of MIC.

The EIS data were fitted with the two-time constant model shown in Figure 16. The fitting results are shown in Table 9. Table 9 shows that R_{ct} values were much larger than R_b values, indicating charge transfer control in the MIC. R_{ct} values of the coupon incubated with no treatment were lower than those of coupons incubated with 100 ppm THPS. The charge transfer resistance of coupons treated with 100 ppm THPS + 100 ppm D-mix was higher than that treated with 100 ppm THPS alone as shown in Table 9.

Figure 57 shows PDS conducted at the end of the 7-day incubation for samples incubated with different biocide treatments. Scans were done only once because a wide range of potential applied could damage the biofilm. The fitted Tafel parameters are listed in Table 10. The i_{corr} values for the samples incubated with no treatment control, 100 ppm THPS alone, and 100 ppm THPS + 100 ppm D-mix treatment were 7.24 ± 0.61 μA/cm^2, 3.98 ± 0.43 μA/cm^2, and 2.29 ± 0.37 μA/cm^2, respectively, suggesting that D-amino acids enhanced THPS thus reducing MIC. The PDS results are consistent with weight loss and pitting data trends.

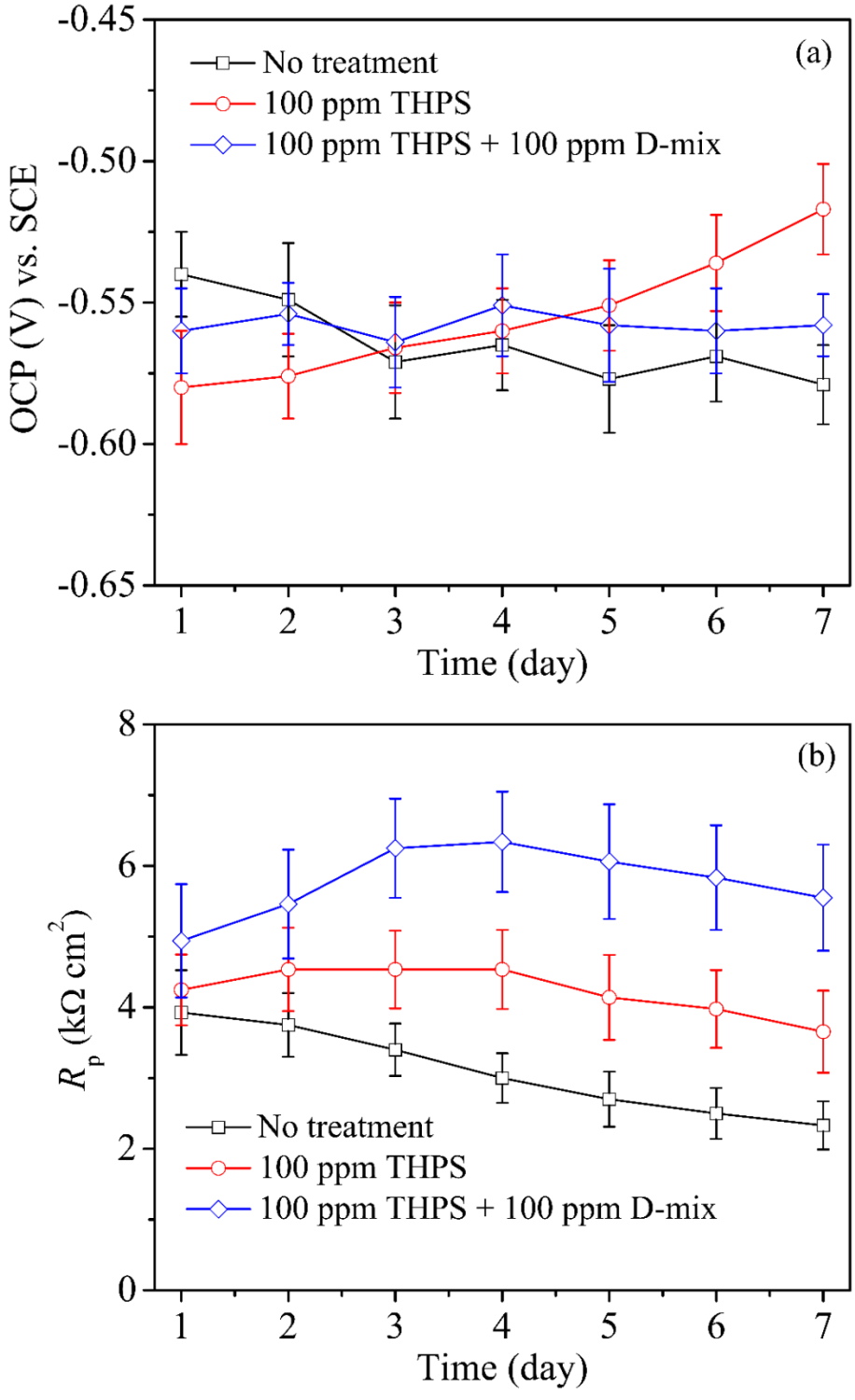

Figure 55. Variations of OCP (a) and polarization resistance (b) versus time for samples incubated with and without treatment during the 7-day incubation test. (The standard deviation calculated from 3 independent samples in 3 different experimental batches.)

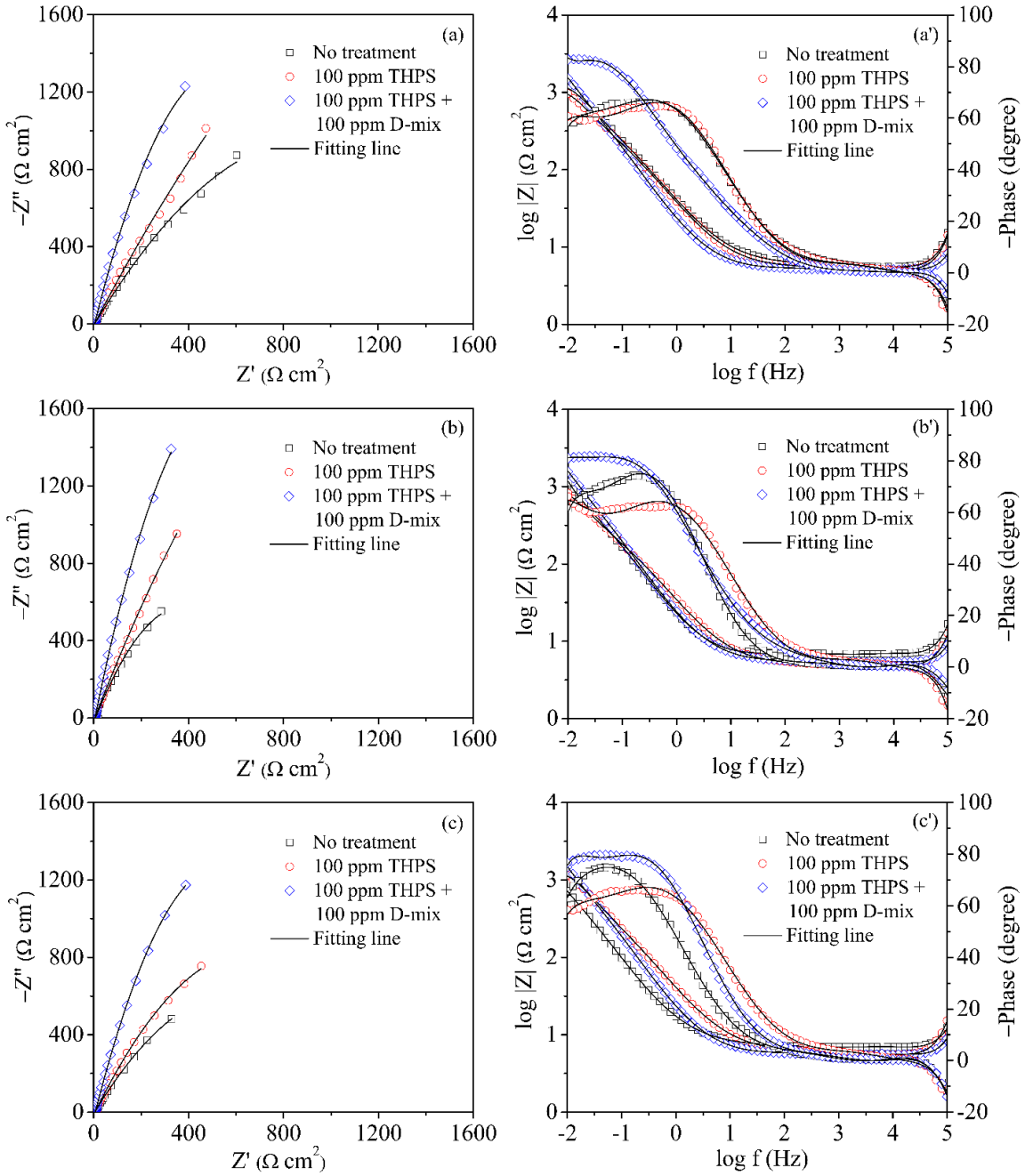

Figure 56. Nyquist and Bode plots for coupons incubated with and without biocide treatment during the 7-day incubation test: day 1 (a, a′), day 4 (b, b′), and day 7 (c, c′). (EIS was conducted under stable OCP between 10^{-2} and 10^{5} Hz with a sinusoidal voltage signal (10 mV amplitude).)

Table 9. Fitted EIS parameters of samples incubated with and without treatment during the 7-day incubation test (The standard deviation calculated from 3 independent samples in 3 different experimental batches.)

Day	R_s (Ω cm^2)	Y_b (Ω^{-1} cm^{-2} s^n)	n_b	R_b (Ω cm^2)	Y_{dl} (Ω^{-1} cm^{-2} s^n)	n_{dl}	R_{ct} (kΩ cm^2)
No treatment							
1	9.1 ± 2.3	0.0045 ± 0.0023	0.85 ± 0.09	9.9 ± 1.9	0.0033 ± 0.0011	0.81 ± 0.11	4.0 ± 0.5
4	10.2 ± 2.4	0.0057 ± 0.0026	0.88 ± 0.12	10.4 ± 2.5	0.0045 ± 0.0018	0.83 ± 0.15	3.1 ± 0.5
7	9.4 ± 2.2	0.0065 ± 0.0021	0.92 ± 0.06	9.4 ± 1.8	0.0105 ± 0.0036	0.79 ± 0.16	2.2 ± 0.4
100 ppm THPS treatment							
1	10.4 ± 2.8	0.0039 ± 0.0015	0.85 ± 0.11	9.7 ± 1.9	0.0042 ± 0.0016	0.91 ± 0.06	4.8 ± 0.8
4	10.9 ± 2.1	0.0047 ± 0.0021	0.89 ± 0.08	9.2 ± 1.7	0.0055 ± 0.0020	0.80 ± 0.15	5.4 ± 1.4
7	12.3 ± 2.5	0.0076 ± 0.0029	0.91 ± 0.06	9.5 ± 1.3	0.0039 ± 0.0019	0.87 ± 0.06	4.3 ± 1.1
100 ppm THPS + 100 ppm D-mix treatment							
1	8.4 ± 2.1	0.0073 ± 0.0021	0.79 ± 0.13	8.5 ± 1.2	0.0035 ± 0.0014	0.82 ± 0.11	5.2 ± 1.3
4	9.5 ± 2.8	0.0065 ± 0.0019	0.82 ± 0.09	8.6 ± 1.8	0.0047 ± 0.0024	0.85 ± 0.08	6.6 ± 1.5
7	8.7 ± 1.9	0.0045 ± 0.0012	0.93 ± 0.04	7.9 ± 1.7	0.0034 ± 0.0011	0.89 ± 0.09	5.5 ± 1.2

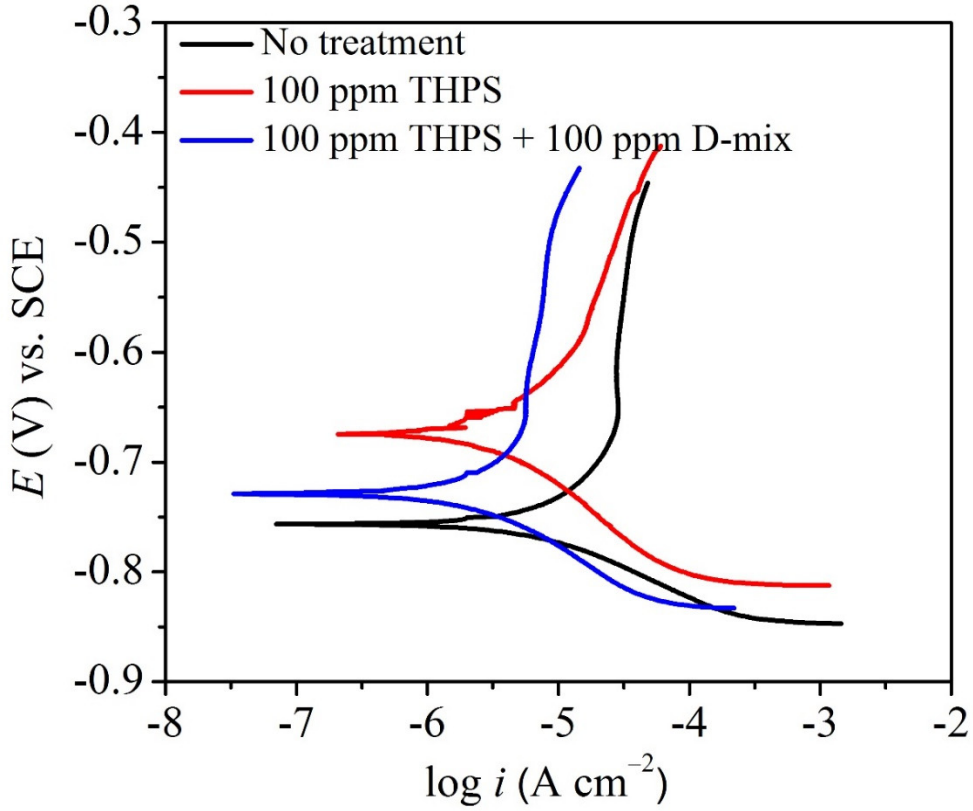

Figure 57. PDS measurements of coupons incubated with and without treatment at the end of the 7-day incubation test.

Table 10. Fitted parameters from PDS (The standard deviation calculated from 3 independent samples in 3 different experimental batches.)

	i_{corr} ($\mu A/cm^2$)	E_{corr} (V) vs. SCE	β_a (V/dec)	β_c (V/dec)
No treatment	7.24 ± 0.61	−0.76 ± 0.07	0.29 ± 0.02	0.05 ± 0.01
100 ppm THPS treatment	3.98 ± 0.43	−0.67 ± 0.05	0.22 ± 0.04	0.11 ± 0.02
100 ppm THPS + 100 ppm D-mix treatment	2.29 ± 0.37	−0.73 ± 0.06	0.28 ± 0.03	0.08 ± 0.02

8.4 Summary

This work demonstrates that an equimolar D-amino acid mixture containing four different D-amino acids enhanced THPS mitigation of a corrosive oilfield biofilm consortium. The combination of 100 ppm THPS + 100 ppm D-mix achieved further reductions of sessile cells compared with the 100 ppm THPS alone treatment. The combination also reduced carbon steel coupon weight loss and pitting corrosion. Electrochemical tests employing LPR, EIS and PDS confirmed the efficacy trend, suggesting that properly conducted electrochemical methods can be used in biocide assessments. The experimental results clearly show that THPS was enhanced by D-amino acids and the presence of other oilfield chemicals did not interfere with the efficacy.

Chapter 9: Enhanced Biofilm Mitigation by Nature-Inspired Peptide A at Sub-ppm Concentrations

9.1 Introduction

In nature, some organisms can keep their surfaces free from biofilm formation by secreting protective chemicals. Sea anemone *Actinia equine* is one example [161]. The marine environment is full of microorganisms. However, *A. equine* can still maintain a biofilm-free exterior. The extract of *A. equina* tentacles was found to possess an ability against biofilm adhesion. Its active component was later identified as Equinatoxin II [161]. This protein has two identical peptide chains. Using this protein as a biofilm dispersal agent for large-scale applications is not practical because of cost and protein stability issues. Thus, efforts were made to identify the functional group in the protein. A bioinformatics search conductive by Dr. Amir Zlotkin discovered that a 12-mer sequence (SVPYDYNWYSNW) in Equinatoxin II is highly conserved in few other organisms such as moss, which possess a biofilm-free exterior [161]. Thus, this 12-mer was chemically synthesized, but it exhibited no anti-biofilm capability, likely because it lacks the 3-D structure in Equinatoxin II. Thus, Peptide A was engineered by adding one L-cysteine residue to each side to make a ring-shaped 14-mer peptide (CSVPYDYNWYSNWC) to emulate the loop shape of the 12-mer sequence in Figure 58.

A project was carried out to evaluate the efficacy of Peptide A in the mitigation of biofilms and MIC caused by the biofilms [162]. The results of this work have been included in a manuscript submitted to International Biodeterioration & Biodegradation.

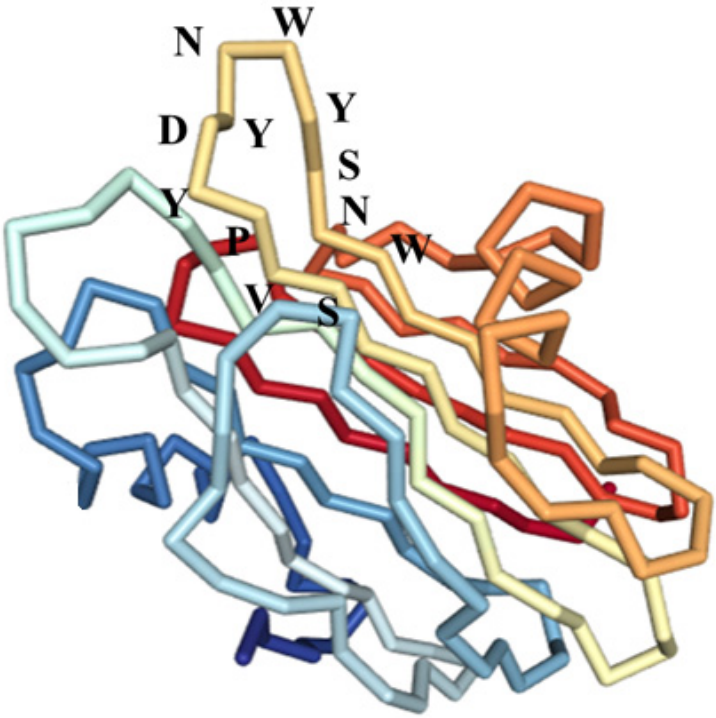

Figure 58. The 3D Equinatoxin II protein structure (one of the two identical peptide chains shown here) that contains the highly conserved 12-mer peptide sequence (SVPYDYNWYSNW from Positions 105 to 116) in a loop-like structure. (3D image generated by online NGL viewer software [163,164] from RCSB Protein Data Bank at http://www.rcsb.org with PDB ID 1IAZ based on X-ray diffraction data from Athanasiadis, et al. [165].)

9.2 Materials and Methods

Biofilm Consortium II described in Section 7.2 was used in this work. Enriched artificial seawater medium (supplemented with 100 ppm L-cysteine as oxygen scavenger) described in Section 5.2 was used to culture Consortium II. Peptide A was synthesized by a commercial peptide company (Bachem AG, Bubendorf, Switzerland). The peptide sequence is cys-ser-val-pro-tyr-asp-tyr-asn-trp-tyr-ser-asn-trp-cys

(CSVPYDYNWYSNWC) with an S-S bond to form a loop-shaped structure. C1018 carbon steel coupons were used for corrosion. Peptide A and THPS solutions were sterilized with a 0.22 μm sterile filter. Detailed information about coupon preparation, vendors of other chemicals used in this work, medium sterilization, deoxygenation and anaerobic manipulation are described in Appendix A.

In each 125 mL anaerobic vial, 5 coupons, 100 mL medium, and 1 mL Consortium II seed culture were added. The initial planktonic cell amount was about 10^6 cells/mL. The initial pH value in the medium was 7.0. Vials were sealed and incubated at 37^{o}C for 14 days. The abiotic control contained all chemicals without inoculation.

During the 14-day incubation, a set of vials were set aside for planktonic cell counts. The details for planktonic cell counting are described in Section 5.2. After the 14-day incubation, coupons were retrieved for APB, GHB, and SRB sessile cell counts using MPN method. Details about biofilm removal and MPN methods are described in Appendix A. Biofilm observation was conducted with SEM and CLSM. The detailed SEM preparation and CLSM staining procedures are described in Appendix A.

After the 14-day incubation, weight loss and culture medium pH were measured. The detailed coupon preparation procedure for weight loss is described in Appendix A. After biofilms and corrosion products were removed using a fresh Clarke's solution, SEM was used to examine pit morphologies. IFM was used to find the maximum pit depth on a coupon. LPR was conducted in 450 mL glass cells filled with 350 mL medium. It was used to monitor the corrosion process during the 14-day incubation. Detailed LPR procedures are described in Appendix A.

9.3 Results and Discussion

9.3.1 Cell counts

Figure 59a shows that the planktonic cell counts in 125 mL vials for the no treatment control and 100 nM Peptide A alone treatment are the same. The data indicate that 100 nM Peptide A did not exhibit a biocidal or biostatic effect against planktonic cells. The sessile cell counts on coupons incubated with and without treatment chemicals after the 14-day incubation are shown in Figure 59b. The SRB, APB and GHB sessile cell counts on the control coupon were 3.3×10^7 cells/cm^2, 7.8×10^4 cells/cm^2, and 6.7×10^4 cells/cm^2 after the 14-day incubation period. When 100 nM Peptide A alone treatment was used, it had a negligible effect for the reduction of the sessile cell count. When 100 ppm THPS was added, this treatment achieved a 1-log reduction in APB, SRB and GHB sessile cell counts compared with the no treatment control. The combination of 100 ppm THPS + 10 nM Peptide A achieved an extra 1-log reduction in SRB sessile cell count vs. the 100 ppm THPS alone treatment. The combination of 100 ppm THPS + 100 nM Peptide A achieved an extra 2-log reduction in SRB sessile cell count and an extra 1-log reduction in APB and GHB sessile cell counts vs. the 100 ppm THPS alone treatment. These data suggest that for a tough biofilm, Peptide A alone was not sufficient. A biocidal effect was required. In turn, Peptide A enhanced the biocide treatment. Figure 59b also shows that similar efficacy was achieved for the 100 ppm THPS + 100 nM Peptide A treatment and the 200 ppm THPS alone treatment. This means that 100 nM Peptide A lowered THPS dosage by half when treating biofilm Consortium II.

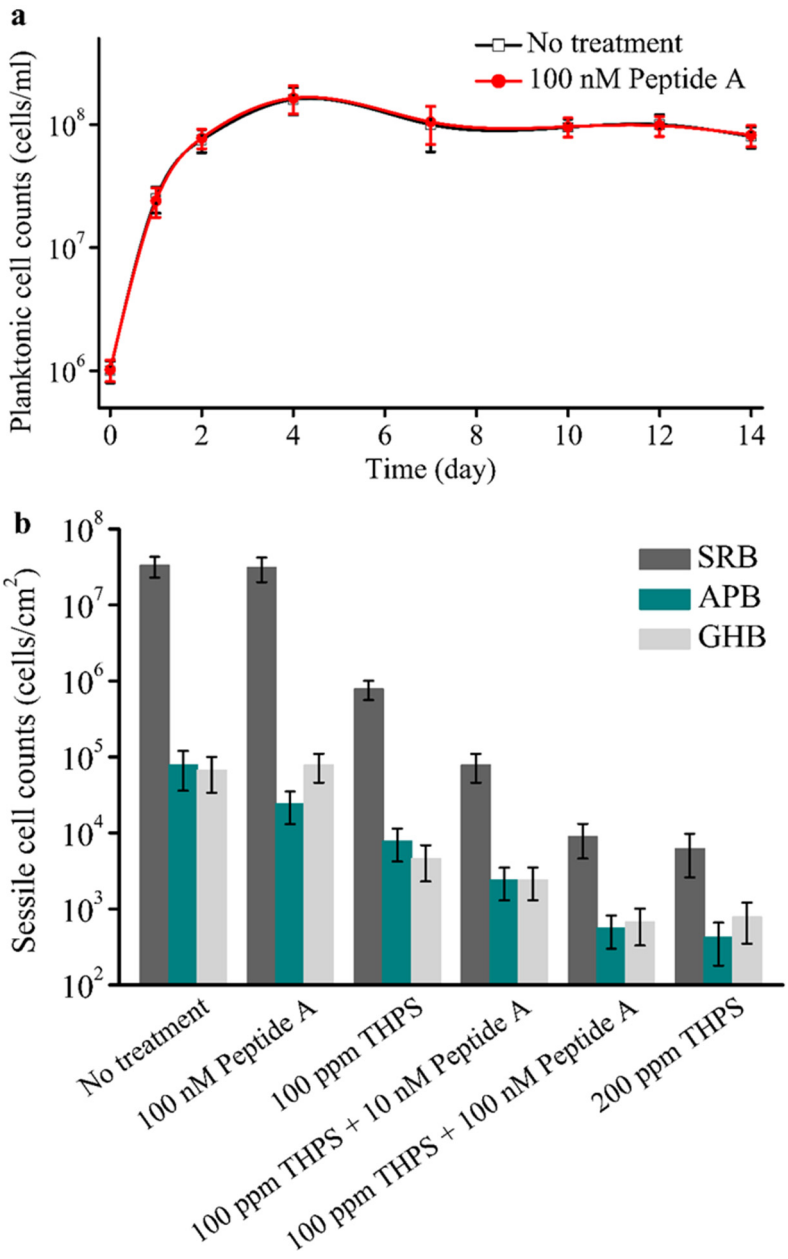

Figure 59. Planktonic cell counts with and without Peptide A in enriched artificial seawater during the 14-day incubation period (a). Sessile cell counts of coupons incubated with different treatments after the 14-day incubation period (b). (The standard deviation calculated from 3 independent samples from 3 different vials in 3 different experimental batches.)

9.3.2 Biofilm examination

Biofilm SEM images of coupons incubated with and without Peptide A treatment in the enriched artificial seawater medium after the 14-day incubation are shown in Figure 60. For the no treatment control in Figure 60a, it shows the biofilm Consortium II was a mixed culture because different cell shapes are seen in SEM images. When the 100 nM Peptide A alone treatment was used, abundant sessile cells are observed seen in Figure 60b, suggesting that Peptide A alone was not effective enough to disperse biofilm Consortium II. When the 100 ppm THPS alone treatment was used, many sessile cells on the coupon surface as seen in Figure 60c. When the combination of 100 ppm THPS + 10 nM Peptide A was used (Figure 60d), sessile cells on the coupon surface were fewer than those on the coupons treated with 100 ppm THPS alone. When 100 nM Peptide A was used to enhance 100 ppm THPS, much fewer sessile cells can be found in Figure 60e. Figure 60f shows similar sessile cell amount as that in Figure 60e, meaning that 100 ppm THPS + 100 nM Peptide A and 200 ppm THPS had a similar efficacy. This means 100 nM Peptide A reduced the THPS dosage by half. Biofilm SEM images here corroborate the sessile cell counts in Figure 59b.

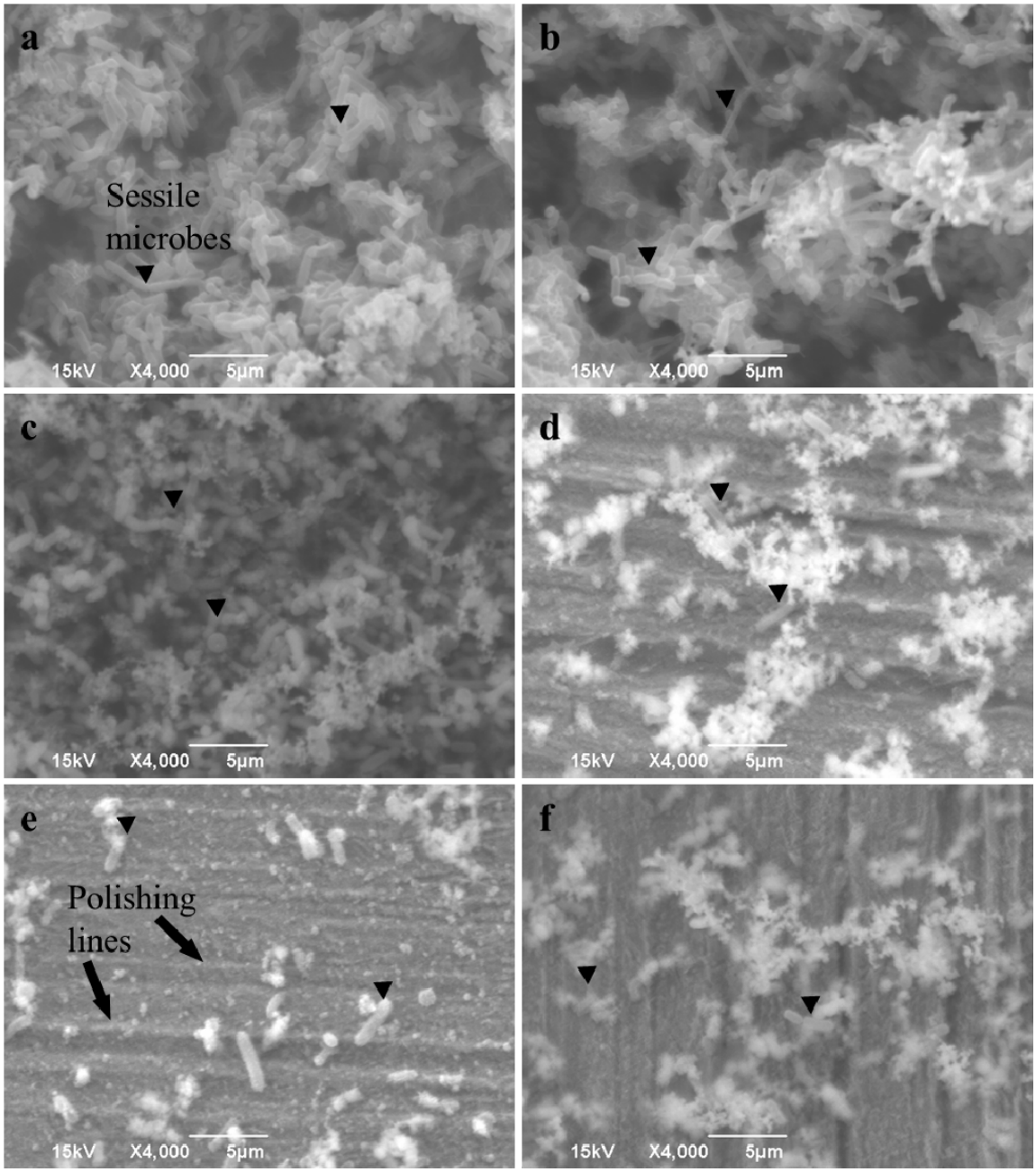

Figure 60. Biofilm SEM images of coupons incubated with and without treatment after 14-day incubation with: no treatment (control) (a), 100 nM Peptide A (b), 100 ppm THPS (c), 100 ppm THPS + 10 nM Peptide A (d), 100 ppm THPS + 100 nM Peptide A (e), and 200 ppm THPS (f).

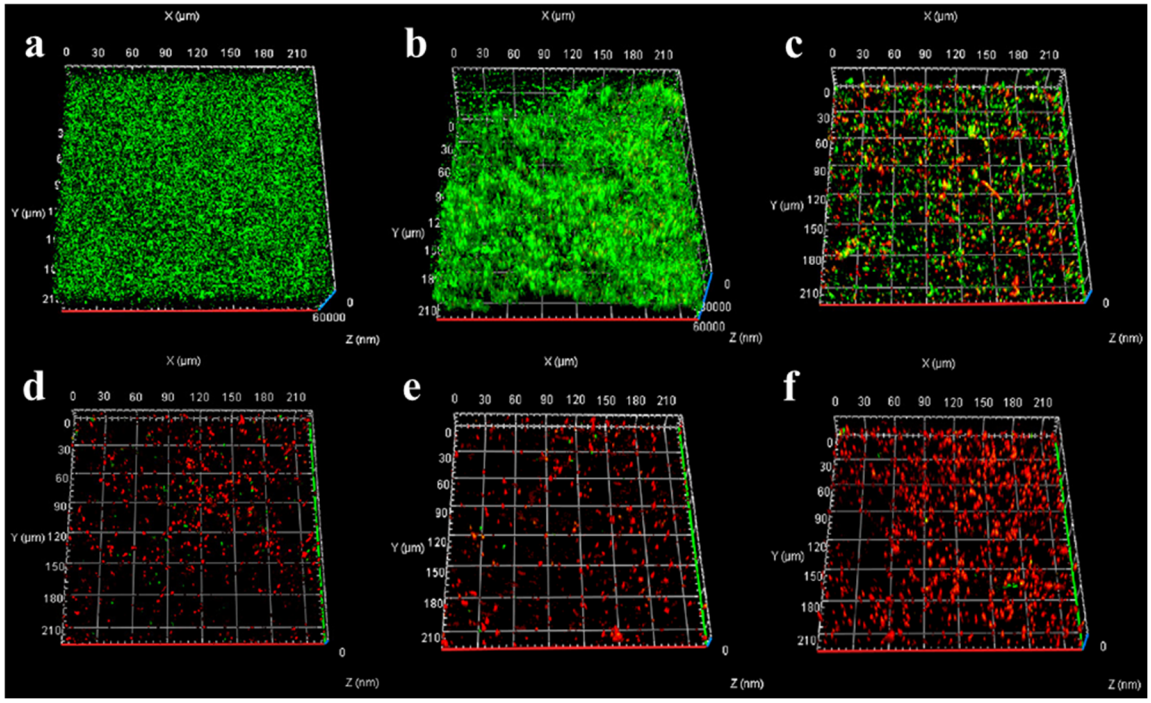

Figure 61. Biofilm CLSM images of coupons incubated with and without treatment after 14-day incubation with: no treatment (control) (a), 100 nM Peptide A (b), 100 ppm THPS (c), 100 ppm THPS + 10 nM Peptide A (d), 100 ppm THPS + 100 nM Peptide A (e), and 200 ppm THPS (f).

3D CLSM images in Figure 61 can be used to assess the biofilm treatment efficacy. Figure 61a and Figure 61b show dense live sessile cells covered on the surfaces of the coupon with no Peptide A treatment (control) and the coupon with 100 nM Peptide A alone treatment, respectively. This shows that Peptide A is not biocidal. When the 100 ppm THPS alone treatment was used, many sessile cells were dead (which could not be revealed by the SEM image in Figure 60c) and the biofilm thickness decreased. There are still many live cells on the coupon surface seen in Figure 61c. When 10 nM Peptide A was used to enhance 100 ppm THPS (Figure 61d), much fewer live sessile cells are seen than those treated with 100 ppm THPS alone. When 100 nM Peptide A was used to

enhance 100 ppm THPS, much fewer live cells are seen in Figure 61e. This means that the increased Peptide A dosage increased the enhancement effect. The efficacies achieved by the combination of 100 ppm THPS + 100 nM Peptide A (Figure 61e) and 200 ppm THPS alone treatment (Figure 61f) were similar, except that Figure 61f has more dead cells than Figure 61e, indicating the dispersal effect of Peptide A instead of the biocidal effect. This comparison also suggests that 100 nM Peptide A cut the THPS dosage by half.

9.3.3 Biocorrosion analyses

The average weight losses for the abiotic control, no treatment control, 100 ppm THPS alone treatment, 100 nM Peptide A alone treatment, 100 ppm THPS + 100 nM Peptide A treatment, 100 ppm THPS + 10 nM Peptide A treatment, and 200 ppm THPS alone treatment were found to be 0.3 mg/cm^2, 10.9 mg/cm^2, 3.8 mg/cm^2, 10.3 mg/cm^2, 1.7 mg/cm^2, 2.5 mg/cm^2 and 1.3 mg/cm^2, respectively, as shown in Figure 62. When 100 nM Peptide A alone treatment was used, it did not reduce the weight loss statistically ($p = 0.69$). This is consistent with the sessile cell count since sessile cells in biofilms are responsible for MIC. When 100 ppm THPS alone treatment was used, it reduced the carbon steel weight loss greatly. When 100 ppm THPS was combined with Peptide A, the combinations further reduced the weight loss. The weight loss for the combination treatment using 100 ppm THPS + 10 nM Peptide A was not significantly different from that for the combination treatment of 100 ppm THPS + 100 nM Peptide A treatment ($p = 0.16$). The combination of 100 ppm THPS + 100 nM Peptide A led to similar weight loss to that achieved by the 200 ppm THPS alone treatment ($p = 0.43$). The weight loss was

almost negligible for the abiotic control, suggesting that the abiotic enriched artificial seawater at pH 7.0 had negligible corrosion under anaerobic condition.

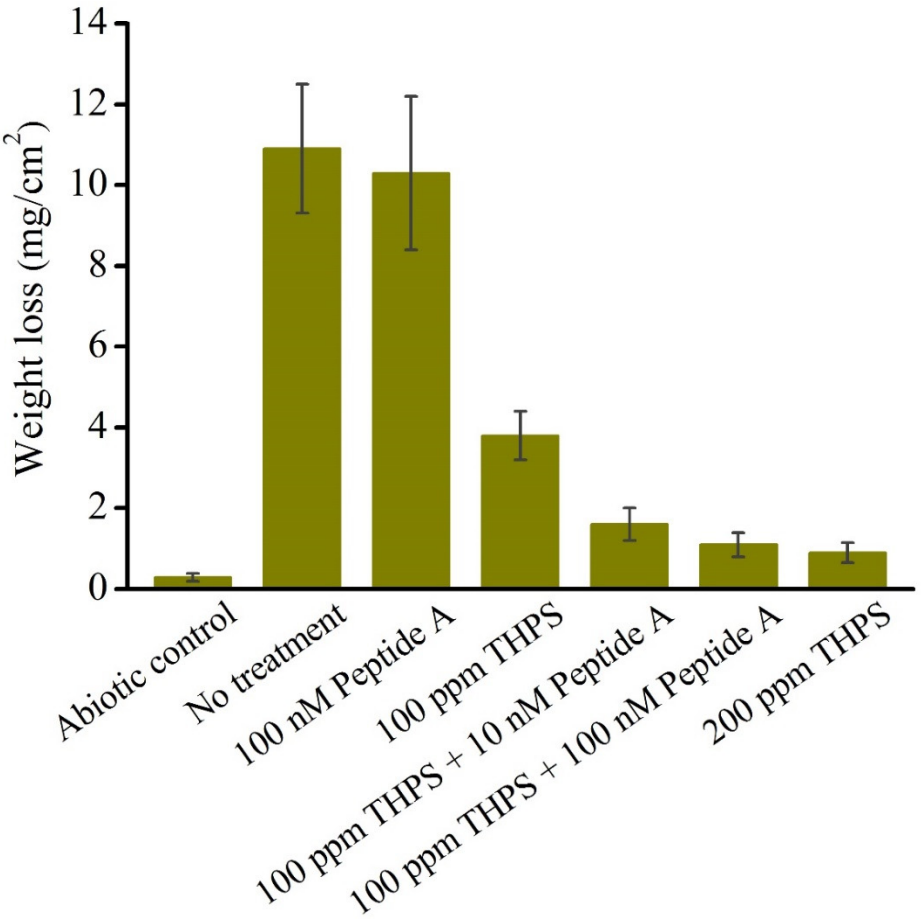

Figure 62. Weight losses of coupons incubated enriched artificial seawater with and without treatment after the 14-day incubation. (The standard deviation calculated from 9 independent samples from 3 different vials in 3 different experimental batches.)

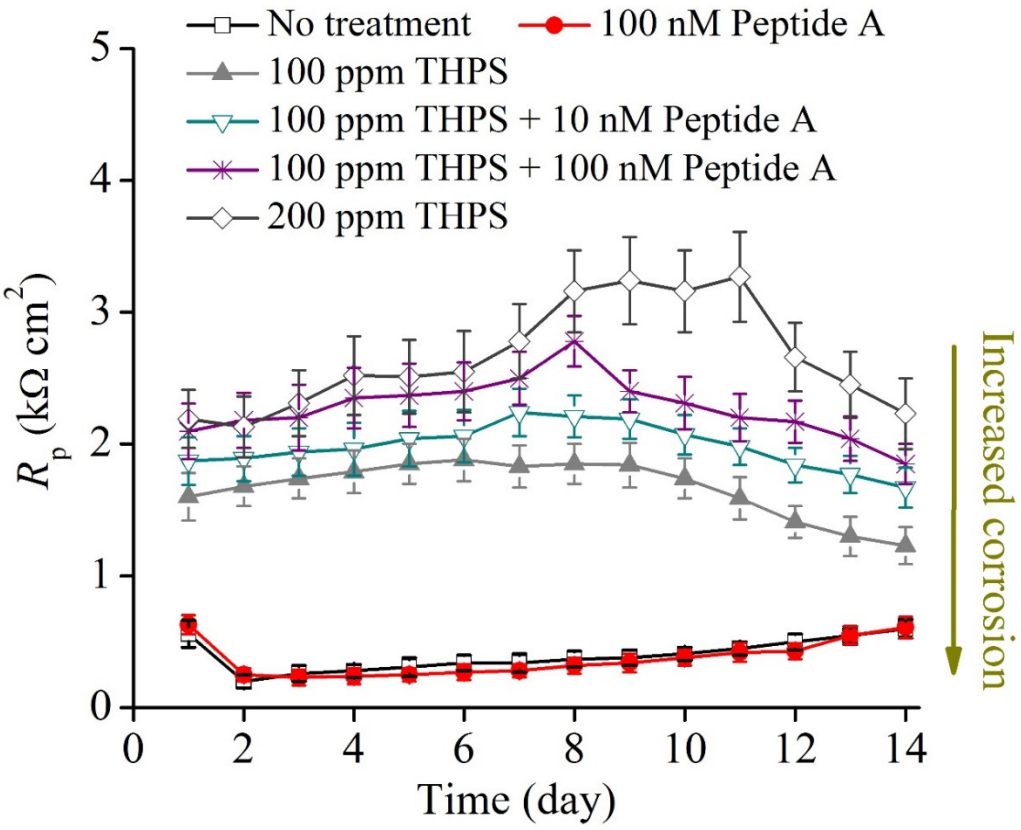

Figure 63. Variations of polarization resistances of coupons with time during the 14-day incubation. (The standard deviation calculated from 3 independent samples in 3 different experimental batches.)

LPR as a non-destructive electrochemical method is used to monitor the corrosion progress during the 14-day incubation. R_p versus time during the 14-day incubation with and without treatment are shown in Figure 63. Unlike weight loss, which needs several days to allow corrosion to be measurable, LPR is fast and provides real-time data [102]. In Figure 63, the R_p values of the no treatment control and the 100 nM Peptide A alone treatment are similar during the 14-day incubation. A higher polarization resistance was observed in the vial treated with 100 ppm THPS alone compared with the no treatment

control, suggesting decreased corrosion. When 100 ppm THPS + 10 nM Peptide A was used, R_p was higher than that treated with 100 ppm THPS alone. When the dosage of Peptide A increased from 10 nM to 100 nM in the combination treatment, R_p increased further. After 7 days during the 14-day incubation, R_p in the 200 ppm THPS alone treatment was slightly higher than that in the treatment of 100 ppm THPS + 100 nM Peptide A. LPR results showed that Peptide A enhanced THPS against biofilm Consortium II, thus reducing corrosion. LPR results here generally corroborate the weight loss data in Figure 62.

Figure 64 shows SEM images that were used to examine pit morphologies on the coupons with and without treatment. After the 14-day incubation, large pits were found on the coupons with no treatment (Figure 64a) and 100 nM Peptide A alone (Figure 64b). Fewer and smaller pits are seen in Figure 64c for the coupon treated with 100 ppm THPS alone. For 100 ppm THPS + 10 nM Peptide A treatment (Figure 64d), 100 ppm THPS + 100 nM Peptide A treatment (Figure 64e), and 200 ppm THPS (Figure 64f) treatment, fewer pits are seen compared with the coupon treated with 100 ppm THPS alone in Figure 64c.

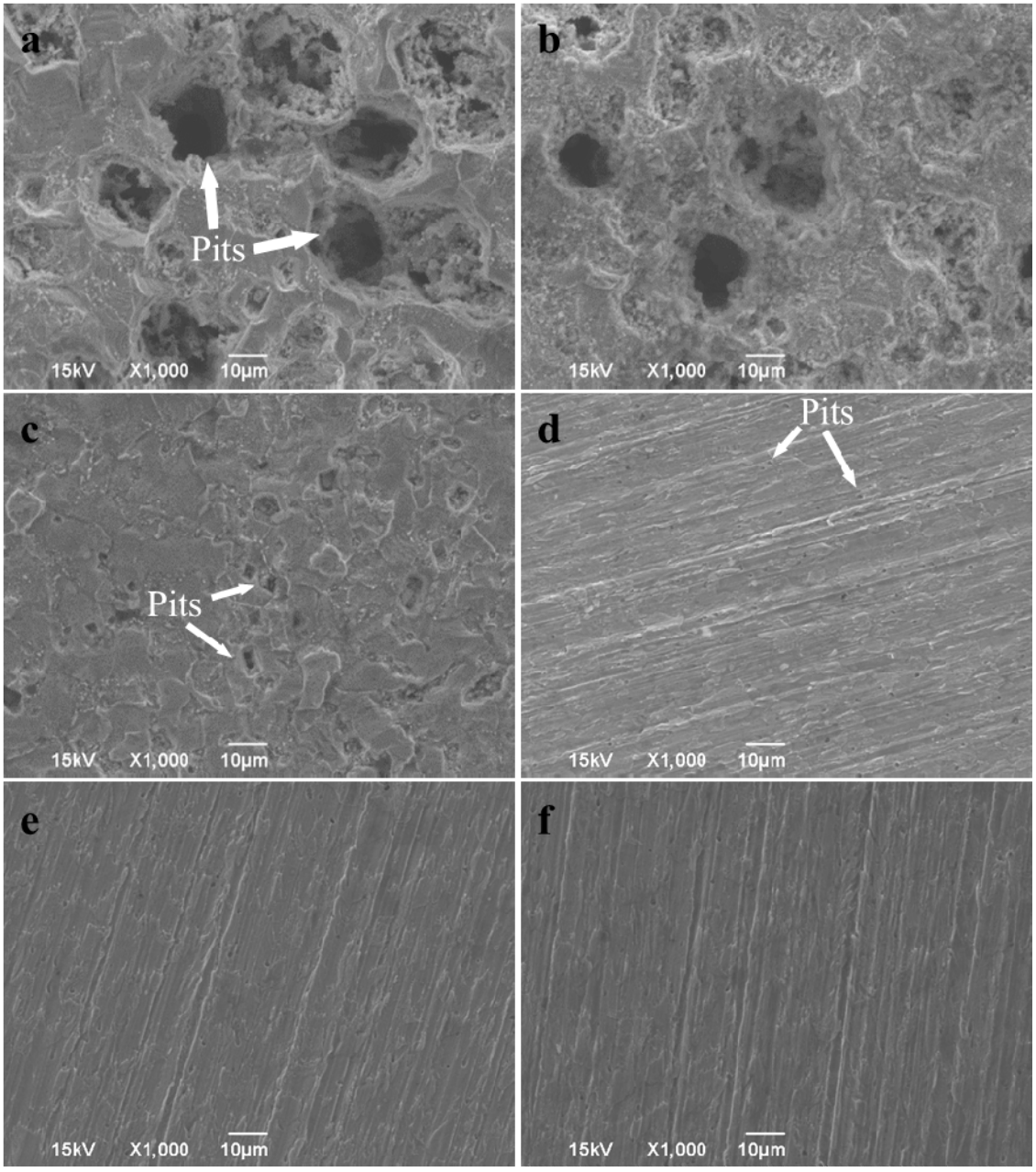

Figure 64. SEM pit morphologies of coupons incubated with and without treatment after 14-day incubation with: no treatment (control) (a), 100 nM Peptide A (b), 100 ppm THPS (c), 100 ppm THPS + 10 nM Peptide A (d), 100 ppm THPS + 100 nM Peptide A (e), and 200 ppm THPS (f).

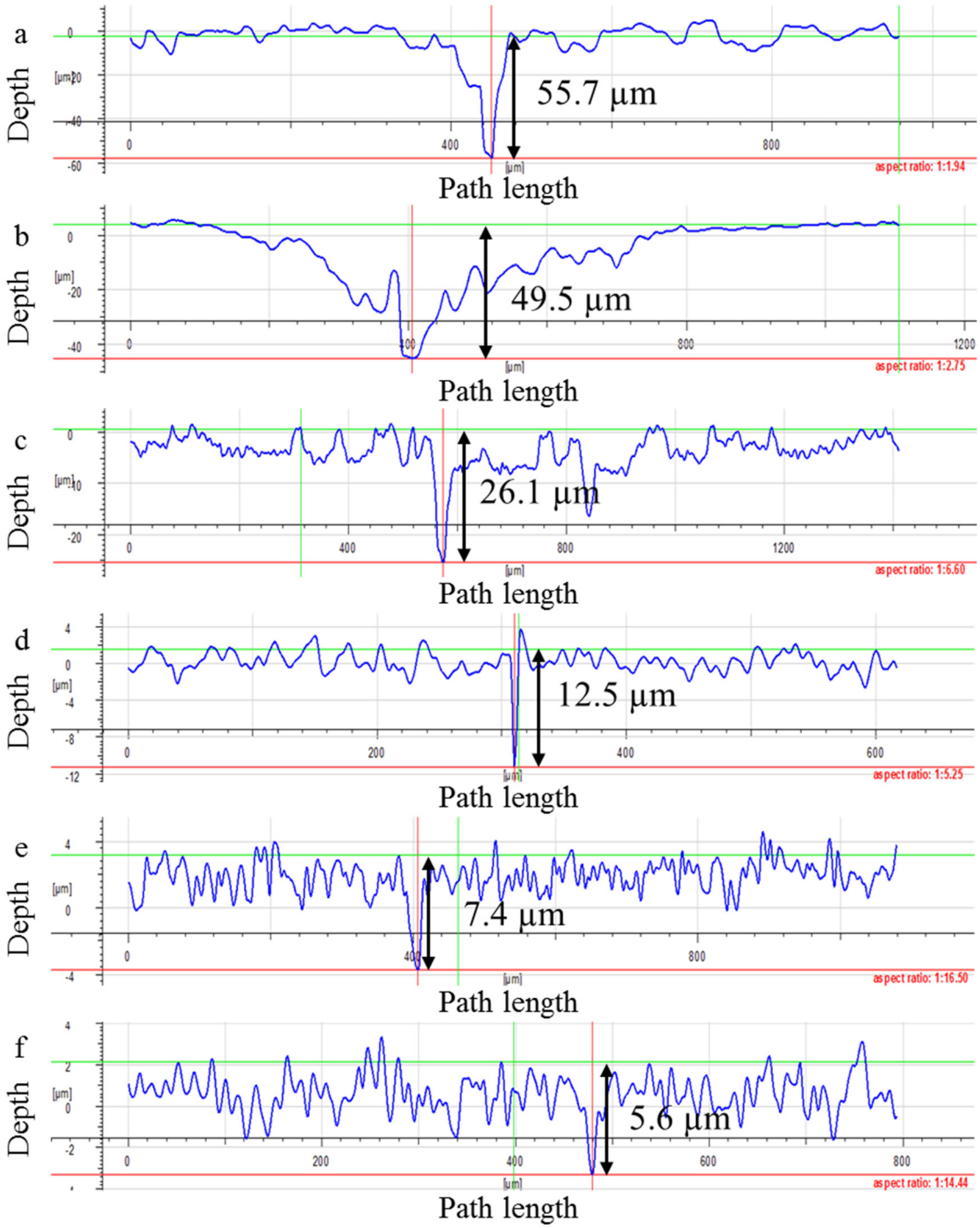

Figure 65. IFM maximum pit depths of coupons incubated with and without treatment after the 14-day incubation with: no treatment (control) (a), 100 nM Peptide A (b), 100 ppm THPS (c), 100 ppm THPS + 10 nM Peptide A (d), 100 ppm THPS + 100 nM Peptide A (e), and 200 ppm THPS (f).

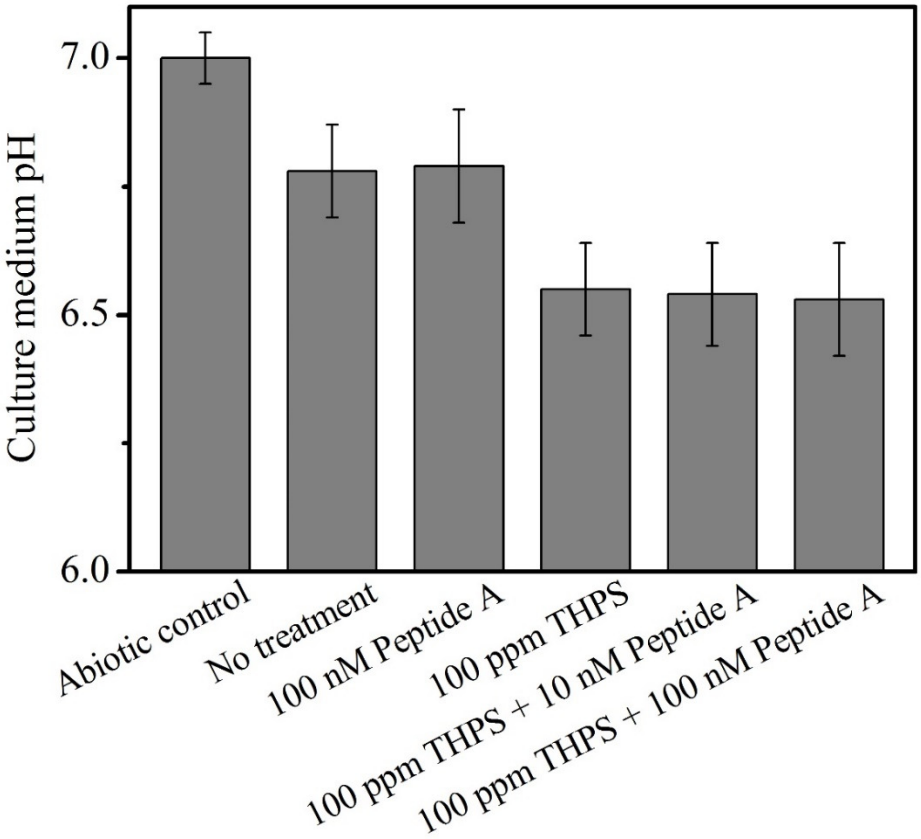

Figure 66. Culture medium pH values after 14-day incubation. (The standard deviation calculated from 3 independent samples in 3 different experimental batches.)

Figure 65 shows the maximum pit depth data for coupons incubated with and without treatment. After the 14-day incubation, the maximum pit depths for no treatment control and 100 nM Peptide A alone treatment were 55.7 μm and 49.5 μm, respectively. When 100 ppm THPS alone treatment was used, it reduced the maximum pit depth to 26.1 μm. The maximum pit depths were further reduced to 12.5 μm and 7.4 μm when treated with 100 ppm THPS + 10 nM Peptide A, and 100 ppm THPS + 100 nM Peptide A, respectively. The 200 ppm THPS alone treatment reduced the maximum pit depth to 5.6 μm. The pit depth data are consistent with the SEM pit images in Figure 64. The

SEM pitting images and IFM maximum pit depth data indicated that Peptide A enhanced THPS in the mitigation of MIC pitting corrosion on carbon steel caused by biofilm Consortium II.

The culture medium pH values after the 14-day incubation with and without treatment in the enriched artificial seawater medium were all above 6.5 (Figure 66). With such near neutral pH, acid corrosion was not a significant factor. The culture medium pH of the abiotic control did not change as expected.

It was found that 100 nM Peptide A alone could achieve almost 1-log sessile cell count reduction of some pure-strain bacteria such as *P. aeruginosa*, and *S. aureus* [161]. However, for biofilm Consortium II, the 100 nM Peptide A alone treatment had a negligible effect on sessile cell reduction (Figure 59b). In addition, the combination of 100 ppm THPS + 100 nM Peptide A and 200 ppm THPS alone treatment showed similar efficacies. These results indicate that a biocidal stress is required to make Peptide A effective against recalcitrant biofilms.

The mechanism by which Peptide A can disperse biofilms has not been elucidated. Typical corrosion inhibitors work by adsorption on a metal surface. This requires a dosage typically in tens of ppm (w/w) [166]. However, the dosages in this work were well below 1 ppm. Thus, a different mechanism is likely. It is speculated that Peptide A could work as a signal molecule that affects the polysaccharide matrix [161]. In-depth investigation of the dispersal mechanisms will be challenging but worthwhile. This non-biocidal agent will unlikely have environmental issues and it is less likely to lead to microbial resistance. Since Peptide A was derived from the marine eco-system

which is abundant with microbes, Peptide A has a high potential to cope with various environmental biofilms.

9.4 Summary

A novel biocide enhancer (Peptide A) at ppb levels was found to enhance 100 ppm of a widely used industrial biocide (THPS) in treating a corrosive oilfield biofilm consortium on C1018 carbon steel in an enriched artificial seawater medium. It also led to enhanced corrosion inhibition. The amino acid sequence in the synthetic peptide was derived from a sea anemone that has a biofilm-free exterior. Because the anti-biofilm ability has an origin in the marine eco-system, Peptide A has a high potential to treat various biofilms. Peptide A can be chemically synthesized or produced via fermentation economically because it is a small peptide. This work presents a successful example that anti-biofilm bioactive molecules can be created with inspiration from nature. It shows that bioinformatics can be very helpful in the process.

Chapter 10: Conclusions

MIC mechanisms and its mitigation were investigated in order to understand MIC better and to find more efficient ways to treat corrosive biofilms. The following conclusions can be made based on the experimental results:

MIC caused by NRB and SRA

- *P. aeruginosa* anaerobically grown as an NRB corroded C1018 carbon steel.
- In the NRB starvation test, starved NRB sessile cells switched from organic carbon to elemental iron as electron donor, causing more corrosion. This supported the BCNR theory, which is parallel to the BCSR theory.
- *A. fulgidus*, a thermophilic SRA, was found corrosive against C1018 carbon steel at 80ºC.
- It was found that under different levels of carbon source starvation, the thermophilic SRA became more corrosive against carbon steel. The corrosion results extended the bioenergetics theory for EET-MIC to SRA.
- Properly conducted electrochemical measurements including LPR, EIS and PDS were helpful in mechanistic MIC studies. They provided corrosion data that were consistent with the weight loss and pitting data trends. Furthermore, electrochemical measurements can capable of providing transient data from the very beginning, while in comparison weight loss and pitting data require a considerable lead time.

Ferrous ion effect on SRB MIC of carbon steel

- Ferrous ion (Fe^{2+}) in a SRB culture medium is known to enhance MIC of carbon steel, but the underlining mechanism is controversial. Results in this work

demonstrated that the enhancement is due to detoxification of H_2S effects by Fe^{2+} that increases the sessile cell density.

- The ferrous ion study provided critical evidence to the theory that SRB MIC against carbon steel with near-neutral broth pH is due to electron harvest by SRB cells for energy production rather than due to H_2S corrosion. In this study, increased corrosion was accompanied by increased dissolved *[*H_2S*]*, while in a previous study using varied headspace volume for H_2S to escape, increase corrosion was accompanied by decreased dissolved *[*H_2S*]* [76]. In both studies, increased corrosion was the result of increased sessile cell count, which led to more electron harvest in EET-MIC.

MIC and its mitigation in EOR

- A commercial EOR polymer was found can be degraded by an oilfield biofilm consortium (Consortium II) in an artificial seawater medium during a 30-day incubation period resulted in 34.5% viscosity loss.
- The polymer utilization by microbes promoted planktonic cell growth in the bulk fluid and SRB sessile cell growth on C1018 carbon steel coupons.
- The promoted SRB sessile cell growth led to more severe corrosion.
- An equimolar D-amino acid mixture of D-tyrosine, D-methionine, D-leucine, and D-tryptophan enhanced THPS against Consortium II in the presence of EOR chemicals and other oilfield chemicals such as corrosion inhibitors and scale inhibitors, thus proving that the biocide cocktail is chemically compatible with the oilfield chemicals.

- The combination of 100 ppm THPS + 100 ppm D-mix achieved further reductions of sessile cells compared with the 100 ppm THPS alone treatment, which led to further reducing carbon steel corrosion.
- Electrochemical tests employing LPR, EIS and PDS confirmed the biocide efficacy results on corrosion mitigation, suggesting that properly conducted electrochemical tests can be used to assess biocide efficacy in corrosion mitigation.

Enhanced biocide treatment using a novel anti-biofilm peptide with ultralow dosage

- A novel biocide enhancer (Peptide A) at ppb levels was found to enhance 100 ppm of a widely used industrial biocide (THPS) in treating biofilm Consortium II on C1018 carbon steel in an enriched artificial seawater medium.
- The enhanced biocide treatment reduced sessile cells on the carbon steel surface, thus reducing the coupon weight loss and pitting corrosion considerably
- It was found that 100 nM (180 ppb) Peptide cut the THPS dosage from 200 ppm to 100 ppm while achieving similar sessile cell count and weight loss reductions.
- This work presents a successful bioinformatics-based modern methodology for discovering a nature-inspired anti-biofilm agent.

References

[1] N. Kip, J.A. van Veen, The dual role of microbes in corrosion, ISME J. 9 (2015) 542–551.

[2] B.J. Little, J.S. Lee, Microbiologically influenced corrosion: an update, Int. Mater. Rev. 59 (2014) 384–393.

[3] D. Walsh, D. Pope, M. Danford, T. Huff, The effect of microstructure on microbiologically influenced corrosion, JOM. 45 (1993) 22–30.

[4] H.A. Gaines, Bacterial activity as a corrosion induced in the soil, J. Ind. Eng. Chem. 2 (1910) 128–130.

[5] J.R. Ibars, D. Moreno, Biofouling and microbiologically influenced corrosion in admiralty brass heat exchanger tubes, Eur. Fed. Corros. Publ. 29 (1999) 53–60.

[6] T. Gu, New understandings of biocorrosion mechanisms and their classifications, J. Microb. Biochem. Technol. 4 (2012) 3–6.

[7] R. Jia, Y. Li, H.H. Al-Mahamedh, T. Gu, Enhanced biocide treatments with D-amino acid mixtures against a biofilm consortium from a water cooling tower, Front. Microbiol. 8 (2017) 1538.

[8] R. Jia, D. Yang, H.B. Abd Rahman, P.A. Hamid, I.K. Salleh, J.M.M. Ibrahim, T. Gu, Laboratory Testing of Enhanced Biocide Mitigation of Microbiologically Influenced Corrosion in Enhanced Oil Recovery, Corrosion/2017 Paper No. 2017-9039, NACE International, New Orleans, Louisiana, 2017.

[9] G.A. Jacobson, Corrosion at Prudhoe Bay: a lesson on the line, Mater. Perform. 46 (2007) 26–34.

[10] A.K. Samant, V.K. Sharma, S. Thomas, P.F. Anto, S.K. Singh, Investigation of premature failure of a well fluid pipeline in an indian Offshore installation, Book-Inst. Mater. 715 (1999) 180–187.

[11] S. Bhat, B. Kumar, S.R. Prasad, M.V. Katarki, Failure of a new 8-in pipeline from group gathering station to central tank farm, Mater. Perform. 50 (2011) 50–54.

[12] L. Hall-Stoodley, J.W. Costerton, P. Stoodley, Bacterial biofilms: from the natural environment to infectious diseases, Nat. Rev. Microbiol. 2 (2004) 95–108.

[13] R.M. Donlan, Biofilms: microbial life on surfaces, Emerg. Infect. Dis. 8 (2002) 881–890.

[14] D. Xu, R. Jia, Y. Li, T. Gu, Advances in the treatment of problematic industrial biofilms, World J. Microbiol. Biotechnol. 33 (2017) 97.

[15] X. Wang, R.E. Melchers, Corrosion of carbon steel in presence of mixed deposits under stagnant seawater conditions, J. Loss Prev. Process Ind. 45 (2017) 29–42.

[16] A.F. Forte Giacobone, S.A. Rodriguez, A.L. Burkart, R.A. Pizarro, Microbiological induced corrosion of AA 6061 nuclear alloy in highly diluted media by *Bacillus cereus* RE 10, Int. Biodeterior. Biodegrad. 65 (2011) 1161–1168.

[17] T. Wu, M. Yan, D. Zeng, J. Xu, C. Sun, C. Yu, W. Ke, Stress corrosion cracking of X80 steel in the presence of sulfate-reducing bacteria, J. Mater. Sci. Technol. 31 (2015) 413–422.

[18] K.M. Usher, A.H. Kaksonen, I. Cole, D. Marney, Critical review: microbially influenced corrosion of buried carbon steel pipes, Int. Biodeterior. Biodegrad. 93 (2014) 84–106.

[19] N.S. Manam, W.S.W. Harun, D.N.A. Shri, S.A.C. Ghani, T. Kurniawan, M.H. Ismail, M.H.I. Ibrahim, Study of corrosion in biocompatible metals for implants: A review, J. Alloys Compd. 701 (2017) 698–715.

[20] E. Zhou, H. Li, C. Yang, J. Wang, D. Xu, D. Zhang, T. Gu, Accelerated corrosion of 2304 duplex stainless steel by marine *Pseudomonas aeruginosa* biofilm, Int. Biodeterior. Biodegrad. 127 (2018) 1–9.

[21] D. Ahmadkhaniha, A. Järvenpää, M. Jaskari, M.H. Sohi, A. Zarei-Hanzaki, M. Fedel, F. Deflorian, L.P. Karjalainen, Microstructural modification of pure Mg for improving mechanical and biocorrosion properties, J. Mech. Behav. Biomed. Mater. 61 (2016) 360–370.

[22] X. Dai, H. Wang, L.-K. Ju, G. Cheng, H. Cong, B.Z. Newby, Corrosion of aluminum alloy 2024 caused by *Aspergillus niger*, Int. Biodeterior. Biodegrad. 115 (2016) 1–10.

[23] E. Ilhan-Sungur, T. Unsal-Istek, N. Cansever, Microbiologically influenced corrosion of galvanized steel by *Desulfovibrio* sp. and *Desulfosporosinus* sp. in the presence of Ag–Cu ions, Mater. Chem. Phys. 162 (2015) 839–851.

[24] Y. Li, D. Xu, C. Chen, X. Li, R. Jia, D. Zhang, W. Sand, F. Wang, T. Gu, Anaerobic microbiologically influenced corrosion mechanisms interpreted using bioenergetics and bioelectrochemistry: A review, J. Mater. Sci. Technol. 34 (2018) 1713–1718.

[25] P.S. Stewart, J.W. Costerton, Antibiotic resistance of bacteria in biofilms, The Lancet. 358 (2001) 135–138.

[26] H.A. Videla, Prevention and control of biocorrosion, Int. Biodeterior. Biodegrad. 49 (2002) 259–270.

[27] J.W. Costerton, The Biofilm Primer, Springer, Berlin-New York, 2007.

[28] I.B. Beech, Sulfate-reducing bacteria in biofilms on metallic materials and corrosion, Microbiol. Today. 30 (2003) 115–117.

[29] L. Yang, M. Givskov, Chemical biology strategies for biofilm control, Microbiol. Spectr. 3 (2015). doi:10.1128/microbiolspec.MB-0019-2015

[30] I.B. Beech, C.C. Gaylarde, Recent advances in the study of biocorrosion: an overview, Rev. Microbiol. 30 (1999) 117–190.

[31] H.C. Flemming, J. Wingender, The biofilm matrix, Nat. Rev. Microbiol. 8 (2010) 623–633.

[32] E. Maunders, M. Welch, Matrix exopolysaccharides; the sticky side of biofilm formation, FEMS Microbiol. Lett. 364 (2017) fnx120.

[33] P.S. Stewart, M.J. Franklin, Physiological heterogeneity in biofilms, Nat. Rev. Microbiol. 6 (2008) 199–210.

[34] K. Jefferson, What drives bacteria to produce a biofilm?, FEMS Microbiol. Lett. 236 (2004) 163–173.

[35] E. Tuomanen, D.T. Durack, A. Tomasz, Antibiotic tolerance among clinical isolates of bacteria, Antimicrob. Agents Chemother. 30 (1986) 521.

[36] T.F.C. Mah, G.A. O'Toole, Mechanisms of biofilm resistance to antimicrobial agents, Trends Microbiol. 9 (2001) 34–39.

[37] C. Walsh, Molecular mechanisms that confer antibacterial drug resistance, Nature. 406 (2000) 775–781.

[38] B. Anandkumar, R.P. George, S. Maruthamuthu, N. Parvathavarthini, U.K. Mudali, Corrosion characteristics of sulfate-reducing bacteria (SRB) and the role of molecular biology in SRB studies: an overview, Corros. Rev. 34 (2016) 41–63.

[39] R.K. Bhagobaty, Culture dependent methods for enumeration of sulphate reducing bacteria (SRB) in the oil and gas industry, Rev. Environ. Sci. Biotechnol. 13 (2014) 11–16.

[40] Y. Tanaka, M. Sogabe, K. Okumura, R. Kurane, A highly selective direct method of detecting sulphate-reducing bacteria in crude oil, Lett. Appl. Microbiol. 35 (2002) 242–246.

[41] T. Thorstenson, E. Sunde, G. Bodtker, B.L. Lillebo, T. Torsvik, J. Beeder, Biocide Replacement by Nitrate in Sea Water Injection Systems, Corrosion/2002 Paper No. 2002-2033, NACE International, Denver, Colorado, 2002.

[42] D. Xu, W. Huang, G. Ruschau, J. Hornemann, J. Wen, T. Gu, Laboratory investigation of MIC threat due to hydrotest using untreated seawater and subsequent exposure to pipeline fluids with and without SRB spiking, Eng. Fail. Anal. 28 (2013) 149–159.

[43] R.K. Thauer, E. Stackebrandt, W.A. Hamilton, Energy metabolism phylogenetic diversity of sulphate-reducing bacteria, in: L.L. Barton, W.A. Hamilton (Eds.), Sulphate-Reducing Bacteria: Environmental and Engineered Systems, Cambridge University Press, Cambridge, UK, 2007, pp. 1–37.

[44] D. Enning, J. Garrelfs, Corrosion of iron by sulfate-reducing bacteria: new views of an old problem, Appl. Environ. Microbiol. 80 (2014) 1226–1236.

[45] T.T. Fida, C. Chen, G. Okpala, G. Voordouw, Implications of limited thermophilicity of nitrite reduction for control of sulfide production in oil reservoirs, Appl. Environ. Microbiol. 82 (2016) 4190–4199.

[46] L.M. Gieg, T.R. Jack, J.M. Foght, Biological souring and mitigation in oil reservoirs, Appl. Microbiol. Biotechnol. 92 (2011) 263–282.

[47] D. Xu, Y. Li, F. Song, T. Gu, Laboratory investigation of microbiologically influenced corrosion of C1018 carbon steel by nitrate reducing bacterium *Bacillus licheniformis*, Corros. Sci. 77 (2013) 385–390.

[48] R. Jia, D. Yang, D. Xu, T. Gu, Anaerobic corrosion of 304 stainless steel caused by the *Pseudomonas aeruginosa* biofilm, Front. Microbiol. 8 (2017) 2335.

[49] H. Wan, D. Song, D. Zhang, C. Du, D. Xu, Z. Liu, D. Ding, X. Li, Corrosion effect of *Bacillus cereus* on X80 pipeline steel in a Beijing soil environment, Bioelectrochemistry. 121 (2018) 18–26.

[50] D. Xu, Y. Li, T. Gu, Mechanistic modeling of biocorrosion caused by biofilms of sulfate reducing bacteria and acid producing bacteria, Bioelectrochemistry. 110 (2016) 52–58.

[51] T. Gu, Theoretical modeling of the possibility of acid producing bacteria causing fast pitting biocorrosion, J. Microb. Biochem. Technol. 6 (2014) 68–74.

[52] Y. Kryachko, S.M. Hemmingsen, The role of localized acidity generation in microbially influenced corrosion, Curr. Microbiol. 74 (2017) 870–876.

[53] C.O.A. Olsson, D. Landolt, Passive films on stainless steels—chemistry, structure and growth, Electrochimica Acta. 48 (2003) 1093–1104.

[54] C. Bang, R.A. Schmitz, Archaea associated with human surfaces: not to be underestimated, FEMS Microbiol. Rev. 39 (2015) 631–648.

[55] R.S. Gupta, Protein phylogenies and signature sequences: a reappraisal of evolutionary relationships among archaebacteria, eubacteria, and eukaryotes, Microbiol. Mol. Biol. Rev. 62 (1998) 1435–1491.

[56] J.M. Willey, L.M. Sherwood, C.J. Woolverton, Prescott's Principles of Microbiology, McGraw Hill Higher Education, New York, 2009.

[57] X. Li, J. Liu, F. Yao, W. Wu, S. Yang, S.M. Mbadinga, J. Gu, B. Mu, Dominance of *Desulfotignum* in sulfate-reducing community in high sulfate production-water of high temperature and corrosive petroleum reservoirs, Int. Biodeterior. Biodegrad. 114 (2016) 45–56.

[58] P. Völkl, R. Huber, E. Drobner, R. Rachel, S. Burggraf, A. Trincone, K.O. Stetter, *Pyrobaculum aerophilum* sp. nov., a novel nitrate-reducing hyperthermophilic archaeum, Appl. Environ. Microbiol. 59 (1993) 2918–2926.

[59] R.K. Thauer, A.-K. Kaster, H. Seedorf, W. Buckel, R. Hedderich, Methanogenic archaea: ecologically relevant differences in energy conservation, Nat. Rev. Microbiol. 6 (2008) 579–591.

[60] K.O. Stetter, G. Lauerer, M. Thomm, A. Neuner, Isolation of extremely thermophilic sulfate reducers: evidence for a novel branch of archaebacteria, Science. 236 (1987) 822–824.

[61] J. Beeder, R.K. Nilsen, J.T. Rosnes, T. Torsvik,, T. Lien, *Archaeoglobus fulgidus* isolated from hot North Sea oil field waters, Appl. Environ. Microbiol. 60 (1994) 1227–1231.

[62] K.O. Stetter, R. Huber, E. Blöchl, M. Kurr, R.D. Eden, M. Fielder, H. Cash, I. Vance, Hyperthermophilic archaea are thriving in deep North Sea and Alaskan oil reservoirs, Nature. 365 (1993) 743–745.

[63] T. Gu, K. Zhao, S. Nesic, A Practical Mechanistic Model for MIC Based on a Biocatalytic Cathodic Sulfate Reduction (BCSR) Theory, Corrosion/2009 Paper No. 2009-9390, NACE International, Atlanta, Georgia, 2009.

[64] D. Xu, T. Gu, Carbon source starvation triggered more aggressive corrosion against carbon steel by the *Desulfovibrio vulgaris* biofilm, Int. Biodeterior. Biodegrad. 91 (2014) 74–81.

[65] T. Gu, D. Xu, Why Are Some Microbes Corrosive And Some Not? Corrosion/2013 Paper No. 2013-2336, NACE International, Orlando, Florida, 2013.

[66] D.R. Lovley, The microbe electric: conversion of organic matter to electricity, Curr. Opin. Biotechnol. 19 (2008) 564–571.

[67] C.I. Torres, A.K. Marcus, H.-S. Lee, P. Parameswaran, R. Krajmalnik-Brown, B.E. Rittmann, A kinetic perspective on extracellular electron transfer by anode-respiring bacteria, FEMS Microbiol. Rev. 34 (2010) 3–17.

[68] Y. Huang, E. Zhou, C. Jiang, R. Jia, S. Liu, D. Xu, T. Gu, F. Wang, Endogenous phenazine-1-carboxamide encoding gene *PhzH* regulated the extracellular electron transfer in biocorrosion of stainless steel by marine *Pseudomonas aeruginosa*., Electrochem. Commun. 94 (2018) 9–13.

[69] M. Zhou, H. Wang, D.J. Hassett, T. Gu, Recent advances in microbial fuel cells (MFCs) and microbial electrolysis cells (MECs) for wastewater treatment,

bioenergy and bioproducts: MFCs and MECs for wastewater treatment, bioenergy and bioproducts, J. Chem. Technol. Biotechnol. 88 (2013) 508–518.

[70] Z. Du, H. Li, T. Gu, A state of the art review on microbial fuel cells: A promising technology for wastewater treatment and bioenergy, Biotechnol. Adv. 25 (2007) 464–482.

[71] J. Liu, W. Dou, R. Jia, X. Li, S. Kumseranee, S. Punpruk, T. Gu, *Desulfovibrio vulgaris* Corroded X65 Carbon Steel and Copper with Two Different Types of MIC Mechanisms, Corrosion/2018 Paper No. 2018-10586, NACE International, Phoenix, Arizona, 2018.

[72] B.W.A. Sherar, I.M. Power, P.G. Keech, S. Mitlin, G. Southam, D.W. Shoesmith, Characterizing the effect of carbon steel exposure in sulfide containing solutions to microbially induced corrosion, Corros. Sci. 53 (2011) 955–960.

[73] P. Zhang, D. Xu, Y. Li, K. Yang, T. Gu, Electron mediators accelerate the microbiologically influenced corrosion of 304 stainless steel by the *Desulfovibrio vulgaris* biofilm, Bioelectrochemistry. 101 (2015) 14–21.

[74] W. Fu, Y. Li, D. Xu, T. Gu, Comparing two different types of anaerobic copper biocorrosion by sulfate-and nitrate-reducing bacteria, Mater. Perform. 53 (2014) 66–70.

[75] W. Dou, R. Jia, P. Jin, J. Liu, S. Chen, T. Gu, Investigation of the mechanism and characteristics of copper corrosion by sulfate reducing bacteria, Corros. Sci. 144 (2018) 237–248.

[76] R. Jia, J.L. Tan, P. Jin, D.J. Blackwood, D. Xu, T. Gu, Effects of biogenic H_2S on the microbiologically influenced corrosion of C1018 carbon steel by sulfate reducing *Desulfovibrio vulgaris* biofilm, Corros. Sci. 130 (2018) 1–11.

[77] J.M. Vroom, K.J.D. Grauw, H.C. Gerritsen, D.J. Bradshaw, P.D. Marsh, G.K. Watson, J.J. Birmingham, C. Allison, Depth penetration and detection of pH gradients in biofilms by two-photon excitation microscopy, Appl. Environ. Microbiol. 65 (1999) 3502–3511.

[78] J. Gu, Microbiological deterioration and degradation of synthetic polymeric materials: recent research advances, Int. Biodeterior. Biodegrad. 52 (2003) 69–91.

[79] E. Bayraktarov, R.E. Price, T.G. Ferdelman, K. Finster, The pH and pCO_2 dependence of sulfate reduction in shallow-sea hydrothermal CO_2–venting sediments (Milos Island, Greece), Front. Microbiol. 4 (2013) 69–75.

[80] K.S. George, S. Nešic, Investigation of carbon dioxide corrosion of mild steel in the presence of acetic acid-part 1: basic mechanisms, Corrosion. 63 (2007) 178–186.

[81] S. Nesic, J. Postlethwaite, S. Olsen, An electrochemical model for prediction of corrosion of mild steel in aqueous carbon dioxide solutions, Corrosion. 52 (1996) 280–294.

[82] J. Tiratsoo, The ultimate guide to unpiggable pipelines, Pipelines Int. (2013) 4–5.

[83] Q. Wu, W. Guo, X. Bao, R. Yin, X. Feng, H. Zheng, H. Luo, N. Ren, Enhancing sludge biodegradability and volatile fatty acid production by tetrakis hydroxymethyl phosphonium sulfate pretreatment, Bioresour. Technol. 239 (2017) 518–522.

[84] L. Laopaiboon, N. Phukoetphim, P. Laopaiboon, Effect of glutaraldehyde biocide on laboratory-scale rotating biological contactors and biocide efficacy, Electron. J. Biotechnol. 9 (2006) 358–369.

[85] I. Vance, D.R. Thrasher, Reservoir souring: mechanisms and prevention, in: B. Ollivier, M. Magot (Eds.), Petroleum Microbiology ASM Press, Washington, 2005, pp. 123–142.

[86] I. Raad, I. Chatzinikolaou, G. Chaiban, H. Hanna, R. Hachem, T. Dvorak, G. Cook, W. Costerton, In vitro and ex vivo activities of minocycline and EDTA against microorganisms embedded in biofilm on catheter surfaces, Antimicrob. Agents Chemother. 47 (2003) 3580–3585.

[87] J. Wen, K. Zhao, T. Gu, I.I. Raad, Chelators enhanced biocide inhibition of planktonic sulfate-reducing bacterial growth, World J. Microbiol. Biotechnol. 26 (2010) 1053–1057.

[88] J. Wen, K. Zhao, T. Gu, I.I. Raad, A green biocide enhancer for the treatment of sulfate-reducing bacteria (SRB) biofilms on carbon steel surfaces using glutaraldehyde, Int. Biodeterior. Biodegrad. 63 (2009) 1102–1106.

[89] J. Wen, D. Xu, T. Gu, I.I. Raad, A green triple biocide cocktail consisting of a biocide, EDDS and methanol for the mitigation of planktonic and sessile sulfate-reducing bacteria, World J. Microbiol. Biotechnol. 28 (2012) 431–435.

[90] R. Konno, H. Bruckner, A. D'Aniello, G.H. Fisher, N. Fujii, D-Amino Acids Practical Methods and Protocols: Analytical Methods for D-Amino Acids, Nova Science Pub Inc, New York, 2009.

[91] I. Kolodkin-Gal, D. Romero, S. Cao, J. Clardy, R. Kolter, R. Losick, D-amino acids trigger biofilm disassembly, Science. 328 (2010) 627–629.

[92] H. Xu, Y. Liu, D-amino acid mitigated membrane biofouling and promoted biofilm detachment, J. Membr. Sci. 376 (2011) 266–274.

[93] W.T.K. Kao, M. Frye, P. Gagnon, J.P. Vogel, R. Chole, D-amino acids do not inhibit *Pseudomonas aeruginosa* biofilm formation, Laryngoscope Investig. Otolaryngol. 2 (2017) 4–9.

[94] D. Xu, Y. Li, T. Gu, D-methionine as a biofilm dispersal signaling molecule enhanced tetrakis hydroxymethyl phosphonium sulfate mitigation of *Desulfovibrio vulgaris* biofilm and biocorrosion pitting, Mater. Corros. 65 (2014) 837–845.

[95] R. Jia, D. Yang, Y. Li, D. Xu, T. Gu, Mitigation of the *Desulfovibrio vulgaris* biofilm using alkyldimethylbenzylammonium chloride enhanced by D-amino acids, Int. Biodeterior. Biodegrad. 117 (2017) 97–104.

[96] D. Xu, Y. Li, T. Gu, A synergistic D-tyrosine and tetrakis hydroxymethyl phosphonium sulfate biocide combination for the mitigation of an SRB biofilm, World J. Microbiol. Biotechnol. 28 (2012) 3067–3074.

[97] C.J. Sanchez, K.S. Akers, D.R. Romano, R.L. Woodbury, S.K. Hardy, C.K. Murray, J.C. Wenke, D-amino acids enhance the activity of antimicrobials against biofilms of clinical wound isolates of *Staphylococcus aureus* and *Pseudomonas aeruginosa*, Antimicrob. Agents Chemother. 58 (2014) 4353–4361.

[98] P.S. Zilm, V. Butnejski, G. Rossi-Fedele, S.P. Kidd, S. Edwards, K. Vasilev, D-amino acids reduce *Enterococcus faecalis* biofilms in vitro and in the presence of antimicrobials used for root canal treatment, PloS One. 12 (2017) e0170670.

[99] R. Jia, D. Yang, D. Xu, T. Gu, Mitigation of a nitrate reducing *Pseudomonas aeruginosa* biofilm and anaerobic biocorrosion using ciprofloxacin enhanced by D-tyrosine, Sci. Rep. 7 (2017) 6946.

[100] Y. Li, R. Jia, H.H. Al-Mahamedh, D. Xu, T. Gu, Enhanced biocide mitigation of field biofilm consortia by a mixture of D-amino acids, Front. Microbiol. 7 (2016) 896.

[101] R. Jia, D. Yang, Y. Li, H.H. Al-Mahamedh, T. Gu, Enhancement of Alkyldimethylbenzylammonium Chloride and Tributyl Tetradecyl Phosphonium Chloride Biocides Using D-amino acids against A Field Biofilm Consortium, Corrosion/2016 Paper No. 2016-7279, NACE International, Vancouver, British Columbia, 2016.

[102] R. Jia, D. Yang, H.H. Al-Mahamedh, T. Gu, Electrochemical testing of biocide enhancement by a mixture of D-amino acids for the prevention of a corrosive biofilm consortium on carbon steel, Ind. Eng. Chem. Res. 56 (2017) 7640–7649.

[103] F. Cava, H. Lam, M.A. de Pedro, M.K. Waldor, Emerging knowledge of regulatory roles of D-amino acids in bacteria, Cell. Mol. Life Sci. 68 (2011) 817–831.

[104] H. Lam, D.C. Oh, F. Cava, C.N. Takacs, J. Clardy, M.A. de Pedro, M.K. Waldor, D-amino acids govern stationary phase cell wall remodeling in bacteria, Science. 325 (2009) 1552–1555.

[105] J. Royet, R. Dziarski, Peptidoglycan recognition proteins: pleiotropic sensors and effectors of antimicrobial defences, Nat. Rev. Microbiol. 5 (2007) 264–277.

[106] S.A. Leiman, J.M. May, M.D. Lebar, D. Kahne, R. Kolter, R. Losick, D-amino acids indirectly inhibit biofilm formation in *Bacillus subtilis* by interfering with protein synthesis, J. Bacteriol. 195 (2013) 5391–5395.

[107] F.M. AlAbbas, R. Bhola, J.R. Spear, D.L. Olson, B. Mishra, Electrochemical characterization of microbiologically influenced corrosion on linepipe steel exposed to facultative anaerobic *Desulfovibrio* sp., Int. J. Electrochem. Sci. 8 (2013) 859–871.

[108] B.J. Little, J.S. Lee, Electrochemical Techniques Applied to Microbiologically Influenced Corrosion, John Wiley & Sons, Inc., New Jersey, 2007.

[109] B.J. Little, P.A. Wagner, Application of electrochemical techniques to the study of microbiologically influenced corrosion, in: J.O'M. Bockris, B.E. Conway, R.E. White (Eds.), Modern Aspects of Electrochemistry, Springer, Boston, Massachusetts, 2002, pp. 205–246.

[110] W. Dou, J. Wu, T. Gu, P. Wang, D. Zhang, Preparation of super-hydrophobic micro-needle CuO surface as a barrier against marine atmospheric corrosion, Corros. Sci. 131 (2018) 156–163.

[111] R. Jia, D. Yang, H.B. Abd Rahman, T. Gu, An enhanced oil recovery polymer promoted microbial growth and accelerated microbiologically influenced corrosion against carbon steel, Corros. Sci. 139 (2018) 301–308.

[112] R. Gundersen, B. Johansen, P.O. Gartland, L. Fiksdal, I. Vintermyr, R. Tunold, G. Hagen, The effect of sodium hypochlorite on the electrochemical properties of stainless steels in seawater with and without bacterial films, Corrosion. 47 (1991) 800–807.

[113] H. Li, E. Zhou, D. Zhang, D. Xu, J. Xia, C. Yang, H. Feng, Z. Jiang, X. Li, T. Gu, K. Yang, Microbiologically influenced corrosion of 2707 hyper-duplex stainless steel by marine *Pseudomonas aeruginosa* biofilm, Sci. Rep. 6 (2016) 20190.

[114] J. Xu, R. Jia, D. Yang, C. Sun, T. Gu, Effects of D-Phenylalanine as a biocide enhancer of THPS against the microbiologically influenced corrosion of C1018 carbon steel, J. Mater. Sci. Technol. 35 (2019) 109–117.

[115] J. Liu, R. Jia, E. Zhou, Y. Zhao, W. Dou, D. Xu, K. Yang, T. Gu, Antimicrobial Cu-bearing 2205 duplex stainless steel against MIC by nitrate reducing *Pseudomonas aeruginosa* biofilm, Int. Biodeterior. Biodegrad. 132 (2018) 132–138.

[116] R.S. Dubey, R.S. Dubey, S.N. Upadhyay, A review of electrochemical techniques applied to microbiologically influenced corrosion in recent studies, Indian J. Chem. Technol. 6 (1999) 207–218.

[117] F.K. Sahrani, M.F. Nawawi, G. Usup, A. Ahmad, Open circuit potential and electrochemical impedance spectroscopy studies on stainless steel corrosion by marine sulfate-reducing bacteria, Malays. Appl. Biol. 43 (2014) 141–150.

[118] N.J.E. Dowling, J. Guezennec, M.L. Lemoine, A. Tunlid, D.C. White, Analysis of carbon steels affected by bacteria using electrochemical impedance and direct current techniques, Corrosion. 44 (1988) 869–874.

[119] M.J. Franklin, D.E. Nivens, A.A. Vass, M.W. Mittelman, R.F. Jack, N.J.E. Dowling, D.C. White, Effect of chlorine and chlorine/bromine biocide treatments on the number and activity of biofilm bacteria and on carbon steel corrosion, Corrosion. 47 (1991) 128–134.

[120] F. Mansfield, R. Tsai, H. Shih, B.J. Little, R. Ray, P. Wangner, Results of Exposure of Stainless Steels and Titanium to Natural Seawater, Corrosion/1990 Paper No. 109, NACE International, Houston, Texas, 1990.

[121] J.M. Sasser, D.J. Fieldhouse, C.N. Carter, Computer assisted identification of bacteria based on fatty acid analysis, Phytopathology. 74 (1984) 882–882.

[122] M.J. Franklin, D.E. Nivens, J.B. Guckert, D.C. White, Technical note: effect of electrochemical impedance spectroscopy on microbial biofilm cell numbers, viability, and activity, Corrosion. 47 (1991) 519–522.

[123] H. Liu, T. Gu, G. Zhang, W. Wang, S. Dong, Y. Cheng, H. Liu, Corrosion inhibition of carbon steel in CO_2-containing oilfield produced water in the presence of iron-oxidizing bacteria and inhibitors, Corros. Sci. 105 (2016) 149–160.

[124] D. Yang, Mechanism and Mitigation of Biocorrosion by Nitrate Reducing *Pseudomonas aeruginosa* against Stainless Steel, Master Thesis, Ohio University, 2016.

[125] R. Jia, D. Yang, J. Xu, D. Xu, T. Gu, Microbiologically influenced corrosion of C1018 carbon steel by nitrate reducing *Pseudomonas aeruginosa* biofilm under organic carbon starvation, Corros. Sci. 127 (2017) 1–9.

[126] A.B. Bjornson, J.G. Michael, Contribution of humoral and cellular factors to the resistance to experimental infection by *Pseudomonas aeruginosa* in mice I. Interaction between immunoglobulins, heat-labile serum factors, and phagocytic cells in the killing of bacteria, Infect. Immun. 4 (1971) 462–467.

[127] E.F. DeLong, Everything in moderation: archaea as 'non-extremophiles,' Curr. Opin. Genet. Dev. 8 (1998) 649–654.

[128] R. Jia, D. Yang, H.B. Abd Rahman, T. Gu, Laboratory testing of enhanced biocide mitigation of an oilfield biofilm and its microbiologically influenced corrosion of carbon steel in the presence of oilfield chemicals, Int. Biodeterior. Biodegrad. 125 (2017) 116–124.

[129] R. Jia, D. Yang, D. Xu, T. Gu, Carbon steel biocorrosion at 80°C by a thermophilic sulfate reducing archaeon biofilm provides evidence for its utilization of elemental iron as electron donor through extracellular electron transfer, Corros. Sci. (2018). doi:10.1016/j.corsci.2018.09.015.

[130] X. Jiang, S. Nesic, F. Huet, B. Kinsella, B. Brown, D. Young, Selection of electrode area for electrochemical noise measurements to monitor localized CO_2 corrosion, J. Electrochem. Soc. 159 (2012) C283–C288.

[131] Y. Chen, L. Ju, Method for fast quantification of pitting using 3D surface parameters generated with infinite focus microscope, Corrosion. 71 (2015) 1184–1196.

[132] H.-P. Klenk, R.A. Clayton, J.F. Tomb, O. White, K.E. Nelson, K.A. Ketchum, R.J. Dodson, M. Gwinn, E.K. Hickey, J.D. Peterson, others, The complete genome sequence of the hyperthermophilic, sulphate-reducing archaeon *Archaeoglobus fulgidus*, Nature. 394 (1998) 101.

[133] W. Lee, W.G. Characklis, Corrosion of mild steel under anaerobic biofilm, Corrosion. 49 (1993) 186–199.

[134] R.A. King, J.D.A. Miller, D.S. Wakerley, Corrosion of mild steel in cultures of sulphate-reducing bacteria: effect of changing the soluble iron concentration during growth, Br. Corros. J. 8 (1973) 89–93.

[135] R.A. King, J.D.A. Miller, J.S. Smith, Corrosion of mild steel by iron sulphides, Br. Corros. J. 8 (1973) 137–141.

[136] R. Jia, D. Yang, D. Xu, T. Gu, Electron transfer mediators accelerated the microbiologically influence corrosion against carbon steel by nitrate reducing *Pseudomonas aeruginosa* biofilm, Bioelectrochemistry. 118 (2017) 38–46.

[137] P. Elliott, S. Ragusa, D. Catcheside, Growth of sulfate-reducing bacteria under acidic conditions in an upflow anaerobic bioreactor as a treatment system for acid mine drainage, Water Res. 32 (1998) 3724–3730.

[138] B. Kiilerich, W. van de Ven, A. Nielsen, J. Vollertsen, Sulfide precipitation in wastewater at short timescales, Water. 9 (2017) 670.

[139] M.A.M. Reis, J.S. Almeida, P.C. Lemos, M.J.T. Carrondo, Effect of hydrogen sulfide on growth of sulfate reducing bacteria, Biotechnol. Bioeng. 40 (1992) 593–600.

[140] J.R. Postgate, The Sulfate-reducing Bacteria, Cambridge University Press, Cambridge, London, 1984.

[141] J. Ning, Y. Zheng, D. Young, B. Brown, S. Nešić, Thermodynamic study of hydrogen sulfide corrosion of mild steel, Corrosion. 70 (2014) 375–389.

[142] H. Liu, Y. Cheng, Mechanism of microbiologically influenced corrosion of X52 pipeline steel in a wet soil containing sulfate-reduced bacteria, Electrochimica Acta. 253 (2017) 368–378.

[143] J.A. Berges, D.J. Franklin, P.J. Harrison, Evolution of an artificial seawater medium: improvements in enriched seawater, artificial water over the last two decades, J. Phycol. 37 (2001) 1138–1145.

[144] Y. Konishi, N. Yoshida, S. Asai, Desorption of hydrogen sulfide during batch growth of the sulfate-reducing bacterium *Desulfovibrio desulfuricans*, Biotechnol. Prog. 12 (1996) 322–330.

[145] A.C. Alvarez Yela, M.A. Tibaquirá Martínez, G.A. Rangel Piñeros, V.C. López, S.H. Villamizar, V.L. Núñez Vélez, W.R. Abraham, M.J. Vives Flórez, A.F. González Barrios, A comparison between conventional *Pseudomonas aeruginosa* rhamnolipids and *Escherichia coli* transmembrane proteins for oil recovery enhancing, Int. Biodeterior. Biodegrad. 112 (2016) 59–65.

[146] J.J. Sheng, A comprehensive review of alkaline–surfactant–polymer (ASP) flooding, ASIA-Pac. J. Chem. Eng. 9 (2014) 471–489.

[147] G. Voordouw, Production-related petroleum microbiology: progress and prospects, Curr. Opin. Biotechnol. 22 (2011) 401–405.

[148] C.M. Aitken, D.M. Jones, S.R. Larter, Anaerobic hydrocarbon biodegradation in deep subsurface oil reservoirs, Nature. 431 (2004) 291–294.

[149] R.K. Bhagobaty, Culture dependent methods for enumeration of sulphate reducing bacteria (SRB) in the Oil and Gas industry, Rev. Environ. Sci. Biotechnol. 13 (2014) 11–16.

[150] F. Shi, L. Zhang, J. Yang, M. Lu, J. Ding, H. Li, Polymorphous FeS corrosion products of pipeline steel under highly sour conditions, Corros. Sci. 102 (2016) 103–113.

[151] R. Jia, D. Yang, H.B. Abd Rahman, T. Gu, Investigation of the Impact of An Enhanced Oil Recovery Polymer on Microbial Growth and MIC, Corrosion/2018 Paper No. 2018-10567, NACE International, Phoenix, Arizona, 2018.

[152] D.C. Standnes, I. Skjevrak, Literature review of implemented polymer field projects, J. Pet. Sci. Eng. 122 (2014) 761–775.

[153] C. Li, D. Zhang, X. Li, S.M. Mbadinga, S. Yang, J. Liu, J. Gu, B. Mu, The biofilm property and its correlationship with high-molecular-weight polyacrylamide degradation in a water injection pipeline of Daqing oilfield, J. Hazard. Mater. 304 (2016) 388–399.

[154] D.A.Z. Wever, F. Picchioni, A.A. Broekhuis, Polymers for enhanced oil recovery: A paradigm for structure–property relationship in aqueous solution, Prog. Polym. Sci. 36 (2011) 1558–1628.

[155] F. Ma, L. Wei, L. Wang, C.C. Chang, Isolation and identification of the sulphate-reducing bacteria strain H1 and its function for hydrolysed polyacrylamide degradation, Int. J. Biotechnol. 10 (2008) 55–63.

[156] M. Bao, Q. Chen, Y. Li, G. Jiang, Biodegradation of partially hydrolyzed polyacrylamide by bacteria isolated from production water after polymer flooding in an oil field, J. Hazard. Mater. 184 (2010) 105–110.

[157] I. Lafortune, P. Juteau, E. Déziel, F. Lépine, R. Beaudet, R. Villemur, Bacterial diversity of a consortium degrading high-molecular-weight polycyclic aromatic hydrocarbons in a two-liquid phase biosystem, Microb. Ecol. 57 (2009) 455–468.

[158] S. Yang, S. Richter, W. Robbins, S. Nešić, Evaluation of The Protectiveness of A Paraffin Layer in CO_2 Corrosion of Mild Steel, Corrosion/2012 Paper No. 2012-1323, NACE International, Salt Lake City, Utah, 2012.

[159] T. Gu, R. Jia, T. Unsal, D. Xu, Toward a better understanding of microbiologically influenced corrosion caused by sulfate reducing bacteria, J. Mater. Sci. Technol. (2018). doi:10.1016/j.jmst.2018.10.026.

[160] L. Mi, G.A. Licina, S. Jiang, Nonantibiotic-based *Pseudomonas aeruginosa* biofilm inhibition with osmoprotectant analogues, ACS Sustain. Chem. Eng. 2 (2014) 2448–2453.

[161] A. Zlotkin, Dispersion and detachment of cell aggregates, 9,284,351 B2, 2016.

[162] R. Jia, D. Yang, A. Zlotkin, Y. Li, T. Gu, A Novel Peptide at A Very Low Concentration Enhanced Biocide Treatment of Corrosive Biofilms, Corrosion/2017 Paper No. 2017-8950, NACE International, New Orleans, Louisiana, 2017.

[163] A.S. Rose, A.R. Bradley, Y. Valasatava, J.M. Duarte, A. Prlić, P.W. Rose, Web-based molecular graphics for large complexes, in: ACM Press, 2016: pp. 185–186.

[164] A.S. Rose, P.W. Hildebrand, NGL Viewer: a web application for molecular visualization, Nucleic Acids Res. 43 (2015) W576–W579.

[165] A. Athanasiadis, G. Anderluh, P. Maček, D. Turk, Crystal structure of the soluble form of equinatoxin II, a pore-forming toxin from the sea anemone *Actinia equina*, Structure. 9 (2001) 341–346.

[166] M. Yadav, D. Behera, U. Sharma, Nontoxic corrosion inhibitors for N80 steel in hydrochloric acid, Arab. J. Chem. 9 (2016) S1487–S1495.

[167] S. Sutton, The most probable number method and its uses in enumeration, qualification, and validation, J. Valid. Technol. 16 (2010) 35–38.

[168] ASTM G1-03(2017)e1, Standard Practice for Preparing, Cleaning, and Evaluating Corrosion Test Specimens, ASTM International, West Conshohocken, PA, 2017, www.astm.org

Appendix A: Experimental Methods Used in Multiple Chapters

A.1 C1018 Carbon Steel Coupon

In all experiments in this project, the coupon used was C1018 (AISI 1018) carbon steel. Its chemical composition is (mass percentage): S 0.012, C 0.200, P 0.017, Cr 0.061, Si 0.044, Ni 0.044, Mo 0.018, Mn 0.900, and Fe balance. The square coupon had only one top surface exposed area of 1 cm^2. The other surfaces were coated with inert polytetrafluoroethylene (Teflon) paint. The exposed surface was polished using abrasive papers with 180, 400, and 600 grit sizes sequentially. After that, they were washed with pure isopropanol and dried anaerobically under UV light for 30 minutes.

A.2 Chemicals and Materials

Unless otherwise indicated, chemicals used in this project were either purchased from Fisher Scientific (Pittsburgh, PA, USA) or Sigma-Aldrich (St. Louis, MO, USA). The 125-mL anaerobic vials were purchased from Wheaton Industries, Inc. (Millville, NJ, USA).

A.3 Sterilization and Deoxygenation

The culture medium and all laboratory tools including anaerobic vials, electrochemical glass cell vessels, aluminum caps and rubber septa for vials, rubber stoppers for the glass cells, tweezers, spargers, pipette tips, and gas filters were autoclaved at 121°C for 20 minutes. All liquid solutions including culture medium, PBS solution, L-cysteine stock solution, D-amino acid stock solution, and biocide stock solution were sparged with filter-sterilized N_2 using stainless steel gas distributors for at least 1 hour to remove dissolved oxygen (Figure 67). After that, L-cysteine was added from a stock solution to all culture media to reach 100 ppm as an oxygen scavenger to

assure that the dissolved oxygen level in the sealed anaerobic vials was below 40 ppb. The L-cysteine stocker solution was sterilized using a 0.22 µm sterile filter (Stericup, Millipore, Bedford, MA, USA). All anaerobic manipulations were conducted in an anaerobic chamber filled with filter-sterilized N_2. The anaerobic chamber was flushed with filter-sterilized N_2 for at least 1 hour each time before use.

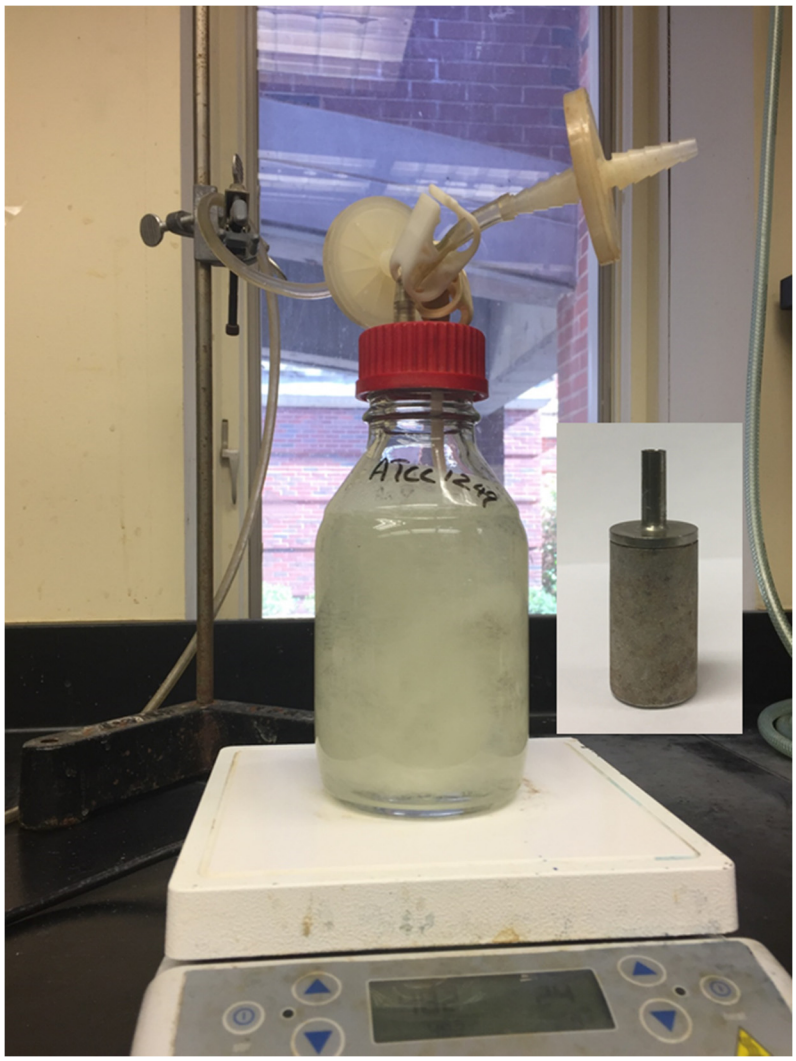

Figure 67. A nitrogen sparging bottle of ATCC 1249 medium with a stainless steel nitrogen gas bubble distributor.

A.4 Sessile Cell Count Using MPN Method

Coupons covered with biofilms and corrosion products were first retrieved from anaerobic vials after a certain period of incubation. Vials were opened in a vented chemical hood. The coupons were then washed with a pH 7.4 PBS solution to remove culture medium and loosely attached planktonic cells. After that, the biofilm on the coupon surface was removed using a sterilized tiny brush in a 10 mL pH 7.4 PBS solution. Then, the 10 mL PBS solution, the coupon, and the brush were put in a conical centrifuge tube and vortexed for more than 30 s to distribute the sessile cells evenly in the 10 mL PBS solution. MPN method was used to enumerate sessile cells. Commercial kits from Biotechnology Solutions (Houston, TX, USA) were used (Figure 68). The phenol red dextrose broth was used for APB enumeration. The modified Postgate's B medium was used for SRB enumeration. The standard bacterial nutrient broth for GHB enumeration. Three rolls of vials were used for MPN. MPN results were interpreted using the MPN table [167].

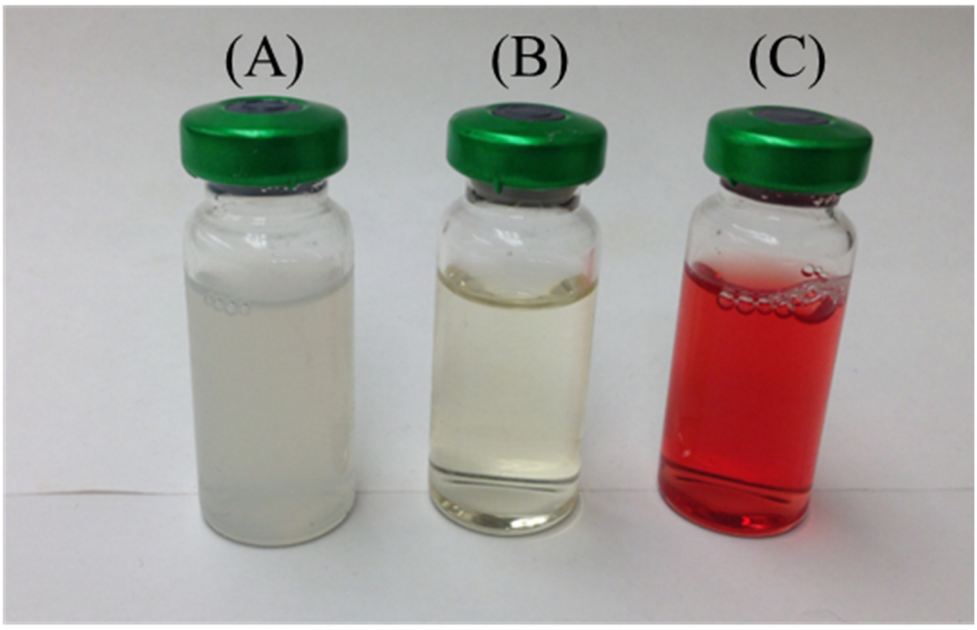

Figure 68. Three culture media used in the MPN method to count the sessile cells: (A) “Modified Postgate's B” for SRB, (B) “Standard Bacterial Nutrient Broth” for GHB, and (C) “Phenol Red Dextrose” for APB.

A.5 Biofilm Observation under SEM

The biofilm morphology on a coupon surface was observed under SEM (Model JSM-6390, JEOL, Tokyo, Japan). Coupons covered with biofilms and corrosion products were first retrieved from anaerobic vials after an incubation period. They were then soaked in 4% (w/w) glutaraldehyde solution for 2 hours to kill and fix the sessile cells. Then, the coupons were dehydrated sequentially with different concentrations (25%, 50%, 75%, and 100% by volume) of isopropanol. Coupons were soaked with each concentration for 5 minutes. After that, coupons were dried using supercritical CO_2 (supplied from a siphoning type of CO_2 cylinder) in a critical point dryer (Model CPD 020, Balzers Union, Liechtenstein). After drying, coupons were stored in a vacuumed

desiccator. Before the SEM observation, biofilms were coated with palladium using a sputter coater (Model Hummer 6.2, Anatech, Hayward, CA, USA) to provide conductivity.

A.6 Biofilm Observation under CLSM

Live and dead cells in biofilms can be detected by CLSM (LSM 510, Carl Zeiss, Jena, Germany). After an incubation period, coupons were first washed with a pH 7.4 PBS solution to remove culture medium, treatment chemicals (if any), and loosely-attached planktonic cells. Then, sessile cells were stained using SYTO 9 and propidium iodide. SYTO 9 is a green-fluorescent stain. Propidium iodide is a red-fluorescent stain. These two dyes are in the Live/Dead® BacLight™ Bacterial Viability Kit L7012 purchased from Life Technologies (Grand Island, NY, USA). The red stain is able to penetrate only dead cells. The dyeing process lasted about 15 minutes. Live cells would show up as green dots while dead cells red when observed under CLSM. Under CLSM, a cell sample can either be in a liquid or on a coupon.

A.7 Weight Loss Measurement

For each weight loss data point, C1018 carbon steel coupons from different vials would be used, some of them from the same batch, some from replicate batches. After an incubation period, biofilms and corrosion products on the coupons were removed using Clarke's solution according to ASTM G1−03 [168]. The chemical composition of Clarke's solution consists of 50 g stannous chloride and 20 g antimony chloride in 1 L hydrochloric acid solution (specific gravity: 1.19). After 1-min cleaning time, 0.1 mg/cm^2 weight loss due to the cleaning process was sometimes observed. The balance (M-120, Denver Instrument, Arvada, CO, USA) used in this work has a readability of 0.1 mg.

A.8 Electrochemical Measurements

Electrochemical tests were conducted in 450 mL glass cells filled with 350 mL culture medium (Figure 69). The working electrode was a carbon steel coupon embedded in epoxy with an exposed 10 mm × 10 mm surface. The counter electrode was a platinum mesh plate. The reference electrode was a saturated calomel electrode (SCE) fitted with a Vycor tip facing the working electrode. In the anaerobic chamber, each glass cell was sealed with a 2.44 inch-diameter rubber stopper. A VersaSTAT 3 potentiostat purchased from Princeton Applied Research (Oak Ridge, TN, USA) was used. Its software was VersaStudio version 2.44.4. LPR was scanned under stable OCP with a potential range of −10 to +10 mV at a rate of 0.167 mV/s. EIS was conducted under stable OCP between 10^{-2} and 10^{5} Hz with a sinusoidal voltage signal (10 mV amplitude). ZSimDemo software with Version 3.30d from EChem Software (Ann Arbor, MI, USA) was used to analyze EIS data. PDS was scanned between −200 mV to and 200 mV vs. the OCP at a rate of 0.167 mV/s. A single working electrode was used to obtain the cathodic potentiodynamic polarization curve followed by the anodic curve. The working electrode was not incubated further because PDS is known to cause film damages on coupons. The PDS curves were processed to obtain Tafel slopes (β_α and β_c), corrosion current densities (i_{corr}), and corrosion potentials (E_{corr}) through Tafel analyses. The electrochemical setup for LPR and PDS in SRA starvation test is shown in Figure 70.

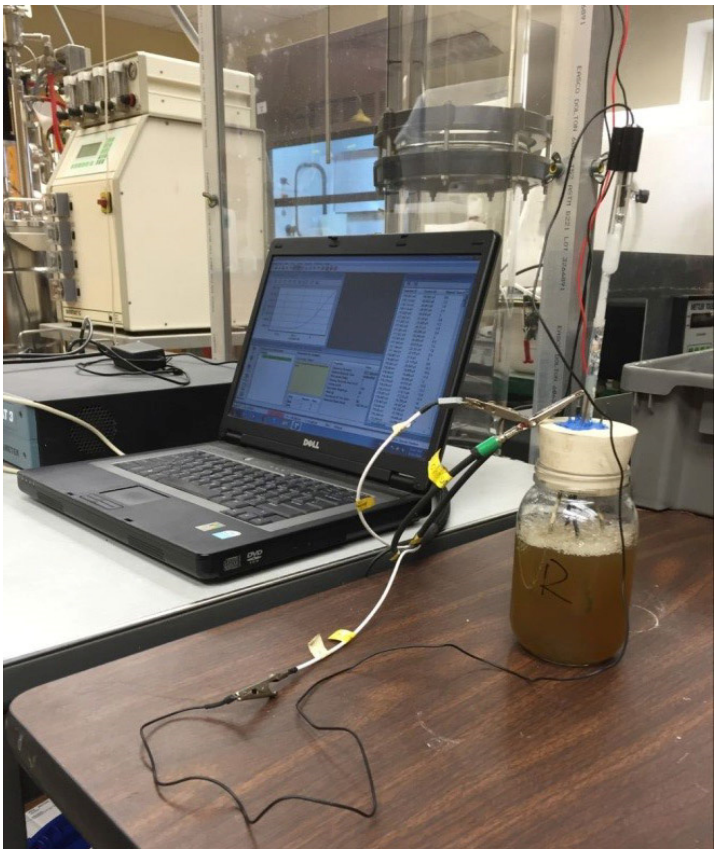

Figure 69. Electrochemical setup for OCP, LPR, EIS and PDS. The brown broth was a *P. aeruginosa* cultured in LB-NO_3 medium.

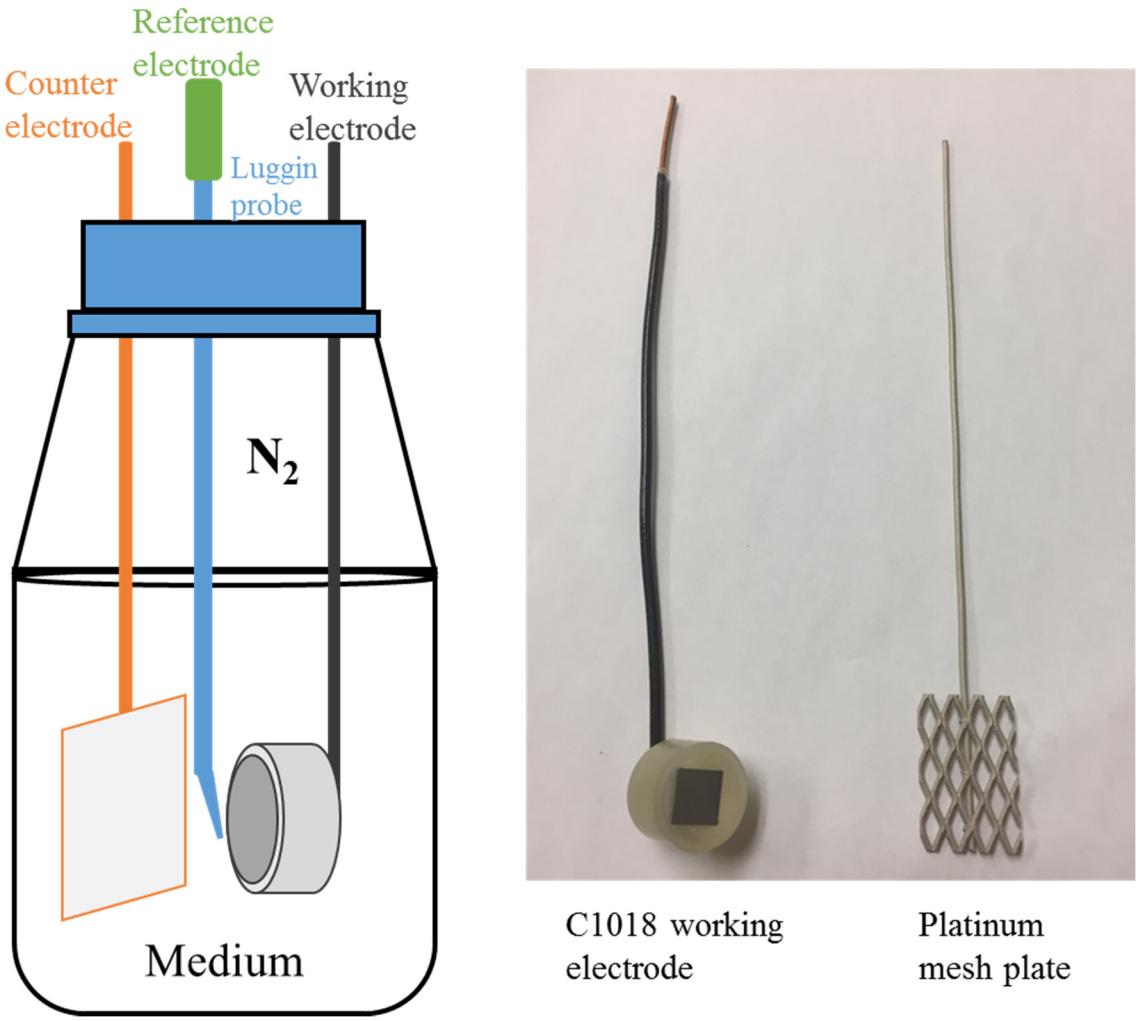

Figure 70. Electrochemical setup for LPR and PDS in SRA starvation test.

Appendix B: Journal Publications

1. **R. Jia,** D. Yang, D. Xu, T. Gu, Carbon steel biocorrosion at 80°C by a thermophilic sulfate reducing archaeon biofilm provides evidence for its utilization of elemental iron as electron donor through extracellular electron transfer, Corros. Sci. (2018). doi:10.1016/j.corsci.2018.09.015.
2. T. Gu, **R. Jia,** T. Unsal, D. Xu, Toward a better understanding of microbiologically influenced corrosion caused by sulfate reducing bacteria, J. Mater. Sci. Technol. (2018). doi:10.1016/j.jmst.2018.10.026.
3. J. Xu, **R. Jia,** D. Yang, C. Sun, T. Gu, Effects of D-Phenylalanine as a biocide enhancer of THPS against the microbiologically influenced corrosion of C1018 carbon steel, J. Mater. Sci. Technol. 35 (2019) 109–117.
4. W. Dou, **R. Jia,** P. Jin, J. Liu, S. Chen, T. Gu, Investigation of the mechanism and characteristics of copper corrosion by sulfate reducing bacteria, Corros. Sci. 144 (2018) 237–248.
5. Y. Huang, E. Zhou, C. Jiang, **R. Jia,** S. Liu, D. Xu, T. Gu, F. Wang, Endogenous phenazine-1-carboxamide encoding gene *PhzH* regulated the extracellular electron transfer in biocorrosion of stainless steel by marine *Pseudomonas aeruginosa*., Electrochem. Commun. 94 (2018) 9–13.
6. **R. Jia,** D. Yang, H.B. Abd Rahman, T. Gu, An enhanced oil recovery polymer promoted microbial growth and accelerated microbiologically influenced corrosion against carbon steel, Corros. Sci. 139 (2018) 301–308.

7. Y. Li, D. Xu, C. Chen, X. Li, **R. Jia,** D. Zhang, W. Sand, F. Wang, T. Gu, Anaerobic microbiologically influenced corrosion mechanisms interpreted using bioenergetics and bioelectrochemistry: A review, J. Mater. Sci. Technol. 34 (2018) 1713–1718.
8. J. Liu, **R. Jia,** E. Zhou, Y. Zhao, W. Dou, D. Xu, K. Yang, T. Gu, Antimicrobial Cu-bearing 2205 duplex stainless steel against MIC by nitrate reducing *Pseudomonas aeruginosa* biofilm, Int. Biodeterior. Biodegrad. 132 (2018) 132–138.
9. **R. Jia,** J.L. Tan, P. Jin, D.J. Blackwood, D. Xu, T. Gu, Effects of biogenic H_2S on the microbiologically influenced corrosion of C1018 carbon steel by sulfate reducing *Desulfovibrio vulgaris* biofilm, Corros. Sci. 130 (2018) 1–11.
10. D. Xu, **R. Jia,** Y. Li, T. Gu, Advances in the treatment of problematic industrial biofilms, World J. Microbiol. Biotechnol. 33 (2017) 97.
11. **R. Jia,** D. Yang, D. Xu, T. Gu, Anaerobic corrosion of 304 stainless steel caused by the *Pseudomonas aeruginosa* biofilm, Front. Microbiol. 8 (2017) 2335.
12. **R. Jia,** D. Yang, H.H. Al-Mahamedh, T. Gu, Electrochemical testing of biocide enhancement by a mixture of D-amino acids for the prevention of a corrosive biofilm consortium on carbon steel, Ind. Eng. Chem. Res. 56 (2017) 7640–7649.
13. **R. Jia,** D. Yang, D. Xu, T. Gu, Electron transfer mediators accelerated the microbiologically influence corrosion against carbon steel by nitrate reducing *Pseudomonas aeruginosa* biofilm, Bioelectrochemistry. 118 (2017) 38–46.
14. **R. Jia,** Y. Li, H.H. Al-Mahamedh, T. Gu, Enhanced biocide treatments with D-amino acid mixtures against a biofilm consortium from a water cooling tower, Front. Microbiol. 8 (2017) 1538.

15. **R. Jia,** D. Yang, H.B. Abd Rahman, T. Gu, Laboratory testing of enhanced biocide mitigation of an oilfield biofilm and its microbiologically influenced corrosion of carbon steel in the presence of oilfield chemicals, Int. Biodeterior. Biodegrad. 125 (2017) 116–124.
16. **R. Jia,** D. Yang, J. Xu, D. Xu, T. Gu, Microbiologically influenced corrosion of C1018 carbon steel by nitrate reducing *Pseudomonas aeruginosa* biofilm under organic carbon starvation, Corros. Sci. 127 (2017) 1–9.
17. **R. Jia,** D. Yang, D. Xu, T. Gu, Mitigation of a nitrate reducing *Pseudomonas aeruginosa* biofilm and anaerobic biocorrosion using ciprofloxacin enhanced by D-tyrosine, Sci. Rep. 7 (2017) 6946.
18. **R. Jia,** D. Yang, Y. Li, D. Xu, T. Gu, Mitigation of the *Desulfovibrio vulgaris* biofilm using alkyldimethylbenzylammonium chloride enhanced by D-amino acids, Int. Biodeterior. Biodegrad. 117 (2017) 97–104.
19. Y. Li, **R. Jia,** H.H. Al-Mahamedh, D. Xu, T. Gu, Enhanced biocide mitigation of field biofilm consortia by a mixture of D-amino acids, Front. Microbiol. 7 (2016) 896

Thesis and Dissertation Services